UCL INSTITUTE OF CARDIOVASCULAR SCIENCE



Detection of Iron and Cobalt by Cardiovascular Magnetic Resonance

Dr Amna Abdel-Gadir

MD(Res) Thesis

UCL

2019

Abdel-Gadir A, Thesis 2019, UCL

DECLARATION

I, Amna Abdel-Gadir confirm that the work presented in this thesis is

my own. Where information has been derived from other sources, I confirm

that this has been indicated in the thesis.

Signature:

Name: Amna Abdel-Gadir

Date: 15th July 2019

ACKNOWLEDGEMENTS

I would like to thank my supervisors Professor James Moon and Dr J Malcolm Walker for their guidance, mentorship, and support throughout my research. I would also like to thank all the research fellows, radiographers, and administrative staff for their endless help on this journey. A very special thanks to the patients as without them this thesis would not have been possible. Finally, I am grateful for my family and friends who have supported me during the more challenging times.

List of collaborators

Dr Juliano Fernandes

Consultants	Fellows
Consulants	Leliow2

Professor James Moon (Primary Supervisor) Dr Sabrina Nordin Dr Malcolm Walker (Secondary Supervisor) Dr Katia Menacho Professor John Porter Dr Maciei Garbowski Dr Charlotte Manisty Dr Stefania Rosmini Dr Anish Bhuva Dr Anna Herrey **Professor Alistar Hart** Dr Giulia Benedetti Mr John Skinner Dr Heerainarain Bulluck Dr Daniel Sado Dr Thomas Treibel Dr Marianna Fontana Mr Reshid Berber Dr Viviana Maestrini Dr Hatai Ngamkasem Dr Yong Vorasettakarnkij Dr Kristopher Knott

Radiographers Administrative staff

Ms Sarah Anderson Mrs Sandy Gardner
Miss Louise McGrath

ABSTRACT

Heart failure remains the leading cause of significant morbidity and mortality in patients with iron or cobalt overload or toxicity, resulting from accumulation of metal in the heart. Survival of patients with iron overload from primary and secondary haemochromatosis has improved with the introduction of the cardiovascular magnetic resonance (CMR) T2* technique allowing a personalised approach to chelator dosing, but this diagnostic test is limited to services with access to the necessary resources. Additionally, limitations have been identified with this technique, which may impact patient outcomes. An alternative MRI measure, T1 mapping, promises major advantages of time and cost over this gold standard. In a single short breath-hold an instant colour map demonstrates the iron content without the need for complex analysis.

More recently, the increasing number of case reports describing fatal cardiomyopathy secondary to high circulating cobalt and chromium from metal-on-metal (MoM) hips has provoked great public concern, strong media coverage, and well profiled litigation cases. Patients are currently risk stratified and monitored for toxicity with crude assessments including measurement of blood levels and echocardiographic assessment of cardiac function, but a diagnostic tool to measure tissue deposition does not exist. Diagnosis depends on invasive myocardial biopsies or post-mortem examinations. As cobalt exhibits similar magnetic properties to iron, CMR has the potential to non-invasively detect tissue deposition of metal ions and act

as a screening tool for patients at risk of systemic toxicity and thus guide management.

The work described in this thesis demonstrates the relationship between the gold standard CMR T2* measurement with T1 mapping. In the largest single centre study for iron overload, 300 adults and 21 paediatric patients at risk of iron overload underwent CMR scans involving both techniques allowing insights into the disease. T1 mapping correlated well with T2* in all patients with iron loading, and potentially diagnosed iron in approximately 50% of patients with a normal T2* value. The utility and ease of the T1 mapping method was further demonstrated in Thailand where 128 scans performed in 2 days demonstrated previously undiagnosed cardiac and liver iron in almost all patients. Scan duration was 4 times faster than a standard non-contrast CMR. These findings had great clinical and cost implications.

Finally, I have shown, in a blinded study involving 90 patients recruited from the UK's national hip prosthesis retrieval service, that patients with high levels of circulating cobalt did not develop heart failure or features suggestive of cardiomyopathy using advanced CMR techniques. In this study, there were no significant differences in ventricular function or tissue characterisation between patients with MoM and non-MoM. Although the results were negative this unique study may provide reassurance to patients and surgeons.

IMPACT STATEMENT

Metal related cardiomyopathy is a global disease resulting from inherited or iatrogenic causes. This work has demonstrated that disease-modifying tests often deemed too expensive can be utilised for patients living in countries with low-income economies to improve outcomes. I have shown that applying new techniques can simplify diagnosis and reduce health care costs. This concept has since been applied in over 10 countries and has provided new insights into other diseases with cardiovascular sequelae. This work also provides reassuring evidence to the over 1 million patients with metal-on-metal hips regarding risk of heart failure even with high blood levels of cobalt and chromium.

FUNDING

This research was funded by grants from the Rosetrees Trust and the UK Thalassaemia Society, to whom I am extremely grateful.

CONTENTS

Declaration		2
Acknowledge	ements	3
Abstract		4
Contents		7
Tables		9
Figures		10
Abbreviation	s	12
Chapter 1 In	troduction	14
1.1 M	etal cardiomyopathy,	15
1.2 lr	on and iron metabolism	16
1.3 lr	on overload	21
1.4 lr	on overload cardiomyopathy	28
1.5 A	ssessment of iron deposition	33
1.6 E	Blood biomarkers of iron status	34
1.7 C	ardiovascular Magnetic Resonance in Iron Overload	35
1.8 M	anagement of iron overload: Chelation therapy	46
1.9 C	obalt	48
1.10	Pathophysiology and complications of cobalt toxicity	50
1.11	Cobalt cardiomyopathy	51
1.12	Assessment of cobalt toxicity	54
1.13	Management of cobalt toxicity	55
Chapter 2 R	esearch Aims	56
Chapter 3 G	eneral methodology	59
3.1 E	thical approval	59

3.2 Study population	59
3.3 CMR protocols	61
3.4 Imaging analysis	64
3.5 Statistical analysis	65
Chapter 4 Results: Myocardial iron quantification by T1 mapping	66
Chapter 5 Results: Ultrafast CMR for iron in the developing world	90
Chapter 6 Results: CMR for cobalt	112
Chapter 7 Discussion and Conclusion	133
Chapter 8 Publications	140
Chapter 9 References	146

TABLES

Table 1. Iron overload syndromes	22
Table 2. Causes of raised serum ferritin	. 35
Table 3. Systemic effects of cobalt toxicity	. 50
Table 4. Factors distinguishing cobalt cardiomyopathy from non-ischaemic	
cardiomyopathy	. 53
Table 5. Comparison of CMR measurements in patients with normal T2*	
and low T1 versus normal T2* and normal T1	.80
Table 6. Patient baseline characteristics	.82
Table 7. CMR parameters between baseline scans and follow-up scans	. 83
Table 8. Grouping of paediatric patients according to T2* and T1 values	. 84
Table 9. Thailand patient baseline characteristics 1	00
Table 10. Interstudy repeatability in 10 patients and 6 healthy volunteers 10	04.
Table 11. Incidental anatomical findings in the Thailand group using CMR.1	05
Table 12. Patient demographics by study group1	123
Table 13. Summary of CMR and biomarker results	126

FIGURES

Figure 1. Distribution of iron in adults	17
Figure 2. Uptake of iron-transferrin complex	19
Figure 3. The effects of iron overload on the heart, liver, and endocrine	
organs	27
Figure 4. Iron uptake, storage, and toxicity in a myocyte	29
Figure 5. Post-mortem myocardial biopsy	30
Figure 6. Spectrum of illness and the development of heart disease in iro	n-
overload	32
Figure 7. Myocardial T2* image demonstrating a mid-short axis slice	37
Figure 8. Myocardial T2* image showing images acquired over 8 predefined	
echo times	38
Figure 9. Dark blood T2* image of a mid-LV short-axis slice	40
Figure 10. T2* map generated with black blood T2* sequence	41
Figure 11. Modified Look-Locker Inversion Recovery (MOLLI) sequenc	е
for T1 mapping	43
Figure 12. Examples of native T1 maps from a healthy volunteer	14
Figure 13. Generation of an ECV map in a healthy volunteer4	6
Figure 14. Examples of T1 mapping in iron loading states	55
Figure 15. Bright blood and dark blood myocardial T2* CMR	
analysis5	56
Figure 16. The healthy volunteer population T2* and T1 values scatter5	59
Figure 17. Correlation between T1 mapping and T2* in patients with	
haemoglobinopathies and in healthy volunteers	61

Figure 18. Correlation between T1 and T2* in patients with values less tha	n
20ms	62
Figure 19. Correlation between T1 and T2* in patients with myocardial	Γ2*
values greater than 20ms	.62
Figure 20. Correlation between T1 and T2* in patients with T2* values less	;
than 29ms	.63
Figure 21. Ultrafast scanning protocol	81
Figure 22. Native T1 myocardial short axis map using the ShMOLLI	
technique	82
Figure 23. T2* of the liver with region of interest shown	83
Figure 24. Correlation between T2* and T1 mapping in patients	86
Figure 25. Significant extra-cardiac findings	106
Figure 26. Patient with severe cardiac iron loading and evidence of extens	ive
extramedullary haematopoiesis	107
Figure 27. Flow diagram of the study methods	117
Figure 28. CMR images of late gadolinium enhancement	126
Figure 29. T1 maps and LGE images of a patient with mid-wall fibrosis	127
Figure 30. Examples of ECV maps of a 4Ch view and a SAX slice	128

ABBREVIATIONS

BBT2* Bright blood T2*

CMR Cardiovascular magnetic resonance

CoC Ceramic-on-ceramic

DBT2* Dark blood T2*

DFO Desferrioxamine

DMT1 Divalent metal transporter1

BNP Brain natriuretic peptide

DPO Deferiprone

ECG Electrocardiogram

ECV Extra-cellular volume

Fe²⁺ Ferrous iron

Fe³⁺ Ferric iron

GRE Gradient echo

FISP Fast imaging with steady state precession

HASTE Half-Fourier Acquisition Single-shot Turbo Spin Echo

HH Hereditary haemochromatosis

ICC Intraclass correlation coefficient

LGE Late gadolinium-enhancement

LPI Labile plasma iron

LV Left ventricle

LVEDVi Left ventricular end-diastolic volume index

LVESVi Left ventricular end-systolic volume index

LVEF Left ventricular ejection fraction

MHRA Medicines and Healthcare products Regulatory Agency

MOLLI Modified look locker inversion recovery

MoM Metal-on-metal

MoP Metal-on-polyethylene

MRI Magnetic resonance imaging

NTBI Non-transferrin bound iron

PPB Parts per billion

ROI Region of interest

ROS Reactive oxygen species

RV Right ventricle

SAX Short axis

SD Standard deviation

SF Serum ferritin

ShMOLLI Shortened modified look locker inversion recovery

SSFP Steady state free precession

TAPSE Tricuspid annular plane systolic excursion

TE Echo time

TEQAS Trace Elements External Quality Assessment Scheme

TM Thalassaemia major

TTE Transthoracic echocardiogram

WIP Work in progress

CHAPTER 1: INTRODUCTION

This chapter is partly based on the following publications:

- Amna Abdel-Gadir, Thomas Treibel, James Moon. Myocardial T1 Mapping:
 Where are we now and where are we going? Research Reports in Clinical
 Cardiology 2014, 5:339-34
- Amna Abdel-Gadir, Emmanuel Ako, J Malcolm Walker. Standards for the Clinical Care of Children and Adults with Thalassaemia in the UK. 3rd ed.
 2016. Chapter 17: Management of the cardiovascular system; p.102-112
- Katia Menacho, <u>Amna Abdel-Gadir</u>, James Moon, Juliano Lara Fernandes.
 T2* mapping techniques: iron overload assessment and other potential clinical applications. Magnetic Resonance Imaging Clinics of North America 2019, 27(3):439-451

1.1 Metal cardiomyopathy

The prevalence of secondary metal-related cardiomyopathy is increasing(1).

Unlike other forms of cardiomyopathy, heart failure related to iron and cobalt deposition is reversible if diagnosed and treated early.

Iron overload has become a global health concern due to the increasing number of patients requiring frequent blood transfusions for survival, and patients affected by inherited iron loading conditions such as haemochromatosis.(1) Cardiac iron deposition over time leads to heart failure and premature death.(2) Monitoring of cardiac iron with cardiac magnetic resonance (CMR) has revolutionised the management of these patients and changed the disease course.(3) However patients who are likely to benefit the most live in countries where access to life saving investigations is scarce creating a large disparity across the globe. Treatment and diagnostic methods are available but not utilised effectively highlighting a dire need for change.

Cobalt shares similar chemical and physical properties with iron. The reversible nature of cobalt toxicity was first noted in the 1960's when increased consumption of beer stabilised with cobalt foam caused acute heart failure resolving with abstinence.(4) Resurgence of iatrogenic cobalt cardiomyopathy secondary to toxicity from failing metal-on-metal (MoM) hip prostheses has caused great concern(5, 6). Over 1 million MoM hip prostheses have been implanted worldwide.(7) Wear and corrosion has led to the release of nanoparticle debris and metal ions locally around the joint and into the circulation with resulting effects.(8, 9) This has led to nationwide

device recall, surgical hip revisions, and the development of a mandatory screening programme. Concerns regarding cardiotoxicity have been further fuelled by the reported 3-fold increased risk of heart failure in men with MoM prostheses.(10) Screening for toxicity relies on symptoms and established organ dysfunction, highlighting the need for a diagnostic non-invasive measurement of cobalt deposition. To date there is no such measurement.

In this chapter, a review of iron and cobalt metabolism and the cardiac manifestations of overload are described. Diagnostic CMR methods for myocardial metal deposition to benefit patients most affected, are explored.

1.2 Iron and iron metabolism

Iron is an essential element for many metabolic processes including oxygen transport, mitochondrial respiration, nucleic acid replication, and signalling, but in excess iron can be toxic when in its free form.(11, 12) A healthy male human body contains approximately 35 to 45mg of iron per kilogram of body weight, with lower amounts found in premenopausal women as a result of menstruation.(11, 13) More than 2 thirds of iron is incorporated into haemoglobin in developing erythroid precursors and mature red cells, and 10- 15% is present in myoglobin, enzymes and cytochromes.(11) The remaining body iron serve as storage depots in hepatocytes, in the form of ferritin, and in reticuloendothelial macrophages (figure 1).(11)

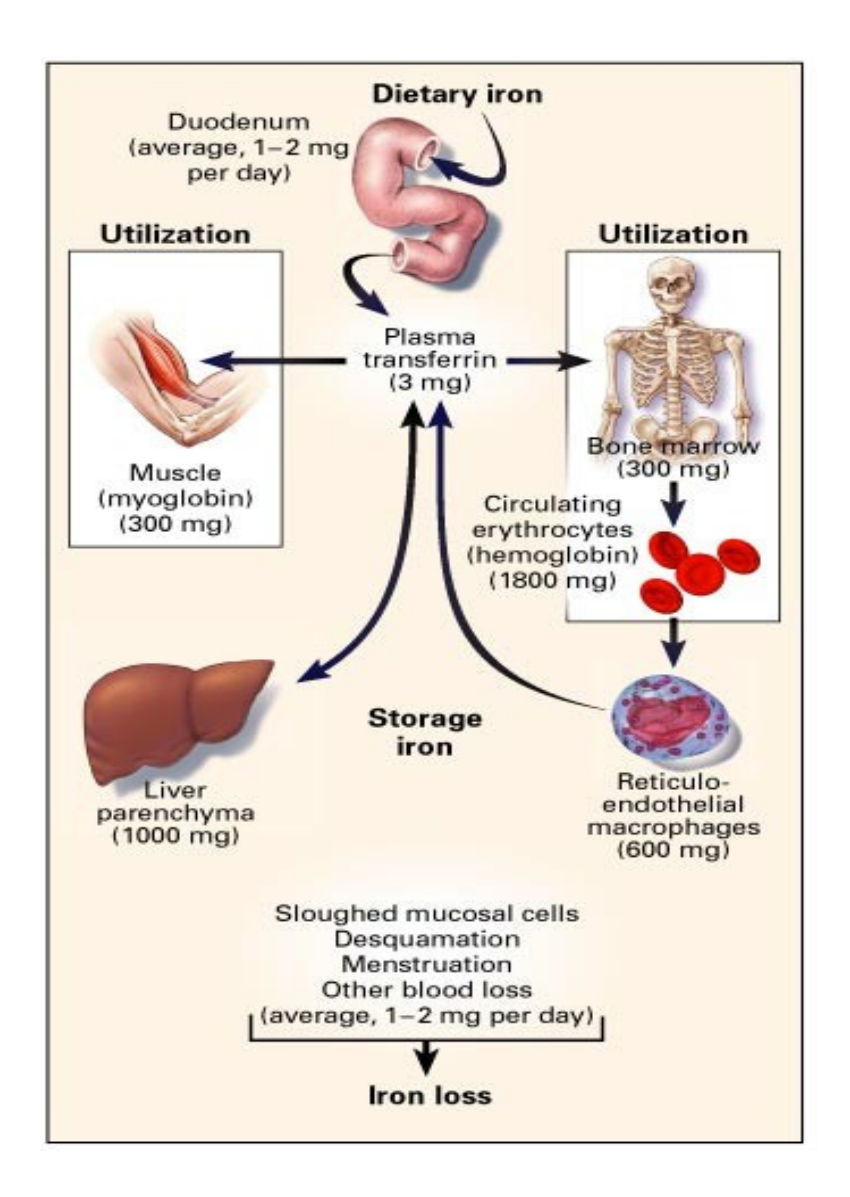


Figure 1. Distribution of iron in adults. Approximately, 1-2mg of iron enters the body daily. 10% of dietary iron is absorbed by duodenal enterocytes and circulates bound to plasma transferrin. Iron is stored in parenchymal cells of the liver and reticuloendothelial macrophages. Adapted from Andrews N.(11)

1.2.1 Iron absorption

The body absorbs approximately 1-2mg of dietary iron per day.(14) This is absorbed in 2 forms: non-heme found in both plants and animal protein,

and heme found in animal sources. Although specific transport mechanisms for the absorption of heme iron remain unknown and not fully understood, the absorption is largely efficient and not influenced by other dietary constituents.(15)

Conversely, non-heme, mainly found in the oxidised ferric form (Fe³⁺), is highly insoluble, not easily absorbed, and absorption is influenced by many dietary components including tannins and phytates.(15) Ferric iron must be reduced prior to intestinal absorption by duodenal enterocytes. This process is mediated by a ferric reductase, duodenal cytochrome b, expressed in the duodenal brush border, which is then taken up by divalent metal transporter1 (DMT1).(16) The enterocytes lining the absorptive villi close to the gastroduodenal junction are responsible for all iron absorption.(11) Absorbed iron can either be stored in the enterocytes or enter the circulation.

1.2.2 Iron in circulation

Circulating iron is mainly bound to transferrin, the major iron transport protein. In healthy adults, approximately one third of transferrin is saturated with iron, and virtually all circulating iron is bound to transferrin.(14) All nucleated cells have the capacity to use transferrin bound iron.

Transferrin, a glycoprotein, can carry 2 ferric iron molecules, maintains iron in a redox inert state, and delivers iron for uptake via transferrin receptors on the surface of erythroid precursor (figure 2).(14) The complexes within

the cells form specialised endosomes. A change in pH within the endosomes results in iron release from transferrin and enters the cytoplasm via DMT1. In erythroid cells, most iron moves into the mitochondria, whilst in nonerythroid cells, iron is stored as ferritin and haemosiderin.(11) Once iron is released, transferrin is recycled to the cell surface and can be used for further cycles of iron binding and uptake.(11)

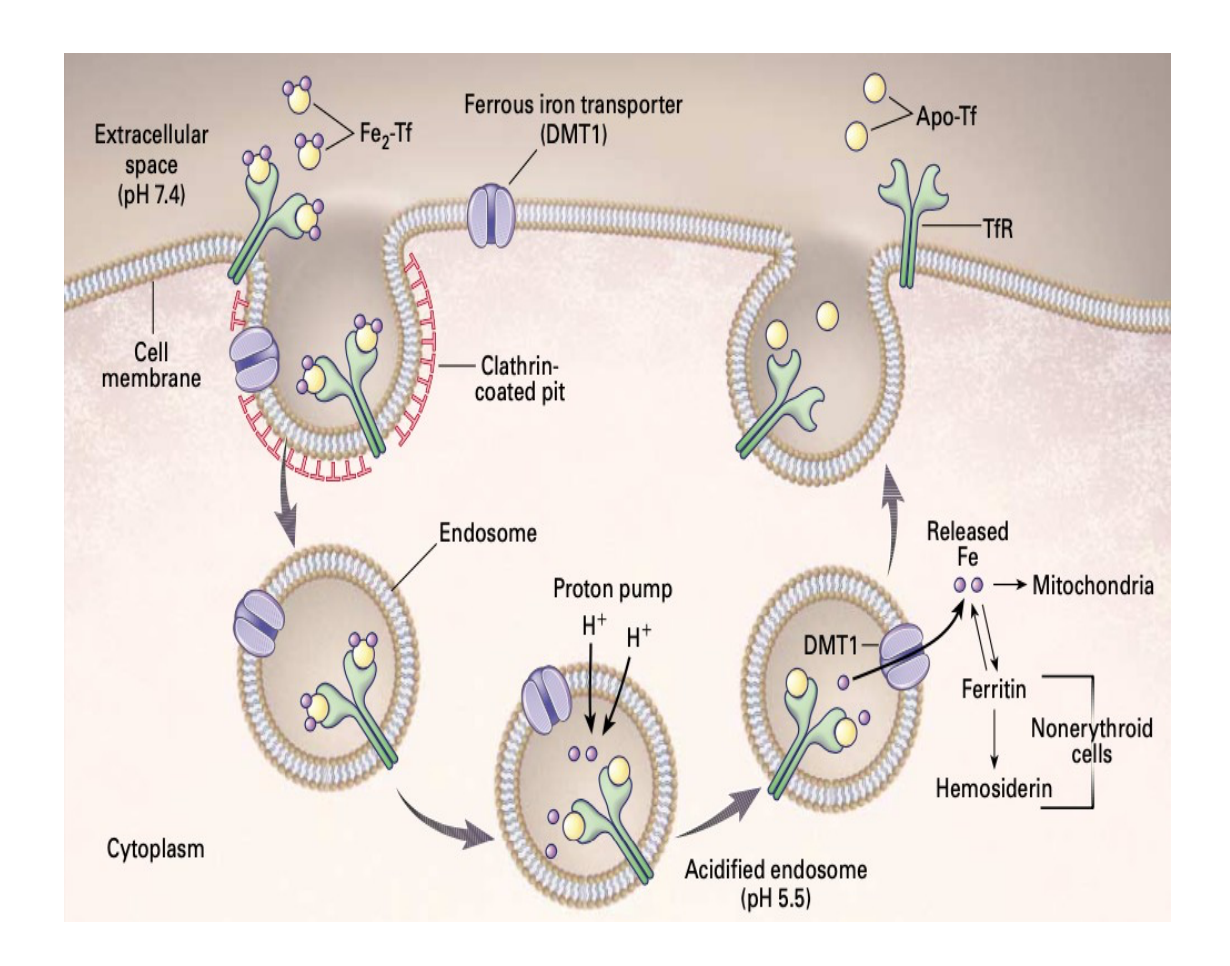


Figure 2. Uptake of iron-transferrin (Fe₂-Tf) complex on the surface of erythroid precursors. Adapted from Andrews N(11)

1.2.3 Iron storage

Iron storage is an important component of iron haemostasis providing a reservoir of non-toxic iron from which iron be used for future needs. Ferritin, the major intracellular iron storage protein, is found in all cells of the body with high concentrations in bone marrow macrophages, the spleen and the liver.(17). It is comprised of 24 monomer subunits and can store up to 4000 iron atoms as Fe³⁺.(17). The accumulation of high concentrations of iron-laden ferritin leads to ferritin molecule aggregates that bind to lysosomes. This process leads to the degradation of ferritin and the generation of hemosiderin, which is a mixture of ferritin and peptides.(18) Iron can be mobilised from both ferritin and hemosiderin when required.

1.2.4 Regulation of iron absorption

The regulation of iron metabolism is complex as the human body does not have an active regulatory mechanism for its excretion.(11) Control is based on a finely balanced system of iron absorption from the gastrointestinal tract and loss, via sloughing of the intestinal mucosa, desquamation of skin, and menstrual blood loss. (11) The circulating peptide hormone hepcidin plays a key role in the regulation of systemic iron homeostasis. Produced mainly by hepatocytes, hepcidin modulates serum iron levels by inhibiting iron release from duodenal enterocytes, macrophages, and hepatocytes.(11) Hepcidin reduces iron release into the plasma by binding to the iron exporter ferroportin. The binding triggers ubiquitination of ferroportin resulting in endocytosis of the ligand-receptor

complex and subsequent proteolysis. This degradation process reduces the delivery of iron into the plasma.(19, 20)

1.3 Iron overload

Under normal physiological conditions, total body iron is approximately 3 to 5g. In conditions of iron excess, iron exceeds the carrying capacity of transferrin and a toxic non-transferrin bound iron (NTBI) is measurable in the plasma.(21) Labile plasma iron (LPI), a component of NTBI, can be taken up by organs including the liver, pancreas, and heart.

Iron overload syndromes encompass a wide range of hereditary and acquired conditions (Table 1).

Inherited iron overload	Acquired iron overload	
syndromes	syndromes	
HFE related haemochromatosis Type 1) C282Y/C282Y C282Y/H63D Other HFE mutations	Iron loading anaemias Thalassaemias Sideroblastic anaemia Aplastic anaemia Pyruvate kinase deficiency	
Juvenile haemochromatosis (Non-HFE Type 2) • Subtype A - hemojuvelin mutations • Subtype B - Hepcidin mutations	 Acquired anaemias Myelodysplasia Myelofibrosis Aplastic anaemia Leukaemia Long term dialysis 	
Transferrin receptor 2 haemochromatosis (Non-HFE Type 3)	Chronic liver diseaseHepatitis C infectionsNAFLDAlcoholic liver disease	
Ferroportin diseases (Non-HFE Type 4) • Classical • Non-classical	MiscellaneousFriedreich's ataxiaAceruloplasminaemiaIncreased dietary intake	

Table 1. Iron overload syndromes. Syndromes broadly divided into 2 groups: inherited and acquired (also commonly referred to as secondary). HFE: high iron (Fe), NAFLD: non-alcoholic liver disease. Adapted from Siddique A et al and Kremastinos et al (22, 23)

In hereditary haemochromatosis (types 1- 3), iron overload is a result of excessive absorption of dietary iron, whilst ferroportin diseases (type 4) result in impaired iron release from macrophages in the liver, spleen, and bone.(24, 25)

In the acquired syndromes, iron loading is an inevitable consequence of repeated blood transfusion therapy, and is directly related to the number of transfusions required.(26) One unit of packed red blood cells contains approximately 200-250mg of iron, which is more than 100 times the quantity absorbed from the diet daily, and combined with mildly increased gastrointestinal iron uptake due to hepcidin suppression, total body iron increases.(27, 28) In non-transfused thalassaemia, iron absorption can be up to 10-15 times normal.(29)

In both hereditary and acquired iron overload, as iron loading progresses the levels of NTBI increase. The uptake and deposition of free iron in the heart, liver and endocrine glands can manifest with symptoms secondary to organ dysfunction (figure 3).

1.3.1 Common conditions associated with iron overload

<u>HFE- related haemochromatosis (type 1)</u> is the most common inherited disorder of iron metabolism with a prevalence of 1 in 200 to 1 in 500 in the Caucasian population.(30) Inherited in an autosomal recessive pattern, gene mutations encoding proteins involved in iron metabolism lead to inappropriately high duodenal iron absorption from birth.(31) Myocardial

siderosis has been reported in 33% of newly presenting genetically confirmed haemochromatosis patients with ferritin values greater than 1000µ g/L, and was commonly associated with left ventricular dysfunction.(32)

<u>Thalassaemia</u> is the most common single-gene disorder worldwide encompassing a group of autosomal recessive inherited disorders of haemoglobin synthesis resulting in the reduction or absence of a normal haemoglobin molecule. The World Health Organisation estimate that 1.5% of the world's population are heterozygous carriers of thalassaemia mutations and approximately 60,000 homozygous infants are born every year with the severe phenotype thalassaemia major (TM).(33) Over 200 mutations of the \}-globin have been identified accounting for the variability in clinical presentations. Production of \}-globin chains in the haemoglobin A molecule is severely impaired in \rightarrow-thalassaemia major with ineffective erythropoiesis, resulting in hepcidin suppression, dietary hyperabsorption, and secondary iron overload.(34) Erythroid hyperplasia leads to medullary expansion with facial deformities and osteoporosis. Extramedullary haematopoiesis results in massive splenomegaly and hepatomegaly, and enlargement of paraspinal and pulmonary masses of erythroid cells. Approximately 80% of those affected die within the first 5 years of life from complications of anaemia if left untreated. Lifelong blood transfusions to maintain haemoglobin levels between 9-10g/dl, typically begins in the first year of life, to reduce ineffective erythropoiesis. This leads to inevitable iron

overload, which before the introduction of chelation therapy culminated in death from heart failure or arrhythmias in childhood.(35)

<u>Sickle-cell anaemia</u> is one of the most common severe monogenic disorders of haemoglobin(36). The substitution of a single nucleotide in the β-globin gene results in a haemoglobin (HbS) molecule that polymerises in low oxygen states. The sickled red blood cells are removed prematurely from circulation resulting in a chronic haemolytic anaemia. Erythrocyte transfusions, simple or exchange, have an established role in the management of acute and chronic complications of sickle cell disease with an increasing number of children on regular transfusion therapy for primary and secondary stroke prevention.(36, 37) Net iron accumulation from transfusions are slower than in TM due to differences in transfusion regimes and because patients tend to be in a negative iron balance due to intravascular haemolysis.(13) With hypertransfusion this negative balance diminishes.

Myelodysplastic syndromes (MDS) are a heterogeneous group of bone marrow disorders characterised by ineffective haematopoiesis. Approximately 2000 patients are diagnosed per year in the UK. Low and intermediate risk MDS patients often survive close to a decade with transfusion therapy, with transfusion requirements comparable to patients with TM, and therefore at risk of iron overload(38, 39). Iron accumulation may start before transfusions begin due to upregulation of cytokines

inhibiting hepcidin production resulting in increased iron absorption from the gut.(13)

Other conditions: Iron overload also occurs in a number of rare transfusion-dependent anaemias and inherited haemolytic anaemias such as Diamond-Blackfan and pyruvate kinase deficiency respectively. Maldistribution of iron, in the absence of total body iron overload, plays a role in other diseases with cardiac dysfunction such as Friedreich's ataxia(40).

1.3.2 Complications of iron overload

Iron overload occurs when there has been a sustained period of exposure from red cell transfusion or increased absorption via the gastrointestinal tract. Iron loading can vary among individuals and is determined by the underlying disease(13). The main organs affected by iron loading are the liver, endocrine glands, and the heart (figure 3). The mechanism of toxicity in parenchymal cells of all organs involved is via the formation of hydroxyl radicals which targets carbohydrates, proteins, and DNA.(25)

In inherited iron overload conditions, iron accumulates in hepatocytes and bile duct epithelium. In transfusional iron overload, iron deposition occurs primarily in the reticuloendothelial system (Kupffer cells), and accumulates in hepatocytes in smaller amounts when present in excess.(41) The liver loads first due to its capacity to store iron with early cirrhotic changes seen in childhood in patients with thalassaemia.(42) Once cirrhosis develops the

risk of hepatocellular carcinoma increases in older patients with thalassaemia and sickle cell disease.(43)

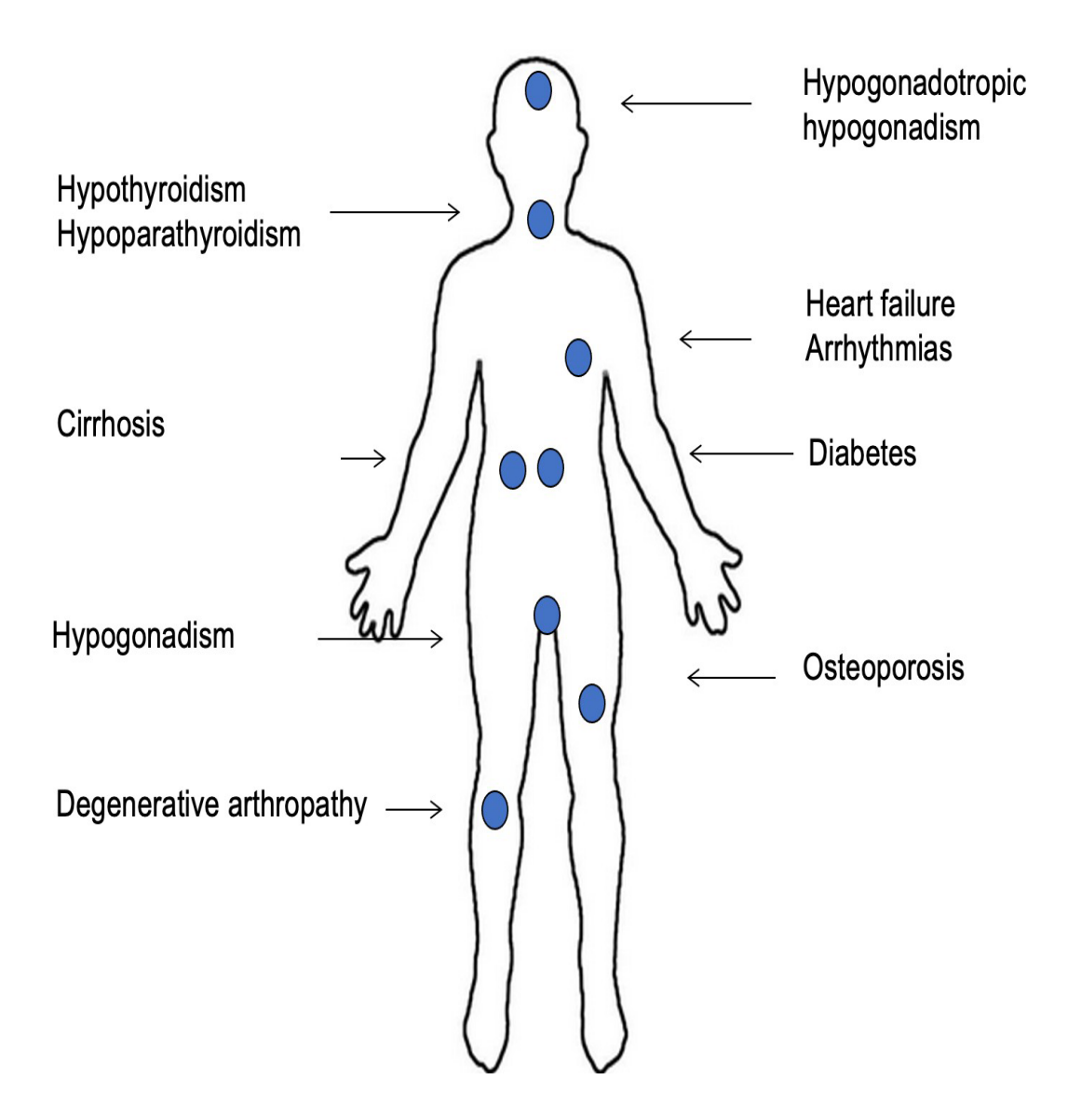


Figure 3. The effects of iron overload on the heart, liver, and endocrine organs. Cardiac failure, liver dysfunction and cirrhosis, and endocrine abnormalities including hypothyroidism, hypogonadotropic hypogonadism, and diabetes mellitus can result from iron deposition.

Dysfunction from iron deposition affects most glands. Delayed puberty due to pituitary iron deposition is commonly seen.(44) Involvement of the pancreas results in overt diabetes mellitus or impaired insulin secretion.(45) Thyroid and parathyroid involvement are also commonly seen.(2)

Myocardial iron uptake is much slower in comparison with hepatic uptake, and thus myocardial iron overload develops at a later stage in comparison with hepatic iron overload.(23)

1.4 Iron overload cardiomyopathy

Iron overload cardiomyopathy remains the leading cause of morbidity and mortality in patients with iron overload, with deaths usually occurring in the second and third decades of life. (2, 46) It is defined as impaired systolic or diastolic function secondary to iron deposition in the heart independent of other processes.(1) Iron loading in the heart begins with an accumulation of 20g of iron.(47)

Cell and animal studies suggest that iron, in the ferrous form, enters the myocytes via the DMT1, L-type and T-type calcium channels(48, 49, 50)(figure 4). NTBI uptake has been shown to be rapid in cardiomyocytes.(51)

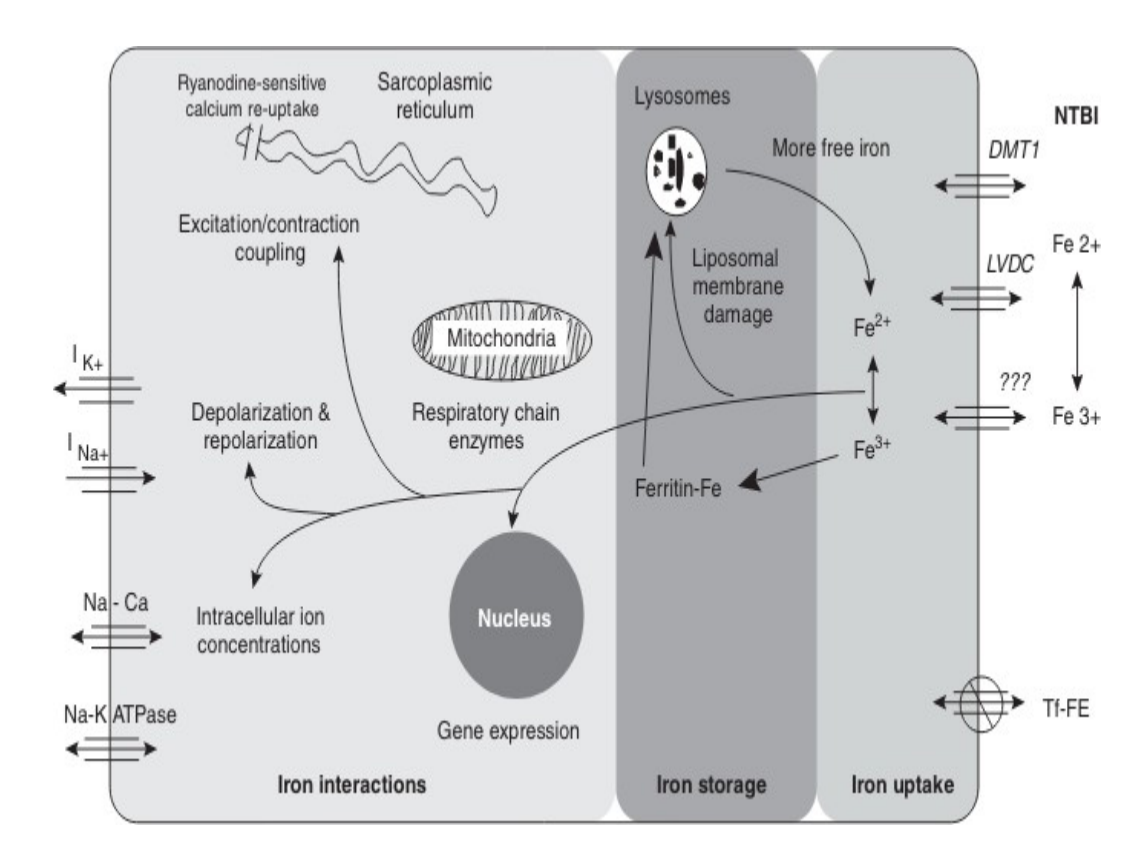


Figure 4. Iron uptake, storage, and interactions in a myocyte. Ferric and ferrous iron are rapidly buffered and stored. DMT1: divalent metal transporter1; LVDC: L-Type voltage-dependent channels; NTBI: non- transferrin bound iron. Adapted from Wood et al.(52)

Iron in the heart is stored in 3 forms: ferritin, hemosiderin, and LPI (figure 5). Labile iron is catalysed via the Fenton reaction converting ferrous to ferric iron generating hydroxyl ions to form reactive oxygen species (ROS). Excessive free iron in the heart is toxic via a number of mechanisms including damage to membranes by lipid peroxidation, damage to mitochondria and respiratory chains, interference with electrical function, promoting fibrosis and altered gene expression.(2)

Histological data has shown that iron deposition in the myocardium is not uniform. Deposition of iron is greatest in the subepicardium of the left ventricle (LV) wall, followed by the subendocardial wall and papillary muscles. The right ventricle (RV), atria and conduction system contain less iron.(53, 54, 55) The LV can have approximately 20% more iron than the RV.(55)

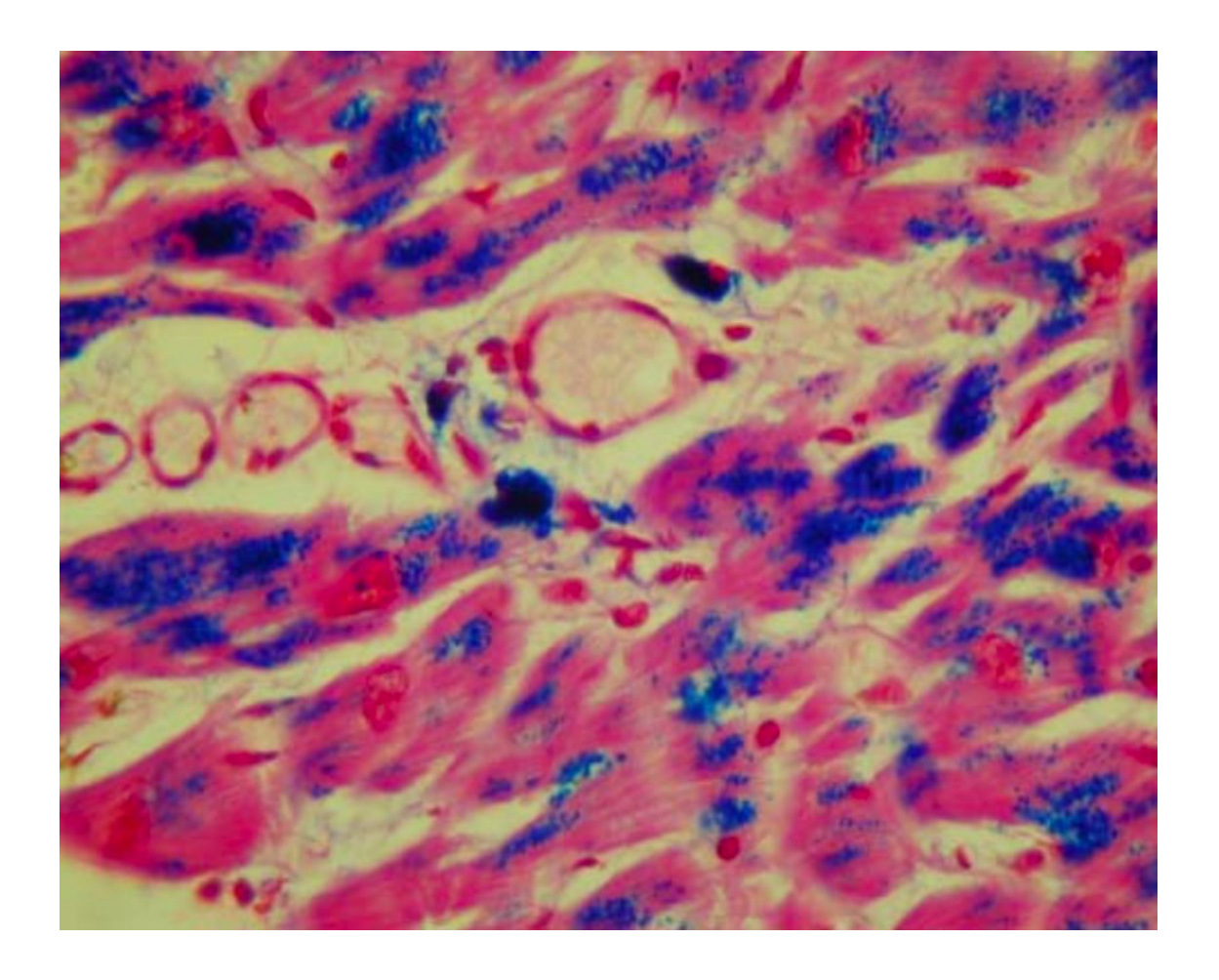


Figure 5. Post-mortem myocardial biopsy in a patient with severe iron overload. Iron is stained by Prussian blue and illustrates a heavy iron presence within the myocytes. Adapted from Walker JW.(21)

1.4.1 Clinical presentation of cardiac iron

Symptoms relating to myocardial iron loading can vary according to the aetiology of the disease and on the severity of disease. Patients may be asymptomatic early in the disease process, while severe disease can present with symptoms related to heart failure including progressive dyspnoea and fluid retention (figure 6).(1)

Two distinctive forms of cardiomyopathies are recognised: dilated and restrictive.(2, 23) The restrictive phenotype is characterised by LV dysfunction with restrictive filling and preserved systolic function. The dilated phenotype is characterised by ventricular remodelling, chamber dilatation, and reduced systolic function.(23) In almost all patients, irrespective of the underlying aetiology, the restrictive phenotype with prominent diastolic dysfunction is seen early in the disease with progression to the dilated phenotype (figure 6).(46) Diastolic dysfunction is a recognised prognostic marker of increased mortality in iron overload.(46) Altered excitation-contraction coupling, the development of fibrosis, and increased myocytes loss secondary to apoptosis may modify the onset of heart failure.(46)

Right ventricle impairment has been demonstrated with tissue Doppler imaging velocity and strain imaging using echocardiography, and with cardiovascular magnetic resonance imaging in patients with early disease. (2, 56)

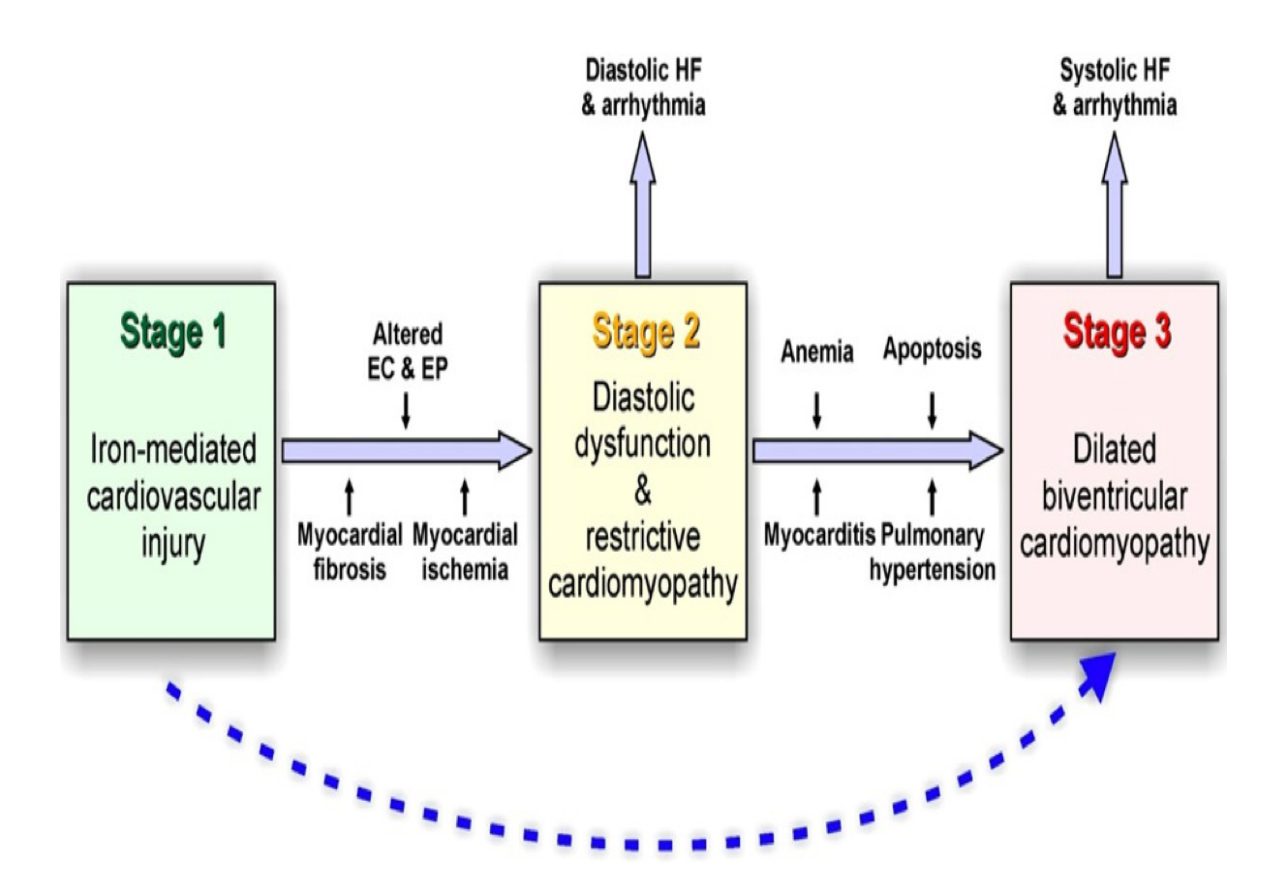


Figure 6. Spectrum of illness and the development of heart disease in iron-overload. Broken line indicates that some patients may progress rapidly to the dilated cardiomyopathy phase. EC, Excitation-Contraction Coupling, EP, Electrophysiology; HF, Heart Failure; PH, Pulmonary Hypertension. Broken lines: some patients progress rapidly to the dilated cardiomyopathy phase. Adapted from Murphy, CJ.(46)

Iron loaded hearts are susceptible to both atrial and ventricular arrhythmias, and can present at any stage of the disease process.(2) Sinoatrial and atrioventricular disease likely results from a combination of iron loading in the node tissue in addition to increased interstitial fibrosis.(46) The presence of

iron deposition in the atria has been shown to correlate with supraventricular tachycardias .(1, 53)

Atrial fibrillation (AF) is the most common arrhythmia in iron-loaded patients with a UK study reporting a 12% incidence, although it is likely that this is underestimated.(57) Paroxysmal AF (PAF) has been documented in 34% of TM patients with normal LV function and in the absence of myocardial iron loading, which may be a late manifestation of historical cardiac iron loading.(21) In severe myocardial iron loading, ventricular arrhythmias are more common in patients with LV dilatation and systolic impairment.(1, 2)

1.5 Assessment of iron deposition

Early diagnosis of iron overload is crucial. Historically total iron burden relied on measurements from liver biopsies, however the relationship between organs, particularly liver and cardiac iron, is not constant.(2) Myocardial biopsies were used to diagnose cardiac iron and guide treatment, but were prone to complications, sampling error as the iron is preferentially distributed in the epicardium, and the right ventricle is relatively spared.(58, 59) Assessments have now largely been replaced by non-invasive methods.

1.6 Blood biomarkers of iron status

Ferritin is found in all cells of the body, but is in high concentrations in bone marrow macrophages, the spleen, and the liver. The subunits can store up to 4000 iron atoms as Fe³⁺.(17) A very small amount of ferritin is found in serum and does not have a role in iron transport or cellular uptake, and is not iron bearing.(17) Correct measurement of serum ferritin (SF) is paramount with international guidelines recommending measurement in laboratories able to dilute samples with high values to give readings within the linear range of the assay.(60) Normal values vary between laboratories but >300ug/L in men and postmenopausal women, and >200ug/L in premenopausal women is regarded as elevated.(17)

SF generally correlates with body iron stores, and increases linearly with the number of blood transfusions.(23) It is relatively easy measure to perform and inexpensive. Despite fluctuating levels with inflammation and other recognised conditions (table 2), SF is considered a useful measure for identifying trends and monitoring therapy. A decreasing trend in SF is a good indication of a fall in body iron burden. SF trends have also been linked with prognosis, and studies have shown a lower risk of cardiovascular disease and mortality when serum levels have been maintained below 2500ug/L over a period of 10 years (61, 62)

Iron accumulation	Raised ferritin without iron accumulation	Cellular damage
нн	Malignancy	Liver disease - Chronic viral hepatitis
Thalassaemias	Hereditary hyperferritinaemia	-Non-alcoholic steatohepatitis
Secondary iron overload -Blood transfusions	Acute and chronic infections	-Liver necrosis
-Excess intake	Chronic inflammatory disorders	Chronic excess alcohol
Infective erythropoiesis	Autoimmune disorders	

Table 2. Causes of raised serum ferritin. HH: Hereditary haemochromatosis.

Adapted from Cullis et al(17)

1.7 <u>Cardiovascular Magnetic Resonance in Iron Overload</u>

Cardiovascular MRI (CMR) is a well-established and highly reproducible assessment of left and right ventricular volumes, function and mass using steady state free precession cine imaging.(63) The T2* sequence is performed in patients with suspected iron loading, and has been shown to provide reproducible quantification of myocardial and hepatic iron load.(64, 65).

1.7.1 T2* imaging

T2* is one of the three fundamental tissue signal MRI rate constants, the others being T2 and T1. T2* is defined as the time constant representing the decay of transverse magnetisation in the presence of local field inhomogeneities and is measured in milliseconds.(66) The MRI signal does

not image the iron particles directly. Paramagnetic ferritin and hemosiderin disrupt the local magnetic field homogeneity causing reduced T2* values in inverse relation to the iron concentration, and darkening of images at a rate proportional to the iron concentration.(67)

For T2* measurements, a single mid-LV short-axis slice is acquired using 8 equally distanced echo times (TE) using a gradient-echo (GRE) sequence on a 1.5T imaging scanner. In a single breathhold, bright blood T2* (BBT2*) images are acquired immediately after the R wave to minimise artefacts caused by blood flow and myocardial wall motion.(65)

A full-thickness region of interest (ROI) is measured in the interventricular septum to include the epicardial and endocardial borders. Care is taken to avoid the superior and inferior cardiac veins as they can cause susceptibility artefacts and erroneous T2* values (figure 7).(2) The interventricular septum has been shown to be a good indicator of global myocardial iron loading.(68)

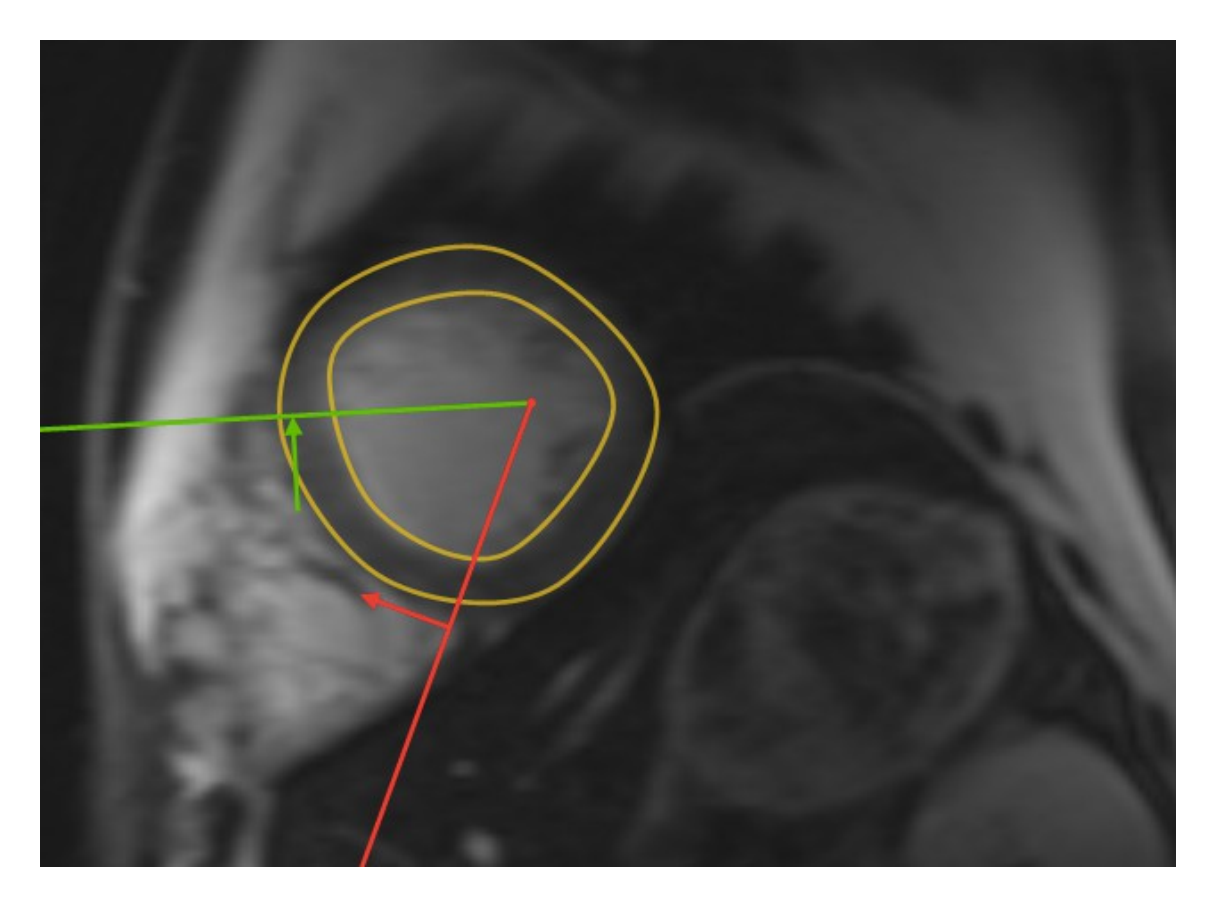


Figure 7. Myocardial T2* image demonstrating a mid-short axis slice. A full thickness region of interest is demonstrated in the interventricular septum.

The signal intensity in each ROI is measured for each the 8 T2* images and the data plotted against the echo time to form an exponential decay curve. Using a truncation model a T2* value is derived (figure 8).

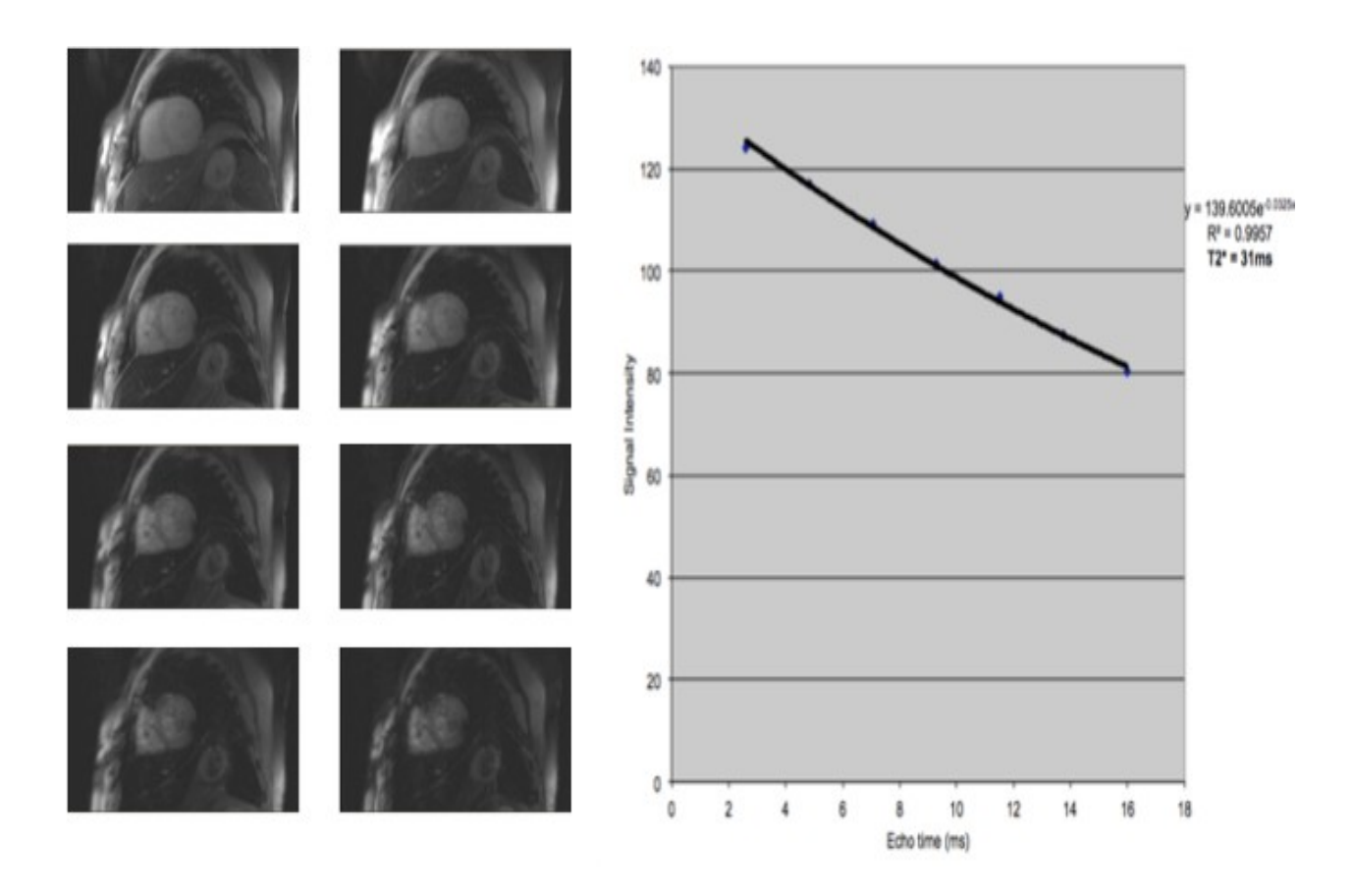


Figure 8. Myocardial T2* image showing images acquired over 8 predefined echo times. The corresponding graph shows the exponential decay curve and the T2* value derived from it.

Cardiac iron levels are inversely related to myocardial T2* values, and thresholds are based on a cohort of normal volunteers.(64) Values greater than 20ms indicate no evidence of iron overload, 14 -20ms mild iron overload, 8-10ms moderate overload, and less than 10ms indicates severe iron overload. The probability of ventricular impairment increases as the T2* value falls. In a multi-centre study of 652 patients with cardiac T2* values less than 10ms, 98% developed heart failure.(57)

The T2* technique has transformed the management of patients with iron loading conditions allowing robust quantification of myocardial iron, however there are recognised limitations with the T2* method including (2, 66, 69, 70):

- Artefacts generated from myocardial motion, and artefacts from blood including ghosting and partial volume effects which can complicate analysis and provide erroneous results.
- Discrimination in patients with iron: the normal range for iron concentration in myocardial tissue is 0.29 0.47mg/g dry weight.(70) Using ex-vivo calibrations the normal range of T2* would be above 40ms ([Fe] = 0.50mg/g dry weight), however to avoid false positives a normal threshold of 20ms has been used, as no healthy volunteers had a T2* value less than 20ms. However, this equates to [Fe] of 1.1mg/g dry weight.
- Sequence acquisition requires 21 heart beats which can result in artefacts from prolonged and inadequate breath holding.
- T2* measurements have thus far been validated at 1.5T, with recommendations that clinical T2* measurements must be limited to 1.5T scanners.(2) T2* values are shorter on 3T, and the potential for artefacts is greater. This adds a further important limitation in the delivery of this test around the world with the growing popularity of 3T scanners due to the greater signal to noise ratio generating superior quality imaging.

 Post-processing analysis can be time consuming, requires specialist programmes, and training is required. This excludes some centres from using the technique or using unvalidated software.

Recent developments of the T2* sequence have attempted to improve measurement accuracy. Using a double inversion recovery pulse to null the signal from blood images are acquired in late diastole generating a dark blood image (figure 9).



Figure 9. Dark blood T2* image of a mid-LV short-axis slice.

A corresponding parametric T2* map is generated allowing a measurement of T2* from the average signal intensities within the region of interest (figure 10). This Siemens Work in Progress (WIP) T2* package is available with permission for research purposes but not validated for clinical use. The sequence thus far has shown good reproducibility compared to the established Bright blood T2* (BBT2*) sequence,(71)

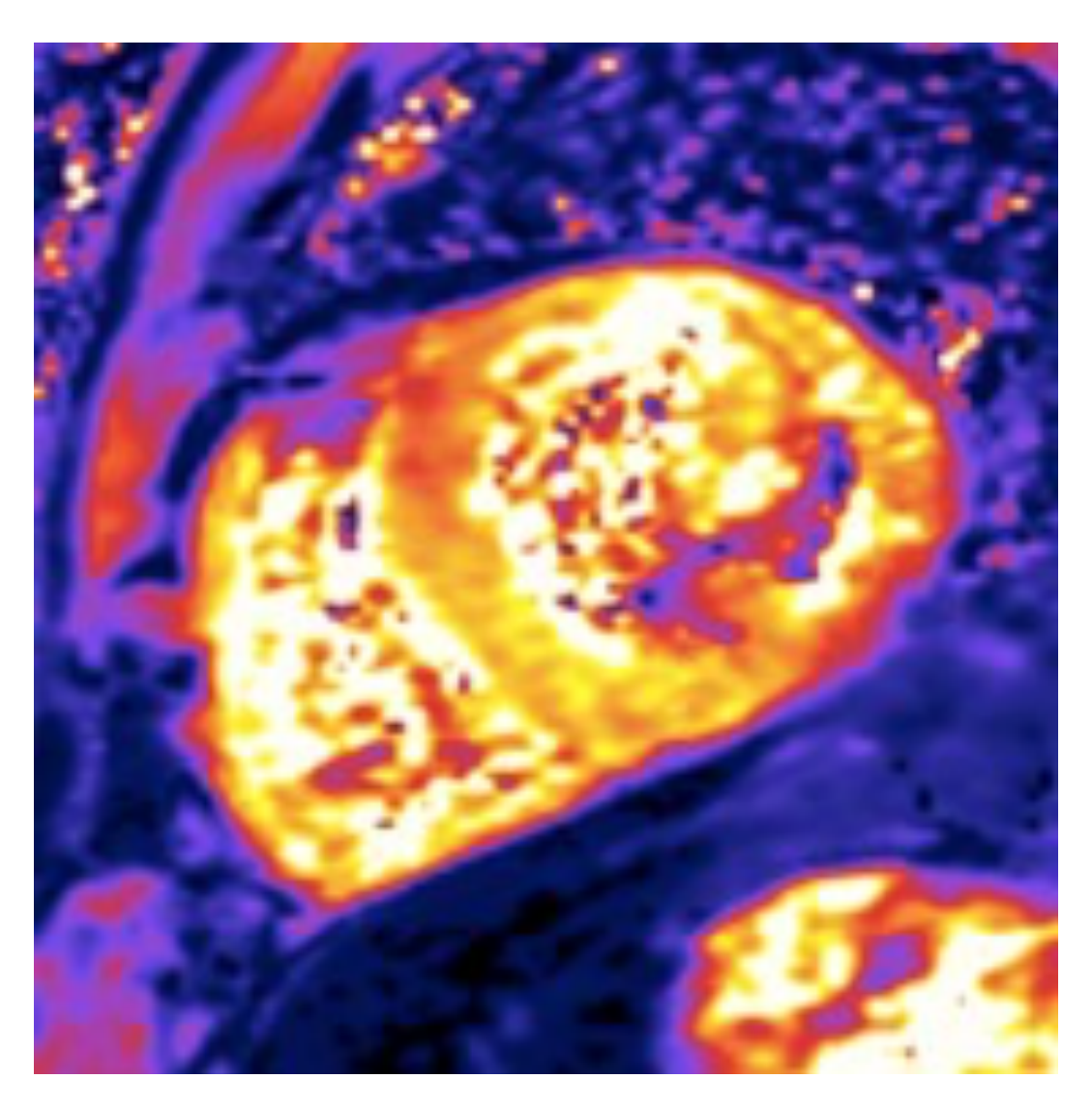


Figure 10. Siemens Work in Progress T2* map generated with black blood T2* sequence.

<u>1.7.2</u> T1 mapping

The presence of iron has previously been shown to correlate with T1 ex-vivo (72), and may aid diagnosis in patients with myocardial iron. T1 is an intrinsic magnetic property that represents longitudinal or spin-lattice relaxation time after excitation of hydrogen atoms.(66) At selected magnetic field strengths each tissue has its own characteristic range of values (expressed in milliseconds), and deviation from these values implies disease. T1 values are increased with the expansion of the extracellular compartment by fibrosis, oedema and amyloid, and reduced in iron, lipid accumulation, and haemorrhage.(73, 74, 75, 76) These changes may be detectable in early disease, and prognostic in some diseases.(77).

T1 measurements were first introduced using the Look-Locker sequence, which required multiple breath-holds to acquire the recovery curve after an initial excitation pulse. Incremental improvements from the original method to the modified look-locker imaging (MOLLI) sequence, with the sampling method 3(3)3(3)5, enabled acquisition of T1 measurements over a single breath hold over 17 successive heart beats.(78, 79) This includes acquisition of 11 images with 3 inversions (3, 3, and 5 images acquired in the beats following inversions with 3 heart beat recovery periods between inversions). All images are acquired at the same delay from the R-wave trigger (figure 11).

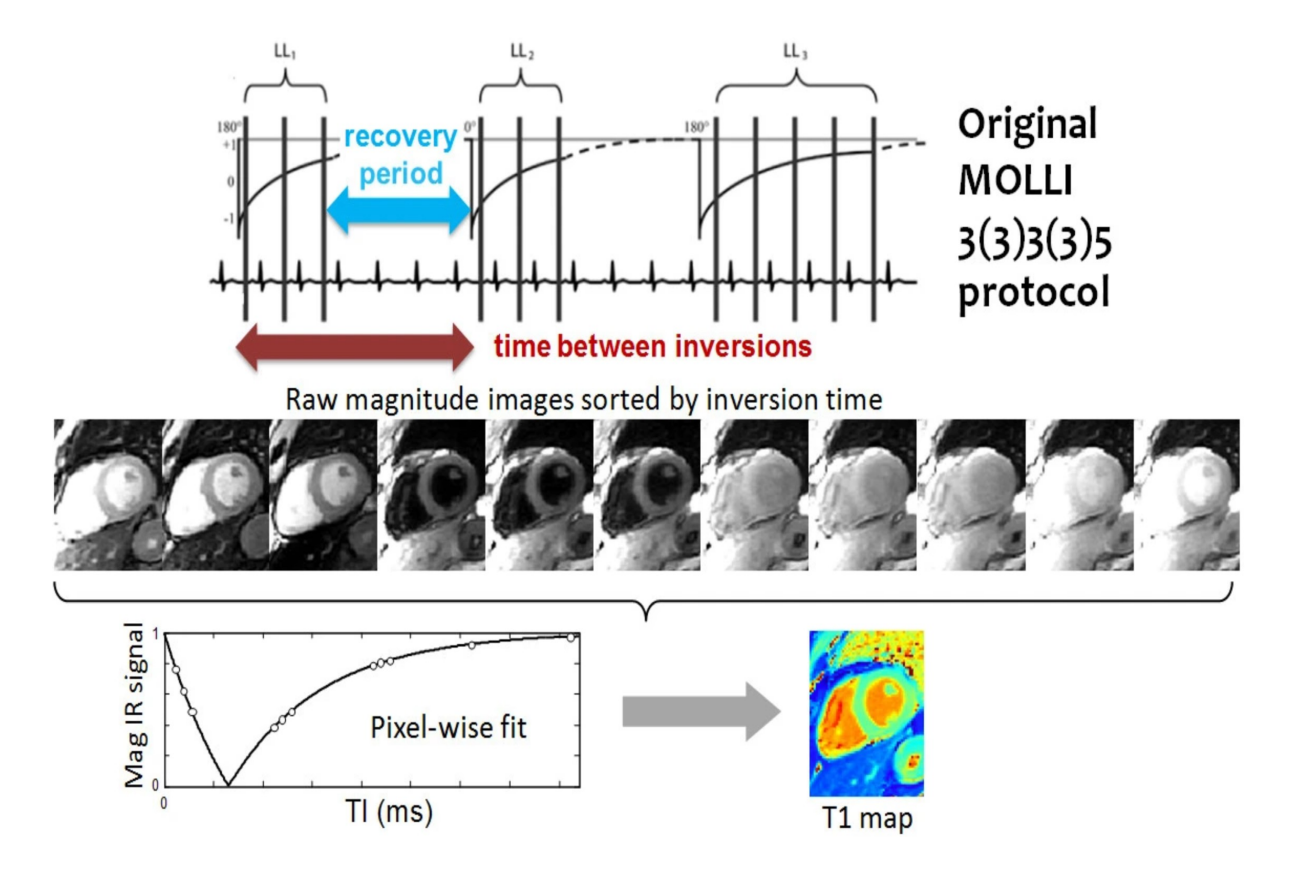


Figure 11. Modified Look-Locker Inversion Recovery (MOLLI) sequence for T1 mapping. Adapted from Kellman P et al.(80)

A further development to the MOLLI sequence has generated the shortened MOLLI (ShMOLLI) sequence with an acquisition time over 9 heartbeats. Newer sequences in development, including saturation recovery single-shot acquisition (SASHA), are independent of heart rate variability and have similar reproducibility compared with MOLLI and ShMOLLI.(81, 82, 83) The generation of parametric maps presents an image that measures T1 and displays the actual values in colour on a pixel-by-pixel basis without the need for post-processing (figure 12).

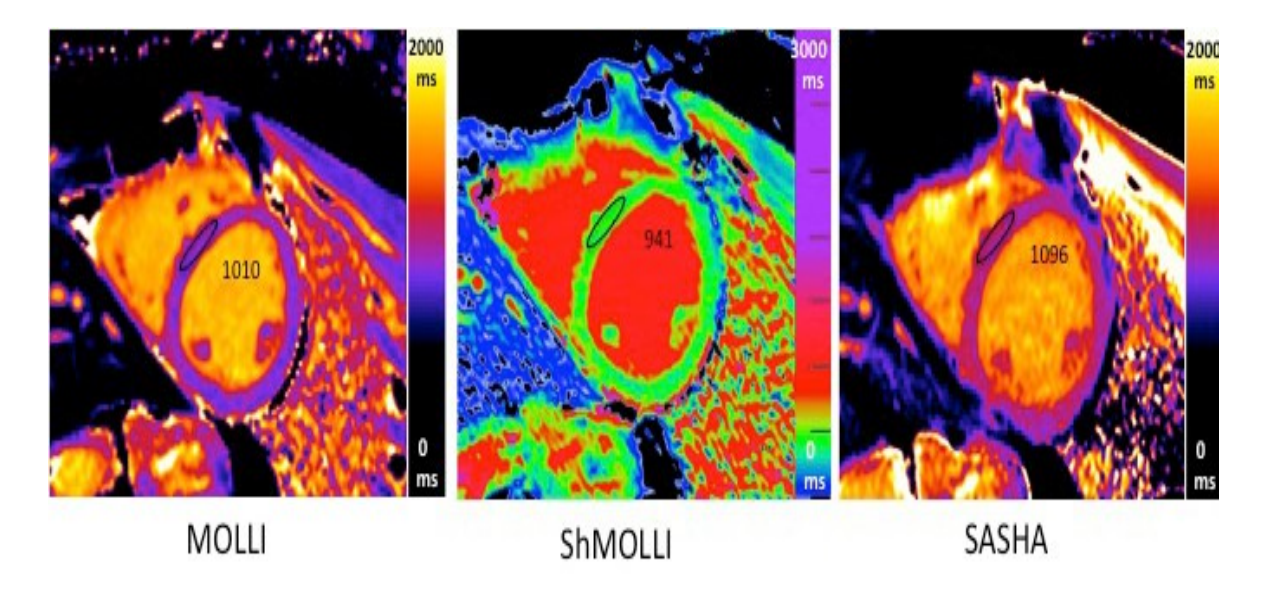


Figure 12. Examples of native T1 maps from a healthy volunteer. 3 different sequences are shown: a) MOLLI; b) ShMOLLI; c) SASHA each demonstrating regions of interest and their respective values. Note the difference in T1 values with each sequence and the difference in look up tables on the right of each image. MOLLI and ShMOLLI can underestimate native. Adapted from Abdel-Gadir et al(84)

The role of T1 mapping in the detection of iron has been promising to date at both 1.5T and 3T, and has been shown to correlate with cardiac iron in vitro.(72) Early data by Sado et al was the first to demonstrate that myocardial T1 mapping has excellent reproducibility and correlates well with T2* in a sample of 88 patients with suspected iron overload.(85) Using the ShMOLLI sequence, T2* was lower in patients than healthy volunteers (836 \pm 138ms versus 968 \pm 32ms, p <0.0001), and no patient with a low T2* value had normal T1 values.

The rise in clinical use of 3T scanners for non-cardiac conditions may provide diagnostic challenges for patients requiring iron quantification as T2* acquisition has not been recommended at 3T.(86) T1 mapping may however be used as a method to quantify iron at 3T where T2* measurements are not possible.(87, 88) Alam et al demonstrated the feasibility of T1 at both 1.5T and 3T, and its superiority to T2* when assessing reproducibility.(87)

1.7.3 Other mapping techniques:

The extracellular space is a dynamic, complex milieu consisting of collagen fibrils, elastin, fibroblasts, macrophages, and other macromolecules.(89) It serves to anchor myocytes, store energy, and provide a protective role.(89) Expansion of the extracellular space occurs with focal fibrosis, diffuse fibrosis, oedema, and infiltrative pathologies. CMR acquisition of T1 after administration of a gadolinium-based extracellular contrast agent, allows an extracellular volume (ECV) measurement. As contrast is confined to the interstitium, ECV reflects interstitial disease. Native and post-contrast T1 images are combined with measurement of blood haematocrit using the following equation to create a map wherein pixel values represent the interstitial volume(90):

$$ECV = (1 - haematocrit)*[\Delta R1_{myocardium}]/[\Delta R1_{blood}]$$

The ECV is displayed as a pixel-by-pixel map (figure 13). ECV has been shown to be a robust marker of diffuse fibrosis and prognostic in certain disease processes including cardiac amyloidosis.(77) Additionally ECV

measurements may be as prognostically important as LV function. In a study with 793 patients followed over 1 year ECV predicted mortality.(91)

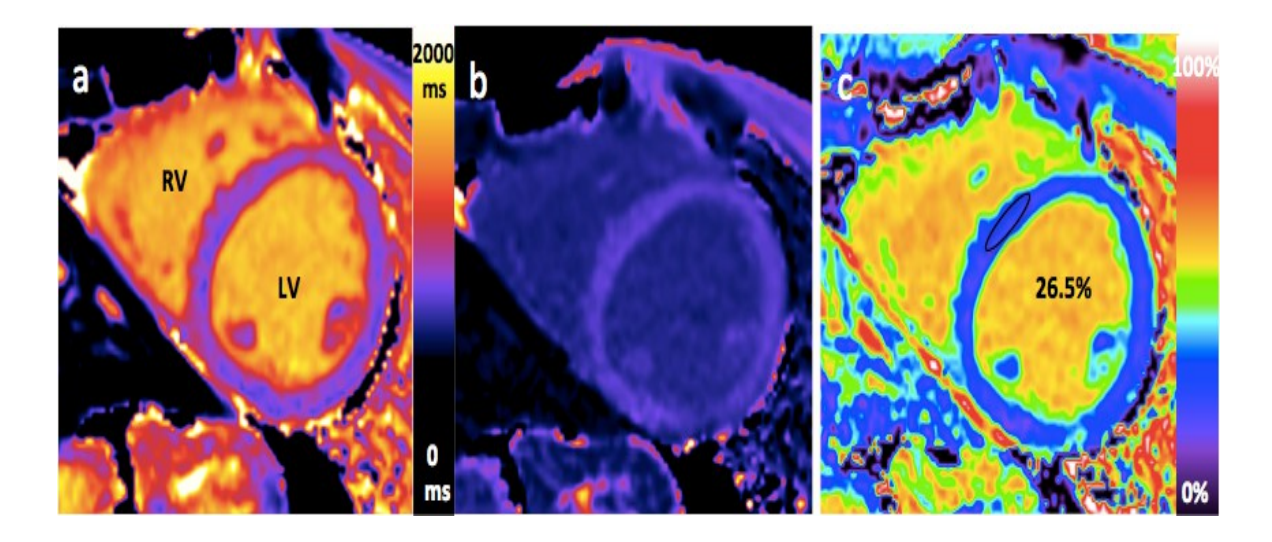


Figure 13. Generation of an ECV map in a healthy volunteer. a) native T1 MOLLI map (myocardial T1 1010ms); b) post-contrast T1 MOLLI map (myocardial T1 615ms); c) ECV map (ECV = 26.5%). Adapted from Abdel-Gadir et al.(84)

1.8 Management of iron overload: Chelation therapy

The prognosis of patients with iron overload has improved significantly with the introduction of chelating agents.(62, 92, 93) Chelation therapies reduce levels of tissue iron, prevent accumulation, neutralize toxic labile iron pools, and have been shown to improve left ventricular systolic function in high-risk patients with heart failure:(2, 21, 27)

 Desferrioxamine (DFO) is a hexadentate ligand that binds to iron in a 1:1 molar ratio. Introduced in the 1960s, DFO has been shown to improve survival in iron overloaded patients with TM. Poorly absorbed by the gastrointestinal tract, DFO typically requires subcutaneous infusions over 8-12 hours due its short half-life of 20minutes, and 24-hour intravenous therapy for more aggressive chelation. This arduous schedule interferes with quality of life resulting in poor patient compliance. Several side effects include allergic reactions, sensorineural hearing loss, and ophthalmic adverse effects.

- Deferiprone is a bidentate ligand that binds to iron in a 3:1 molar ratio. It was the first available oral chelator and is administered daily in three divided doses. It is absorbed rapidly from the upper gastrointestinal tract, and serum concentration peaks at 45 to 60 minutes after ingestion. Agranulocytosis is a rare potential side effect, and this drug is therefore unsuitable in patients with myelodysplastic syndromes. Common side effects include nausea, vomiting, and a transient increase of liver enzymes.
- Deferasirox is a tridentate chelator that binds iron in a 2:1 molar ratio. It is an oral chelator with a half-life of 8-16 hours and thus allows for convenient once daily administration. Peak plasma levels are achieved within 3 hours of ingestion, and excretion is mainly via the faecal route. It is associated with gastrointestinal disturbances, skin rash, and elevations in serum creatinine and liver enzyme levels.

The first studies demonstrating the potential reversibility of iron-induced cardiomyopathy were reported in patients with HH treated with recurrent venesection.(94, 95, 96) In 1983, Freeman first demonstrated that intensification of chelation therapy with high dose DFO reversed subtle

exercise-induced left ventricular dysfunction detected by radionuclide ventriculography.(97) Other groups have since reported the successful reversal of moderate left ventricular dysfunction, NYHA grade 4 heart failure, and arrhythmias with the use of intensive subcutaneous DFO.(98)

1.9 Cobalt

Cobalt is a trace element with chemical properties highly similar to iron.(99) *In vivo*, cobalt exists as either a bivalent cobaltous (2+) or trivalent cobaltic (3+) cation that form complexes with other extra- or intra-cellular molecules to form cobalt oxides, organophosphates, and chlorides.(100) There is approximately 1 to 2mg of cobalt in the human body cobalt found primarily in the liver, heart, and kidneys.(101) Exposure to cobalt in the general population is mainly through ingestion of food and drinking water containing cobalt compounds.(99) The body absorbs cobalt in the small intestine, and shares a common absorptive pathway with iron.(101, 102) Distribution of cobalt is influenced by plasma proteins including albumin and transferrin, and uptake is mediated by a substrate of DMT-1.(103) Excretion of absorbed cobalt occurs predominantly via the kidneys.

In specific quantities, cobalt is an important part of the vitamin B12 complex necessary for the formation of red blood cells. Cobalt also has a role in formation of amino acids, proteins, neurotransmitters, and the synthesis of erythropoietin.(101)

1.9.1 Over exposure to cobalt

The human body can be over exposed to cobalt in many ways. The first notable exposure to cobalt was in the 1960's when it was used to increase foam stability in beer. During that time, almost 25% of all beer sold in the United States contained cobalt.(4) Chronic beer drinkers presented with what was considered a new disease consisting of pericardial effusions and low output states with normalisation on cessation of drinking beer - a phenomenon not seen on consumption of other alcoholic beverages. (104, 105) Cobalt exposure may also occur in processing plants for glass, inks, and paints, and in the hard-metal industry, diamond polishing, and during the manufacture of ceramics. (4, 106) In healthcare, patients with refractory anaemia were treated with cobalt due to its ability to stimulate the production of red blood cells. Athletes have exploited this effect, as an alternative to doping, to artificially increase red blood cell mass and improve exercise performance.(107) More recently, and perhaps the most controversial, is exposure via implanted medical devices. Predominantly composed of cobalt and chromium alloy, wear and corrosion of the metal-onmetal (MoM) implants cause the release of nano-particle debris locally and this has been linked to soft tissue deposition adjacent to the joint.(8, 9) Elevated circulating levels of cobalt and chromium ions causing systemic toxicity have been liked with fatal cardiac, thyroid, and neuro-ocular abnormalities. (4, 108)

1.10 Pathophysiology and complications of cobalt toxicity

Cobalt toxicity can affect multiple organs. In states of both acute and chronic toxicity, excess exposure has been linked with cardiovascular, endocrine, central and peripheral nervous system, and haematological effects (table 3).(99)

Organ	Effects
Cardiac	Cardiomyopathy Heart failure Arrhythmias Pericardial effusions
Hepatic	Hepatomegaly Hepatotoxicity
Respiratory	Occupational asthma Rhinitis Allergic alveolitis Interstitial pneumonia
Endocrine	Hypothyroidism Goitre formation Chronic thyroiditis
Haematological	Polycythaemia
Neurological	Sensorineural hearing loss Tinnitus Visual loss Short-term memory loss
Skin	Occupational contact dermatitis

Table 3. Systemic effects of cobalt toxicity.

Reactions to cobalt exposure depend on the chemical form. In occupational and environmental settings, exposure is predominately to cobalt metal

particles with resulting immune-mediated responses. These cause local adverse tissue reactions including respiratory effects with the inhalation of cobalt dust, and soft tissue collections following corrosion of MoM implants.(99, 109) In medical settings, exposure occurs to both cobalt nano- particles and ions.(99)

Systemic complications of cobalt toxicity arise when cobalt ions enter the circulation and disseminate to different organs. Cobalt ions can cause apoptosis and necrosis through multiple proposed mechanisms including the generation of ROS via a Fenton-type reaction.(110) As seen in iron overload, ROS promote oxidation of proteins, lipids, and carbohydrates leading to cell death.(110) Interruption of mitochondrial function, alteration of calcium and iron homeostasis, DNA fragmentation, and disturbed thyroid iodine uptake have been suggested as possible mechanisms.(99)

1.11 Cobalt cardiomyopathy

Cobalt has a number of reported beneficial actions on the heart including promotion of preconditioning via increased expression of hypoxia-inducible factor-1, it can induce vascular endothelial growth factor, and has a cryoprotective and anti-inflammatory effect preventing adverse cardiac remodelling.(4, 108)

The precise mechanism by which cobalt causes cardiotoxicity is unclear with no recent experimental studies in the literature.(4) Hypotheses include the interference of cobalt with the binding of calcium to sarcolemma, transport into the myocytes, and the inotropic effects of calcium.(111, 112) It may also reduce the generation of ATP by interrupting the citric acid cycle, interfering with mitochondrial respiratory chain enzymes, and promote the generation of ROS.(4) A review of published case reports relating to cobalt cardiomyopathy suggests that isolated elevated cobalt levels requires the co-existence of one or more cofactors including hypothyroidism, alcoholism, and consumption of a low-protein diet.(4, 89)

Similar to iron cardiomyopathy, cobalt can cause a rapidly progressive depression of left ventricular systolic function, which in most cases, reversible with removal of cobalt exposure.(4) Patients can present with a spectrum of symptoms secondary to heart failure including a recognised subacute onset of severe heart failure accompanied by hypotension and cyanosis.(4)

The diagnosis of cobalt cardiomyopathy requires the demonstration of biventricular dilatation and systolic dysfunction at a time when blood and/or tissue concentrations of cobalt are increased, and recovery of systolic function when cobalt levels are within normal limits.(4) Cobalt cardiomyopathy can be distinguished from other causes of non-ischaemic cardiomyopathy based on the clinical presentation, the presence of multi-system involvement, and clinical course (table 4).

	Non-ischaemic cardiomyopathy	Cobalt cardiomyopathy
Predisposing factors	None	Low protein diet Thiamine deficiency Hypothyroidism
Recent history	Non-specific	Anorexia Weight loss
Clinical presentation	Slowly progressive LV dysfunction	Rapid onset
	Asymptomatic	Rapid progression of symptoms
Electrocardiogram	Non-specific	Low voltage Sinus tachycardia
Echocardiogram	Dilated ventricle(s) Impaired systolic function	Dilated ventricles Impaired systolic function
Clinical course	Slowly progressive	Rapidly progressive

Table 4. Factors distinguishing cobalt cardiomyopathy from non-ischaemic cardiomyopathy. Adapted from Packer, M.(4)

Confirming the diagnosis of cobalt cardiotoxicity is challenging, as it requires invasive tissue sampling from endomyocardial biopsies or post-mortem examination for measurement of metal deposition. Various histological changes have been described on light and electron microscopy including interstitial fibrosis, loss of myofibrils, characteristic vacuolar degeneration, and intramyofibril deposits consistent with cobalt.(4, 6, 113, 114)

1.12 Assessment of cobalt toxicity

Diagnosis of acute toxicity can be challenging, and adjunctive tests for multisystem involvement are required to aid the diagnosis. Blood levels are not widely available. Instead, urine cobalt levels are used to estimate exposure and can be used for monitoring, but the results are dependent on the timing of collection and method of analysis. Increased concentrations however are not reliably associated with adverse effects.(4) Whole blood levels are considered to reflect burden more accurately and the preferred method.(4)

Serial measurements of whole blood levels have been recommended by the medical device regulatory bodies, including the US Food and Drug Administration (FDA) and the Medicines and Healthcare products Regulatory Agency (MHRA).(115) In patients with MoM implants a threshold of 7 parts per billion (ppb) (1pbb in equivalent to 1ug/L) is used to track the risk of local soft tissue reactions and the potential for further surgery.(116)

Confirmation of toxicity requires organ tissue sampling, and there are no recommended non-invasive methods for cobalt quantification. The potential use of the CMR T2* sequence was described in a case report of a patient with very high blood metal levels. Abdel-Gadir et al. demonstrated an abnormal T2* result, with tissue sample confirmation, of cobalt deposition in a patient with a failing MoM hip prosthesis.(117) The patient had normal iron serum values and no iron identified in the tissue sample. As cobalt exhibits similar

ferromagnetic properties to iron, the cardiac MRI technique has potential to detect cobalt deposition and be used as a screening tool for patients at risk of systemic toxicity.

1.13 Management of cobalt toxicity

Unlike the management of iron overload, there is very little evidence in the literature for the use of chelation agents in the setting of cobalt toxicity. Evidence for the use of N-acetyl-cysteine and 2,3-dimercaptoproane-1-sulfonate is anecdotal and based on a few case reports.(118, 119, 120, 121) The definitive management of toxicity is removal of the source and organ support, if indicated.

CHAPTER 2: RESEARCH AIMS

The prevalence of metal-related cardiomyopathy is increasing. The prognosis

of patients with cardiac iron has improved significantly since the introduction of

the T2* sequence allowing accurately tailored chelation therapy. As described

in chapter 1, there are technical limitations to this diagnostic test, and the test

is not available and/ or accessible in low-income countries with large

populations at risk of cardiomyopathy. Cobalt exhibits similarities to iron, but at

present non-invasive methods for the detection of systemic toxicity or organ

deposition do not exist.

The aim of this thesis is to investigate the use of novel CMR methods to improve

the diagnostic accuracy of iron and cobalt deposition in the myocardium, and

gain insights into the pathophysiology of metal cardiomyopathy. The work on

iron builds on the initial results from my predecessor Dr Daniel Sado in the use

of T1 mapping for iron.(85)

2.1 T1 mapping in the diagnosis of iron cardiomyopathy

Background: Early data in a small adult population study suggests that T1

mapping correlates well with T2*.(85) In this thesis, the potential role of T1

mapping is further explored including with a larger sample population including

children.

56

Hypothesis: Native T1 will correlate with T2* in the adult and paediatric populations. Additionally, in long-term follow-up of patients undergoing changes in chelation therapy, T1 mapping is a more sensitive measure detecting changes in iron loading earlier than T2*.

2.2 CMR in the developing world for iron detection

Background: Countries that are likely to benefit the most from MRI for iron quantification have limited or no access to scanner time. Traditional CMR methods employ long scanning times resulting in increased costs. This thesis explores the use of abbreviated "ultrafast" protocols using distinctive colour maps for diagnosis of iron loading.

Hypothesis: Ultrafast CMR scans can be diagnostic and cost-effective in the management of iron overload in the developing world.

2.3 CMR for the detection of ferromagnetic metals

Background: Over one million implanted MoM hip prostheses have been implanted worldwide.(7) Elevated circulating levels of cobalt have been linked to fatal cardiac events, and a reported 3-fold increased risk of heart failure, with diagnoses depending on biopsies or autopsies as a non- invasive measure does not exist.(113, 122, 123)

Hypothesis: Myocardial T1 mapping and T2* values would be shortened in patients with MoM hips with high blood metal levels, and changes may be an early marker of organ dysfunction.

CHAPTER 3: GENERAL METHODOLOGY

3.1 Ethical approval for research

There are 3 main cohorts of patients included in this thesis. Ethical approval

was obtained from the UCL/UCLH Joint committees on the Ethics of Human

Research Committee for patients scanned in the United Kingdom. Ethical

approval was obtained from the Institutional Review Board at Chulalongkorn

University for patients recruited in Bangkok, Thailand. All participants were

prospectively recruited and provided written informed consent.

3.2 Study Populations

3.2.1 T1 mapping for iron overload, UCLH, London

Three hundred adult patients (aged 16 years and above) with known

haemoglobin disorders were prospectively recruited for CMR assessment of

iron loading. All patients attending the adult Joint Cardiology and Haematology

Red Cell clinic at University College London Hospital were invited to participate

in the study by the author.

Twenty-one paediatric patients (aged 8 years and above) were referred by the

haematology team for a CMR scan. Parents and legal guardians were

approached prior to the scan appointment, and paediatric patients were asked

for their assent.

All scans were performed at the Heart Hospital, UCLH. Patients with standard

contraindications to MRI scanning were excluded from the study.(124)

59

3.2.2 Ultrafast scanning for iron, King Chulalongkorn Memorial Hospital, Thailand

A total of 100 patients with thalassemia major were recruited for MRI assessment of myocardial and liver iron loading at the King Chulalongkorn Memorial Hospital in Bangkok, Thailand. Patients receiving regular blood transfusions were identified by the Chulalongkorn Thalassemia Support Group and recruited by the Thai collaborators. Blood samples were taken for assessment of ferritin. Patients were scanned at the King Chulalongkorn Memorial Hospital.

3.2.3 CMR for Cobalt, UK

108 patients were recruited from specialist orthopaedic clinics at the Royal National Orthopaedic Hospital, UCL. Patients with metal-on-metal (MoM) or ceramic-on-ceramic (CoC) hip implants in situ for more than 12 months were recruited into the study. Patients were divided into 3 age and sex-matched groups based on their type of prosthesis and blood metal ion levels.

- Group A: CoC implants with normal blood metal ion levels.
- Group B: MoM implants with low metal ion levels.
- Group C: MoM implants with raised metal ion levels.

In addition to standard MRI contraindications, patients with previous hip revision surgery, impaired renal function (estimated glomerular filtration rate of less than 30ml/min) were excluded from this study(124).

3.2.4 Healthy volunteers

Two groups of healthy volunteers are described in this thesis. Fifty healthy volunteers at UCLH and 11 at King Chulalongkorn Hospital were recruited through advertising within the respective hospitals and affiliated universities. All volunteers had no history of symptoms of cardiovascular disease, hypertension, diabetes mellitus, and were not on regular cardioactive medications. All healthy volunteers were scanned at the same centres and same scanner as their respective age-matched study participants. Normal ranges for native T1 values using MOLLI and ShMOLLI sequences were established.

3.3 Cardiovascular Magnetic Resonance Protocols

All CMR scans were performed on a 1.5 Tesla Siemens scanner using a 32-channel phased-array cardiac coil. Images were acquired during breath-hold at end expiration. Each scan included acquisition of pilot imaging, long and short axis left ventricular SSFP cine images, assessment of left ventricular volumes and mass, T2*, and T1 mapping. Specific methodologies used in each study are described in the results chapters, including late gadolinium enhancement (LGE) and ECV imaging.

3.3.1 Pilot images

All studies began with single shot pilot images with the following parameters: repeat time (TR): 3.39ms, echo time (TE): 1.7ms, slice thickness: 5mm, field of view (FoV): 360 x 360mm, read matrix: 256, and flip angle 60°. These images were used to plan further acquisitions.

3.3.2 Cine images

Following piloting imaging steady state free precession (SSFP) cine images were acquired in the long axis planes then short axis for structural and functional assessment. The LV short axis stack, starting at the atrioventricular ring and ending at the apex was acquired using 7mm slice thickness and a gap of 3mm. Retrospective ECG gating was used with 25 phases. Typical fast imaging with steady state precession (FISP) imaging parameters were TE: 1.6ms, TR: 3.2ms, in plane pixel size 2.3 x 1.4mm, slice thickness 7mm, flip angle 60°. Images were optimised by changing these parameters if the patients were unable to breath-hold or had an arrhythmia.

3.3.3 T2* imaging

The standard myocardial BBT2* sequence was acquired, over 21- heart beats, using a single breath-hold ECG-gated multi-echo technique to generate eight images with a range of echo times (TE ranging from 2.59ms -

18.2 ms, slice thickness: 10mm, flip angle: 20°, field of view read/ phase: 400mm/75%). A mid-left ventricular short axis slice was used.

An additional Siemens Work in Progress (WIP) myocardial DBT2* sequence was acquired in 50 UK patients for comparison with BBT2* (TE ranging from 2.8ms - 19.6ms, slice thickness 8mm, flip angle 20°, field of view read/ phase 350mm/75%). A coloured pixel-wise map was generated in-line by the scanner. The WIP sequence was installed by Siemens on the King

Chulalongkorn Memorial Hospital, Thailand MRI scanner for the purpose of the study.

In Thailand, at the request of the local team, a single mid-liver transverse slice was carefully chosen for the liver T2* measurement. Predefined echo times by the scanner vendor, optimised for liver iron loading, were used to generate 12 images (TE ranging from 0.99 - 16.5ms), slice thickness 10mm, flip angle 20°).

3.3.4 T1 mapping

T1 maps were acquired using ShMOLLI and MOLLI sequences (Siemens Myomaps). Motion correction and a non-linear least-square curve fitting were performed with the set of images acquired at different inversion times to generate a pixel-wise coloured T1 map in-line by the scanner.(83)

MOLLI with a 5s(3s)3s sampling protocol was used. This method uses time in seconds rather than heartbeats for sampling. The ShMOLLI sequence was acquired over 9 heartbeats.(83) The same mid-left ventricular short axis slice was used for each sequence. Each slice required one breath hold. Quality control of T1 maps was performed by review of the error maps generated with the sequence, and review of the raw images, looking for any breath-hold artefacts.

3.3.5 Late gadolinium enhancement

Gadolinium (Dotarem, Guerbet S.A., France) was administered intravenously (0.1mmol/kg) as a bolus for assessment of late gadolinium enhancement (LGE). In this thesis, LGE assessment was performed only in the CMR for Cobalt (chapter 6) study. LGE images were acquired in the standard long axis and short axis stack using a fast low angle shot (FLASH) sequence with phase sensitive inversion recovery (PSIR).(125)

3.3.6 ECV maps

Post-contrast MOLLI T1 maps were obtained using the 4s(1s)3s(1s)2s sampling protocol, 15 minutes after contrast injection (0.1mmol/kg of Gd-DOTA), to improve accuracy of T1 values in the 200 - 600ms range(80). Similar acquisition parameters as for native T1 maps were used. ECV was calculated via an off-line software to generate ECV parametric maps generated from coregistration of the native and post-contrast T1 pixel maps together with the patient's haematocrit taken at time of the scan.(126)

3.4 Imaging analysis

Specific details pertaining to each topic are provided in their respective chapters. All studies were reported by the author of this manuscript and Professor James Moon (primary supervisor and Professor of Cardiology) using SCMR standardised reporting guidelines.(127) The author was blinded to patient groupings in the T1 mapping for cobalt study at the time of scanning.

3.5 Statistical Analysis

Specific imaging analysis descriptions will be provided in each relevant chapter. Statistical analysis was performed using IBM SPSS Statistics (version 22) and Stata 14 (StataCorp). Data was tested for assessment of normal distribution using the Shapiro-Wilk test. All continuous variables are expressed as mean \pm standard deviation. Categorical variables are expressed as percentages. Correlations were assessed using either Pearson's correlation coefficient for normally distributed data or Spearman's rho for non- normally distributed data. Inter-study repeatability for T2* and T1 mapping was assessed using intraclass correlation coefficient. A p value of < 0.05 was considered significant.

CHAPTER 4 RESULTS: MYOCARDIAL IRON QUANTIFICATION BY T1 MAPPING

This chapter is based on the abstract and poster presentations listed below. My contribution was obtaining ethical approval, recruitment of patients, consenting, performing, and reporting the scans. I analysed the data and assisted with the statistical analysis. The study conducted in Milan followed on from my work in the UK. We arranged a collaboration with a large Italian thalassaemia centre, I travelled to Milan on 2 occasions, identified relevant patients, analysed 101 CMR scans, and helped write the manuscript. Our Italian collaborators successfully published the paper.

- Amna Abdel-Gadir, Daniel Sado, Stuart Murch, Viviana Maestrini, Stefania Rosmini, Thomas A Treibel, Marianna Fontana, Heerajnarain Bulluck, Stefan K Piechnik, Charlotte Manisty, Anna S Herrey, John Malcolm Walker, John Porter, James Moon. Myocardial iron quantification using T2* and native T1 mapping a 250 patient study. Journal of Cardiovascular Magnetic Resonance 2015 17(Suppl 1):P312.
- Torlasco C, Cassinerio E, Roghi A, Faini A, Capecchi M, <u>Abdel-Gadir A</u>, Giannattasio C, Parati G, Moon JC, Cappellini MD, Pedrotti P. Role of T1 mapping as a complementary tool to T2* for non-invasive cardiac iron overload assessment. PLoS One. 2018 Feb 21;13(2):e0192890
- Amna Abdel-Gadir, Daniel Sado, Katia Menacho, Sabrina Nordin, Louise McGrath, Sara Trompeter, John Porter, Stefan Piechnik, Anna Herrey, Charlotte Manisty, John Malcolm Walker, and James Moon. T1 Mapping for Cardiac Iron in Children. Presented at SCMR 2018, Barcelona, Spain.

4.1 Introduction

Iron loading of the heart remains the leading cause of morbidity and mortality in patients with hereditary and acquired transfusion dependent anaemias. As described in Chapter 1, the human body lacks an active mechanism for excreting iron, and control is based on a finely balanced system of absorption and passive fixed loss.(11, 128) In transfused anaemias heart failure due to cardiac siderosis remains the most common cause of death worldwide.(2) Chelation therapy has improved the prognosis of patients at risk of iron cardiomyopathy, but careful monitoring is required to maximize benefit. The CMR T2* technique allows robust non-invasive cardiac iron quantification, and has been linked to improved survival.(3) This method however has limitations, which may preclude it from benefiting those who may require it the most. Any diagnostic technique has limitations, and often only revealed when an additional method becomes available. The alternative measure this study proposes is native T1 mapping to generate an instantly visible and diagnostic map. (78, 79, 81, 83) Early data suggests myocardial T1 mapping has excellent reproducibility and correlates well with T2*, but the precise relationship between T2* and T1 is not apparent.(129)

The aim of this chapter was to investigate the relationship between T1 mapping and the gold-standard measurement T2* further by:

- assessing the relationship in a large adult and paediatric population at risk of myocardial loading from hereditary and acquired iron loading conditions
- assessing whether T1 mapping has the potential to detect disease earlier than
 T2* by monitoring change over a specified period of time

4.2 Hypotheses

We hypothesised that:

- Native T1 would correlate with T2* in patients with iron loading in both adults and children
- T1 mapping is a more sensitive measure in the detection of iron loading with changes in T1 preceding those in T2*
- T1 will act as a complementary tool in patients with equivocal T2* and highlight which patients may require earlier follow-up

4.3 Materials and methods

The research received approval by the University College London/ University College London Hospitals Joint Committees on the Ethics of Human Research Committee (14/LO/1948). All participants and parents of paediatric patients were provided written informed consent.

4.3.1 Patient cohort

A total of 300 consenting adult patients with known haemoglobin disorders were recruited for CMR assessment at a large single referral centre. Twenty- one paediatric patients were also recruited into the study. Patients were referred from local and national haematology services, with suspected or previously confirmed iron loading.

Fourteen patients who had recent changes to their chelation therapy were invited and recruited for 3 additional scans over the course of 6 months (a

total of 4 scans). In this group, scans 2 and 3 were acquired but not analysed for iron quantification until all 4 scans were completed. Left ventricular function was assessed and relayed to the clinical haematologist to ensure the patients did not develop LV systolic dysfunction.

4.3.2 Normal volunteers

Healthy subjects were recruited through advertising at the local hospital and affiliated University campus. All subjects had no history of cardiovascular disease, hypertension, diabetes mellitus, and were not on regular cardioactive medications. Normal ranges for myocardial T2* and native T1 values, for the scanner used in this study, were established.

4.3.3 CMR scanning

All patients underwent CMR scans with a Siemens 1.5T clinical scanner (Avanto, Siemens Healthcare, Germany). Each scan included acquisition of long and short axis left ventricular SSFP cine images, and assessment of left ventricular volumes, mass, BBT2*, and T1 mapping sequences, using previously published techniques.(65, 83)

Fifty patients had an additional Siemens WIP DBT2* sequence. Native T1 measurements were performed using the ShMOLLI sequence, with measurements as previously published.(83)

Quality control of T1 maps was performed by review of the error maps generated with the sequence, and review of the raw images, looking for any

breath-hold artefacts. T2* and native T1 maps were performed on the same mid-left ventricular short axis slice.

4.3.4 Image analysis

Image acquisition, analyses, and clinical reporting were performed by the author and verified by a Level 3 certified CMR reporter. The author recruited the study participants from a dedicated clinic for patients at risk of cardiac iron loading, therefore was not blinded to their histories, previous imaging, or medications. The second reporter was aware of patients' medical diagnoses prior to analysis, but not the treatment or history of previous iron.

A single region of interest (ROI) was manually traced in the mid-ventricular short axis septum carefully avoiding the endo- and epicardial contours to minimize partial-voluming effect in both T2* and T1 mapping.

T1 values were instantly visible due to change in colour with iron deposition (figure 14). For T2* analysis, a decay curve was calculated using the FDA approved Thalassaemia-Tools plugin for CMR tools (Cardiovascular Imaging Solutions, London, UK). The signal intensity was plotted against each echo time and the T2* value was calculated from the resulting exponential decay curve (figure 15).

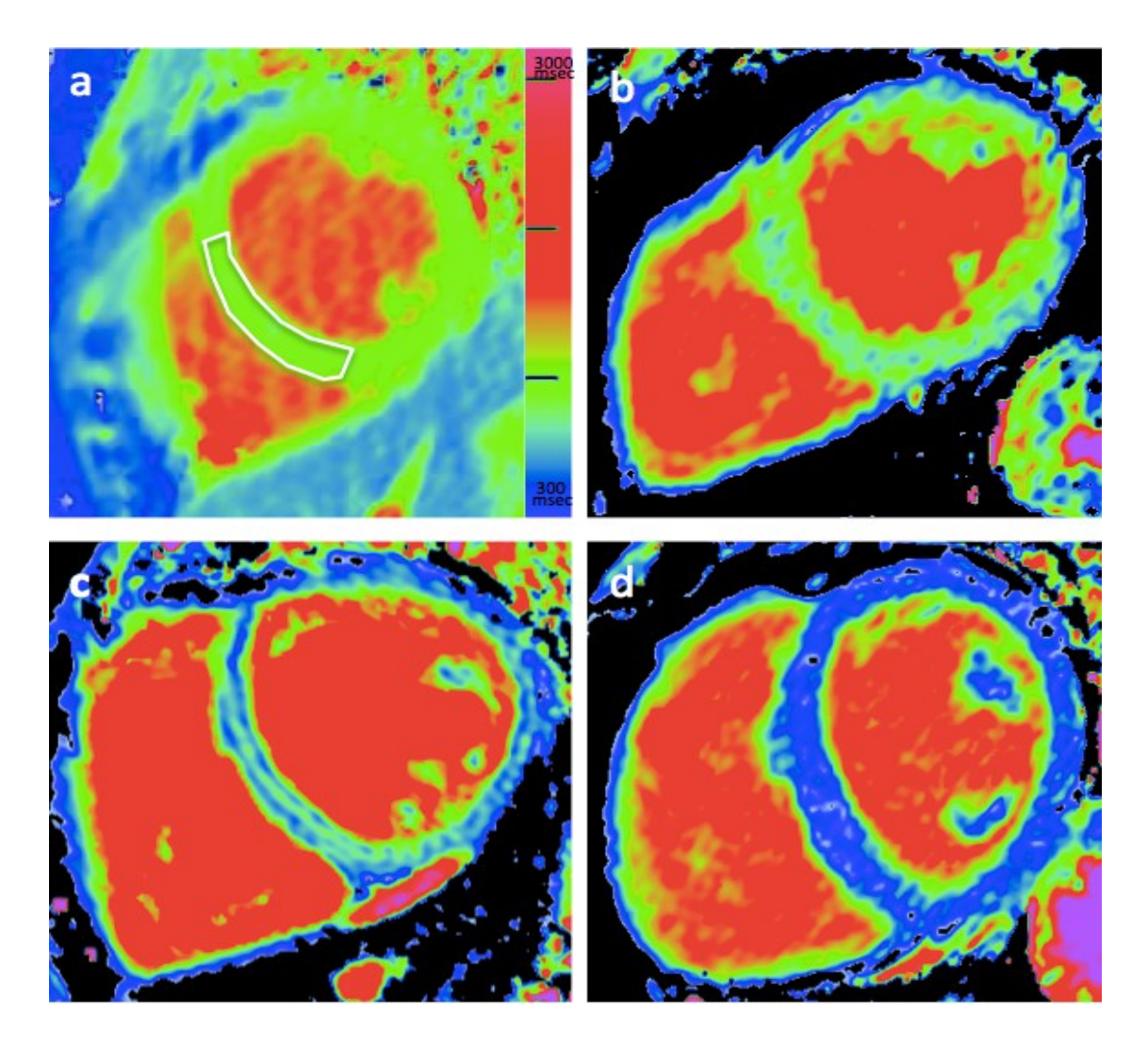


Figure 14. Examples of T1 mapping in iron loading states. Native T1 mapping (ShMOLLI sequence) in myocardial iron overload demonstrating (a) healthy volunteer (with a region of interest drawn) and (b) mild, (c) moderate, and (d) severe iron overload. The colour look up table means that with shorter T1 times, due to the presence of iron allows the myocardium to appear blue.

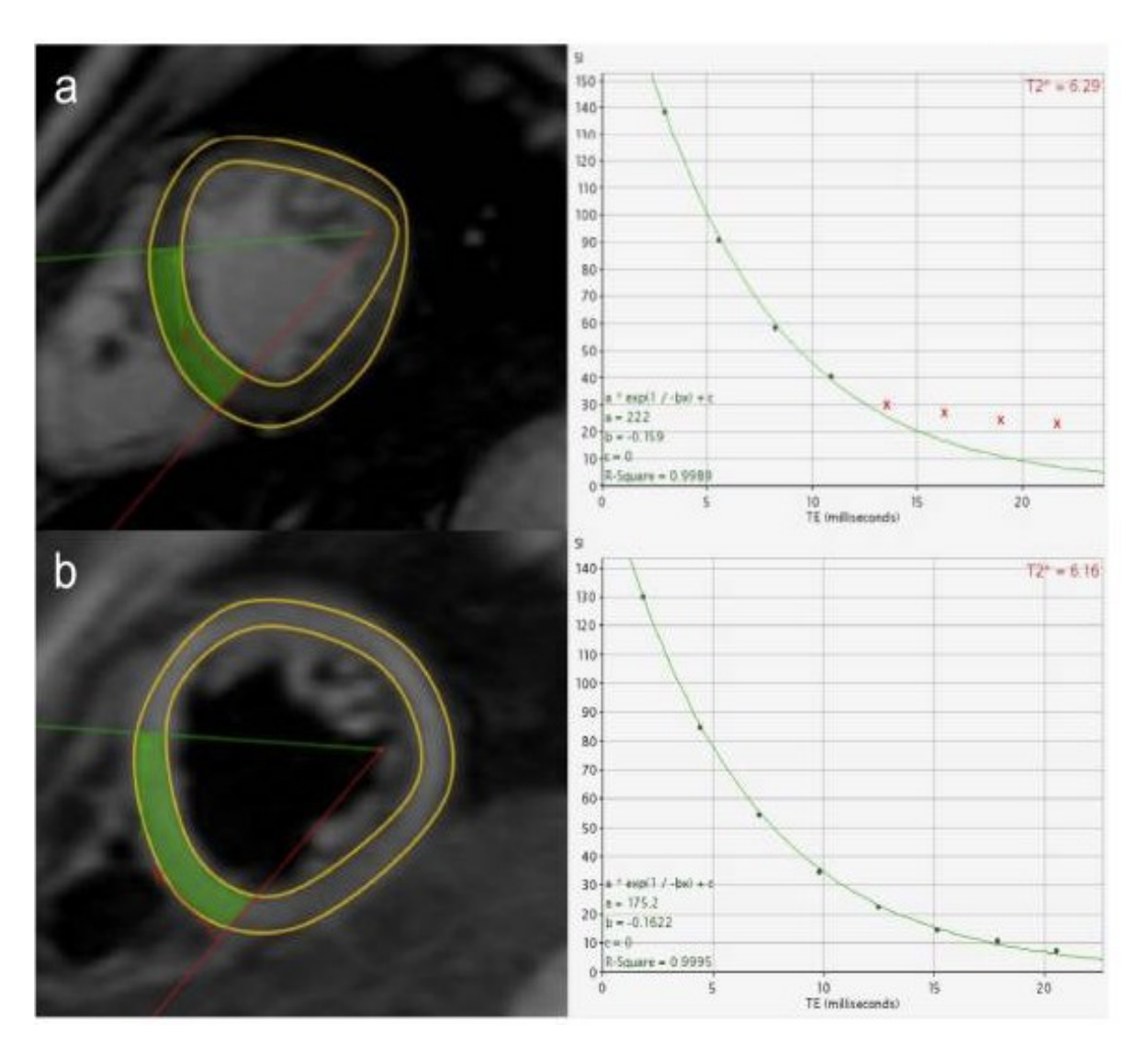


Figure 15. Bright blood and dark blood myocardial T2* CMR analysis. CMR

T2* measurement using a standard approved technique demonstrating the region of interest in the interventricular septum. a) a bright blood sequence demonstrating the measurement of severe myocardial iron using the truncating method; b) dark blood sequence in the same patient. This patient is shown to have severe myocardial iron.

4.3.5 Statistical analysis

Statistical analysis was performed using IBM SPSS Statistics (version 22). All continuous variables are expressed as mean ± standard deviation.

Categorical variables are expressed as percentages. T2* and T1 values are displayed as mean \pm standard deviation. Correlations were evaluated using either Pearson's correlation coefficient or Spearman's rho. A p value of < 0.05 was considered significant. Data between baseline and follow-up visits were compared using paired t-test.

4.4 Results

Adult patients

Three hundred patients were recruited (age 39 ± 15 years; 52% female). The majority of patients had a diagnosis of beta-thalassemia major (n=201), followed by sickle cell disease (n=23), thalassemia intermedia (n=21), hereditary haemochromatosis (n=21), malignancy related anaemias (n=10), sideroblastic anaemia (n=8), Diamond Blackfan anaemia (n= 5), pyruvate kinase deficiency (n=4), aplastic anaemia (n=1), red cell aplasia (n=1), congenital dyserythropoietic anaemia (n=1), congenital haemolytic anaemia (n=1), hereditary spherocytosis (n=1), erythropoietic protoporphyria (n=1) and Haemoglobin H (n=1).

Paediatric patients

Twenty-one paediatric patients were invited to join the study with full consent obtained from the accompanying parent or carer (age 14 ± 2.9 years; 76% male). Referral diseases were beta-thalassaemia major (n= 9), sickle cell anaemia (n =8), and the remainder thalassaemia intermedia, acute lymphoblastic leukaemia, hereditary spherocytosis and congenital sideroblastic anaemia (n= 1 each).

Healthy volunteers

Fifty healthy volunteers were scanned (n=50, age 44 \pm 11; 60% female). All volunteers had normal CMR findings. The healthy range of myocardial T1 was 958ms \pm 30ms; and 33ms \pm 5ms for T2*. The healthy volunteer population scatter was 958ms \pm 3.1% versus 33ms \pm 15% for T1 and T2* respectively demonstrating a five-fold difference (figure 16).

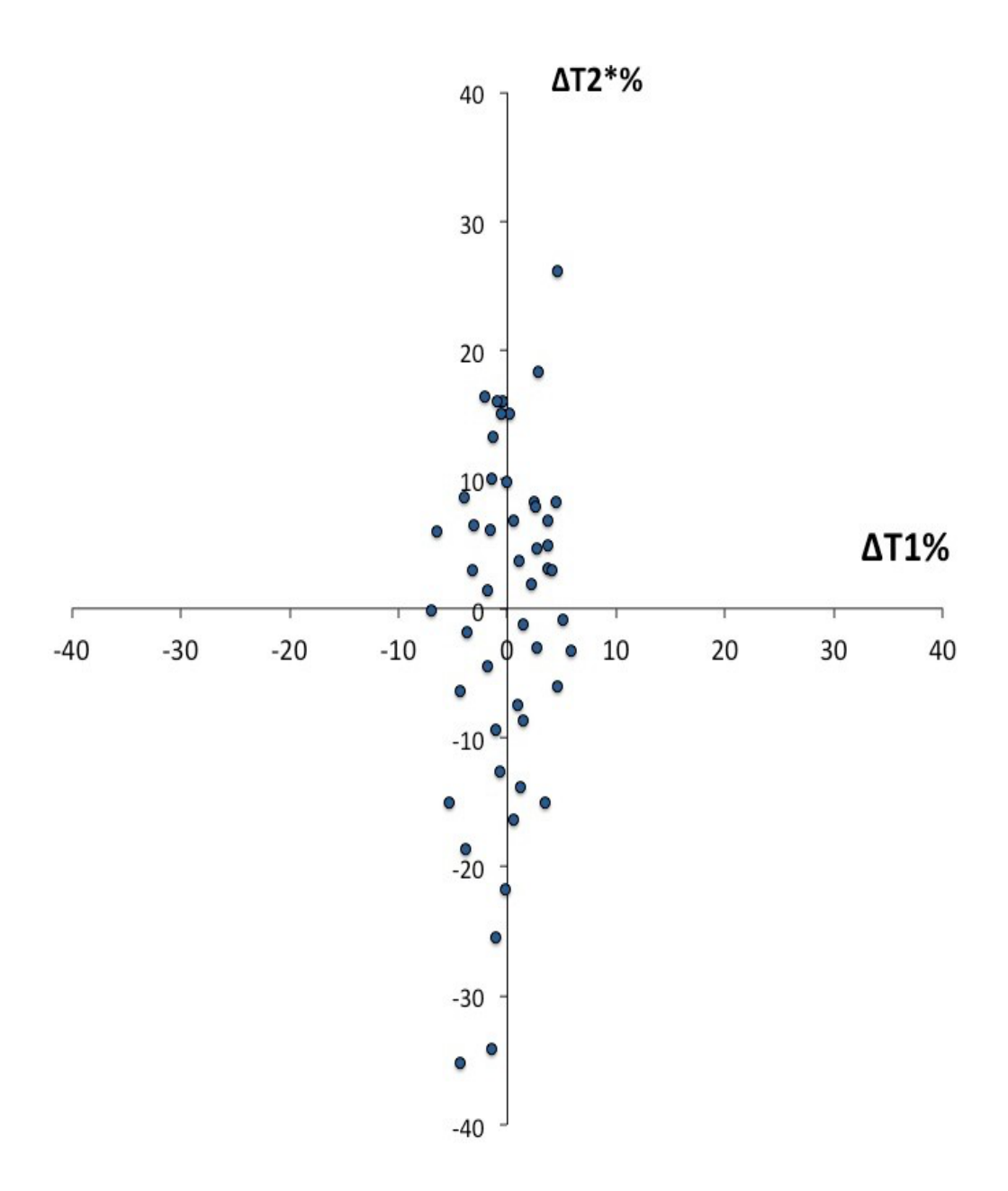


Figure 16. The healthy volunteer population T2* and T1 values scatter. Scatter demonstrating the distribution of T2* and T1 values in the healthy volunteer group. The scatter was 958ms \pm 3.1% for T1 versus 33ms \pm 15% for T2* demonstrating a five-fold difference.

T2* and T1 assessments were completed in all patients and controls. To obtain optimal images for analysis 27% of patients required repeated T2* scans, whilst 12% required repeated T1 maps, p<0.001. ShMOLLI maps were not interpretable in two (0.8%) patients due to the presence of an MRI conditional pacemaker, and the positioning of a PORT-A-CATH implantable venous access system.

4.4.1 Bright blood T2* and T1 mapping

The average myocardial T2* in the patient group was $29.3 \text{ms} \pm 10.6 \text{ms}$ and $850 \text{ms} \pm 118 \text{ms}$ for T1 mapping. As defined by T2*, 56 (18.7%) patients had myocardial iron overload (severe= 22; moderate= 11; mild= 23). Four patients had high T1 values. The lowest BB T2* value was 2.1 ms with a corresponding T1 value of 349 ms.

Across the entire patient cohort there was a significant relationship between T1 mapping and BBT2* with a good association (R²=0.7, p<0.001, figure 17).

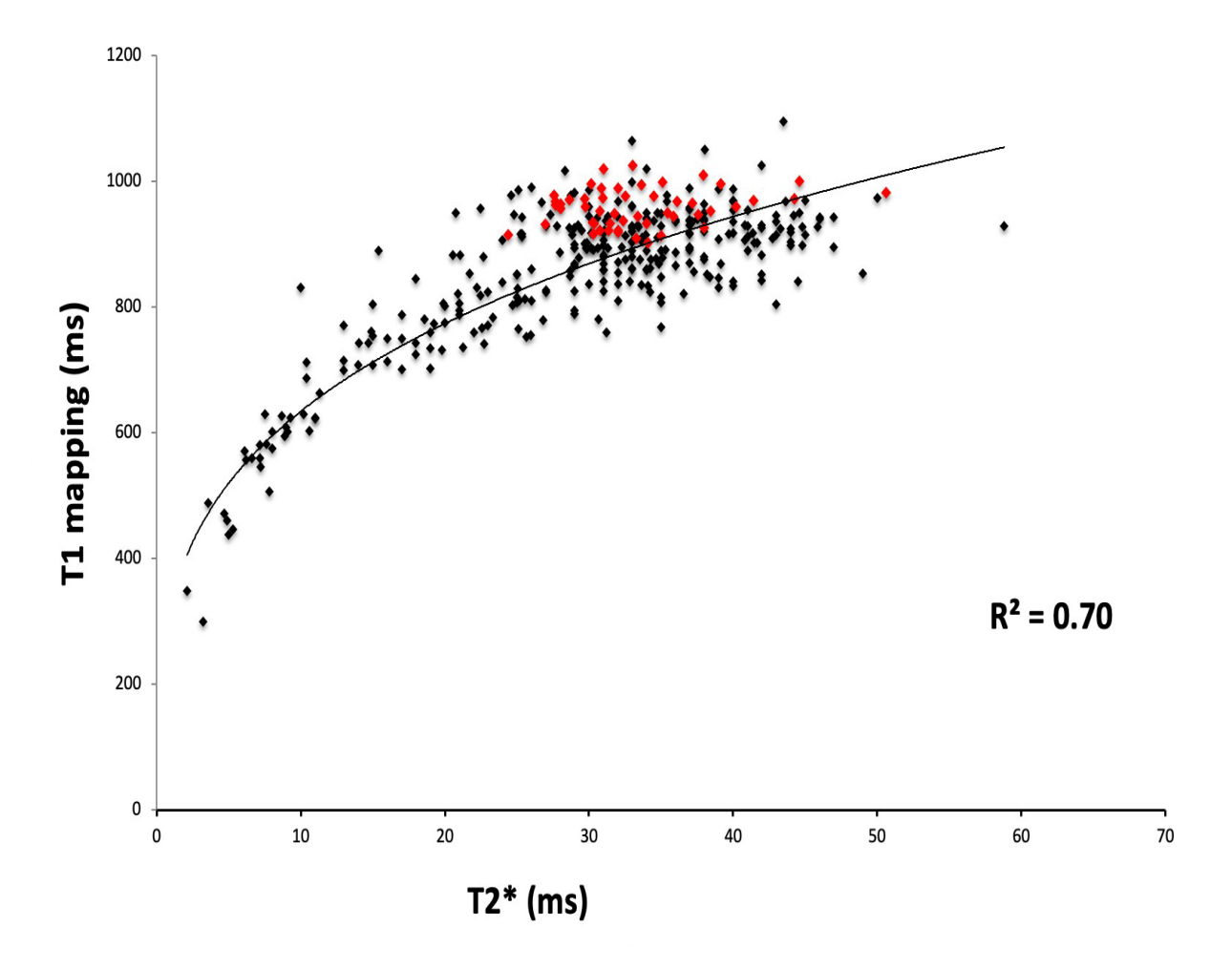


Figure 17. Correlation between T1 mapping and T2* in all patients with haemoglobinopathies. The red dots represent the healthy volunteers all of whom had T2* values greater than 20ms.

This relationship is tighter when T2* is less than 20ms and weaker when greater than 20ms (R^2 =0.75 and R^2 =0.004 respectively, p<0.001, figure 18 and figure 19, respectively). All patients with low T2* values had low T1 values.

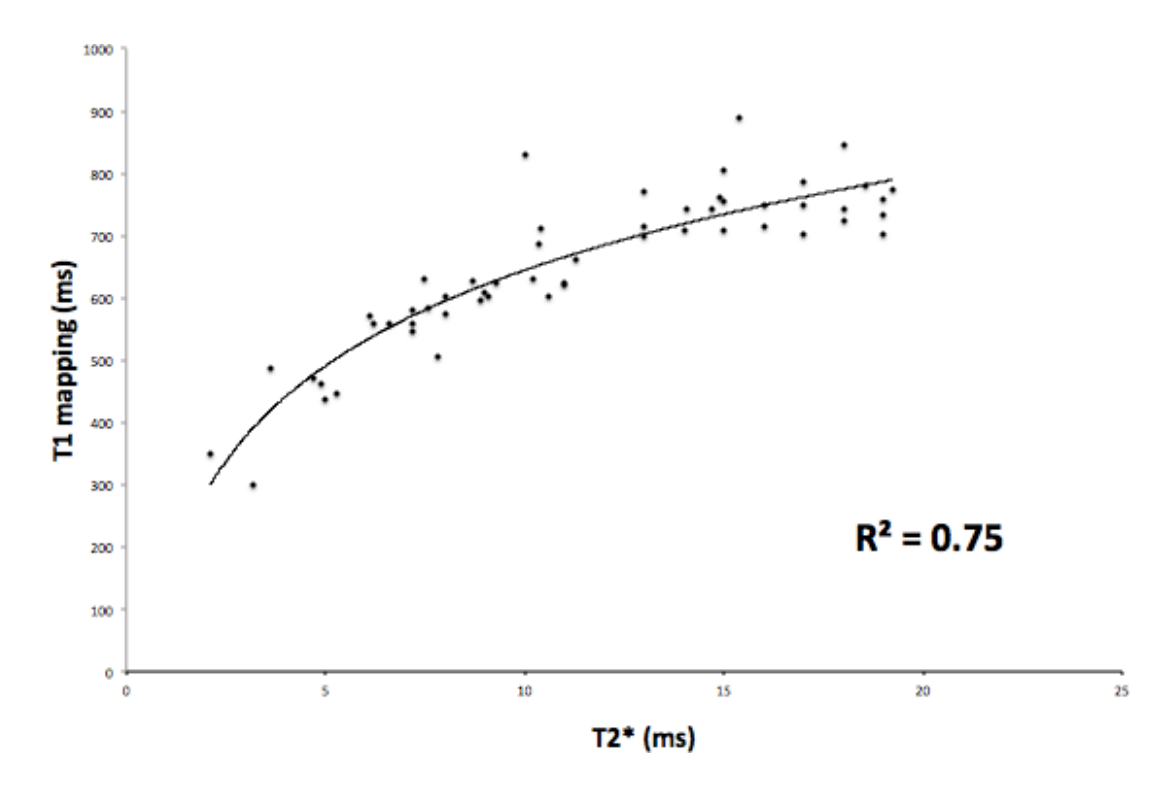


Figure 18. Correlation between T1 and T2* in patients with myocardial T2* values less than 20ms - indicating the presence of iron.

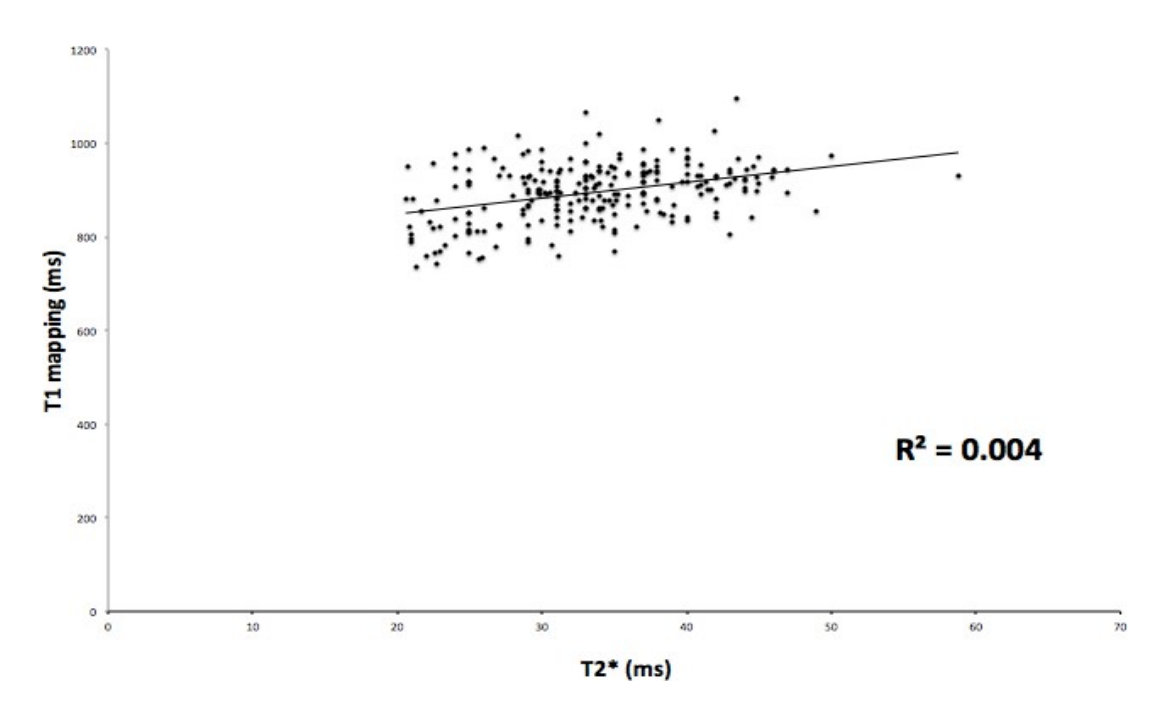


Figure 19. Correlation between T1 and T2* in patients with myocardial T2* values greater than 20ms - indicating the absence of iron.

If T1 from healthy volunteers is assumed as representing the absence of iron overload the lower limit of normal would be 898ms.(86) This would be the equivalent to a T2* lower limit of 29ms. Plotting the relationship between T2* values less than 29ms and T1 demonstrates a stronger association (R^2 =0.78, p<0.001) (figure 20).

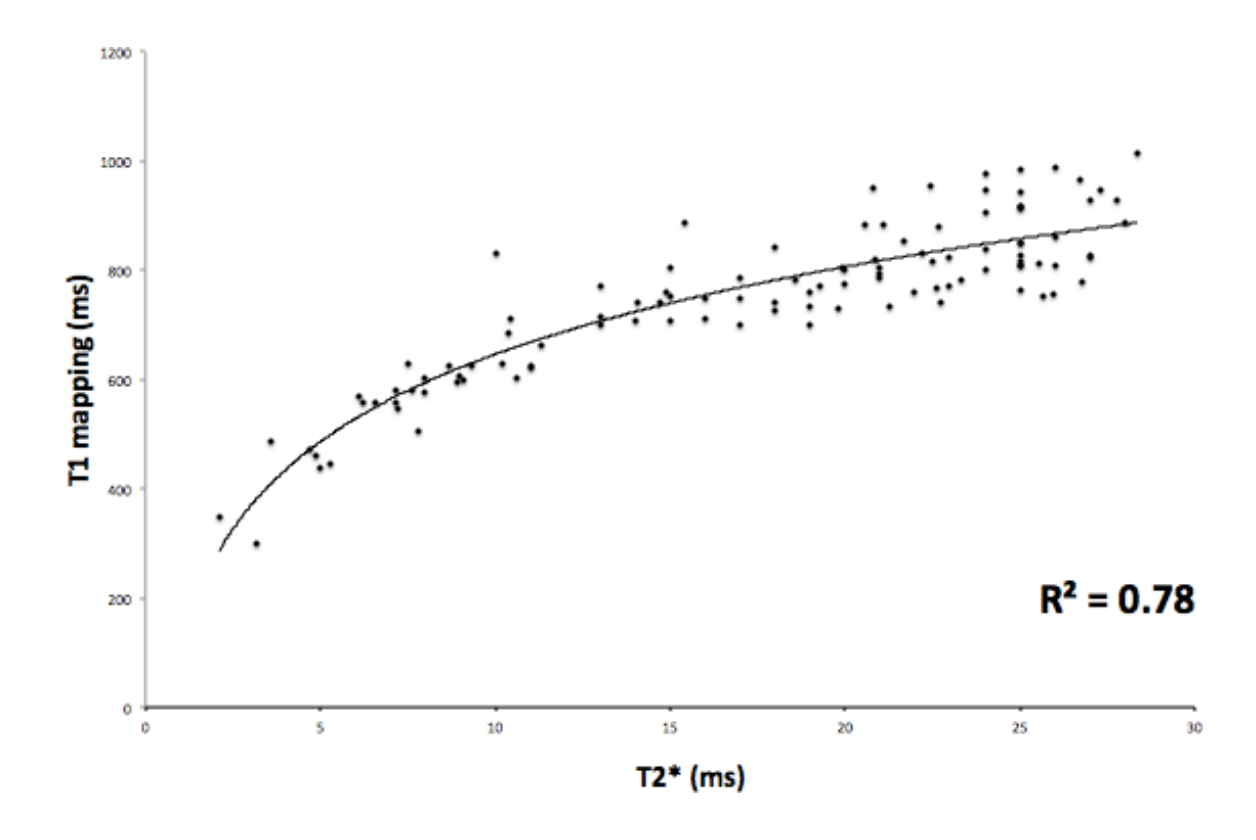


Figure 20. Correlation between T1 and T2* in patients with T2* values less than 29ms corresponding to the lower limit of T1.

Normal T2* and low T1 values in patients

Of the 244 patients with T2* greater than 20ms 118 (48%) had a low T1 (less than 898ms) suggesting that nearly half of this subgroup of patients may have myocardial iron.

Normal T2* and low T1 versus normal T2* and normal T1

A significant difference was noted in left ventricular end-diastolic volumes and tricuspid annular plane systolic excursion (TAPSE) between patients with normal T2* and low T1 compared with normal T2* and normal T1 values. No differences were found in the assessment of left ventricular ejection fraction, mass, and left atrial area between the two groups (table 5).

	Normal T2* Low T1	Normal T2* normal T1	P value
n	118	122	
LVEF (%)	67.0 ± 5.9	67.8 ± 7.0	P= 0.37
MAPSE (mm)	13.4 ± 2.8	13.3 ± 2.7	P=0.9
TAPSE (mm)	20.9 ± 4.5	22.9 ± 3.9	P<0.005
LVEDVi (ml/m²)	74.9 ± 16.7	80.4 ± 19.2	P<0.05
LV mass indexed (g/m²)	64.6 ± 16.2	66.6 ± 16.2	P=0.35
LA area indexed (cm/m²)	12.7 ± 3.0	12.7 ± 2.4	P=0.82

Table 5. Comparison of CMR measurements in patients with normal T2* and low T1 versus normal T2* and normal T1

.

4.4.2 Dark blood T2*

50 patients underwent both DBT2* and T1 mapping sequences in addition to the BBT2* preparation (thalassaemia major (n=40), thalassaemia intermedia (n=3), sickle cell disease (n=2), hereditary haemochromatosis (n=2), Hb H disease (n=1), erythropoietic protoporphyria (n=1), and aplastic anaemia (n=1)).

As expected, there was a good relationship between DBT2* and BBT2* ($R^2 = 0.78$, p< 0.001), and DB T2* and T1 mapping ($R^2 = 0.88$, p< 0.001).

4.4.3 Changing chelation

Fourteen patients undergoing escalation of chelation therapy were recruited for 2-monthly surveillance scans over 6 months (4 scans in total per patient). Baseline characteristics are shown in table 6. Scans were analysed at the end of the 6-month period and relayed to the clinical haematologist leading the patients' care.

Eleven patients had severe myocardial iron and 3 with moderate iron, as identified by T2*, on their first (baseline) scan. All patients with severe and moderate iron had a corresponding low T1 value.

	Patients
N	14
Age (years)	33.7 ± 10.5
Gender (male/female)	7/7
Chelation therapy (number of patients)	
DFO	6
Deferasirox	2
DFO + DPO (combination)	5
DPO + Deferasirox (combination)	1

Table 6. Patient baseline characteristics. Chelation regime on recruitment shown. DFO desferrioxamine; DPO Deferiprone.

Within the 6-month period only one patient (with severe iron on continuous deferoxamine therapy) had 4 scans. Nine patients attended 2 scanning appointments within the 6-month period with mean time between baseline and follow-up scans was 3.4 ± 0.7 months. The remaining patients had one scan within the chelation intensification period.

T2* and T1 changes between scans were concordant in all but 2 patients who had severe myocardial iron secondary to TM and congenital sideroblastic anaemia. In both patients there was a small rise in T2* within the severe category but a fall in T1. There were no significant changes in T2* or T1 between baseline and follow-up scans (p=0.52 and p=0.84, respectively).

There were no significant changes in LV function, left ventricular end diastolic dimension, and TAPSE between the baseline and follow-up scans (EF 58.6 \pm 6.4% vs. 61 \pm 9%, LVEDVi 80.3 \pm 22.5ml/m² vs. 79.6 \pm 18.7ml/m², TAPSE 17 \pm 4.7mm vs. 17 \pm 3.9mm)(table 7).

Baseline scan	Follow-up	P value
6.6 ± 2.6	6.9 ± 2.5	0.52
525 ± 85	527 ± 60	0.84
58.6 ± 6.4	61 ± 9	0.44
80.3 ± 22.5	79.6 ± 18.7	0.85
17 ± 4.7	17 ± 3.9	0.99
	6.6 ± 2.6 525 ± 85 58.6 ± 6.4 80.3 ± 22.5	6.6 ± 2.6 6.9 ± 2.5 525 ± 85 527 ± 60 58.6 ± 6.4 61 ± 9 80.3 ± 22.5 79.6 ± 18.7

Table 7. CMR parameters between baseline scans and follow-up scans. Mean time between baseline and follow-up scans was 3.4 ± 0.7 months.

4.4.4 CMR in paediatric patients

Twenty-one paediatric patients were invited to join the study with full consent obtained from the accompanying parent or carer (age 14 ± 2.9 years; 76% male). Referral diseases were beta-thalassaemia major (n= 9), sickle cell anaemia (n =8), and the remainder thalassaemia intermedia, acute lymphoblastic leukaemia, hereditary spherocytosis and congenital sideroblastic anaemia (n= 1 each).

Mean T2* and native T1 values were 33.1 ± 10.8 ms and 905 ± 101.4 ms, respectively. All patients were able to complete the T1 mapping sequence at first attempt. Across the cohort there was a strong relationship between T2* and T1 (R² = 0.73). Two patients had low T2* indicating the presence of myocardial iron. Overall, 4 patients had low T1 values, including the 2 patients with low T2* (table 8).

	T1 (<898ms)	T1 (>898ms)
T2* (<20ms)	2	0
T2* (>20ms)	2	17

Table 8. Grouping of paediatric patients according to T2* and T1 values.

All patients with iron by T2* had a low T1 value. 2 patients with T2* in the normal range were noted to have low T1 values.

4.5 DISCUSSION

The T2* sequence for iron has changed the management and prognosis of iron loading conditions, allowing non-invasive myocardial monitoring with superiority over surrogates such as serum ferritin.(130, 131, 132) Ferritin and haemosiderin iron alters the behaviour and properties of hydrogen nuclei in water within tissue shortening T1, T2, and T2* times. T1 has shown a potential role in the diagnosis of iron in patients with equivocal T2* values.

In the largest cohort thus far comparing myocardial T1 with T2*, this study has demonstrated a close correlation in the measurement of iron overload (figure 17). The current clinical cut-off value of 20ms has been used to eliminate low false-positive diagnoses, and may misdiagnose mild iron overload as normal.(133) In this study, 48% of patients with normal T2* values were reclassified with myocardial iron overload highlighting its potential utility in the diagnosis of at-risk patients. Furthermore, using the lower limit of normal derived from the healthy volunteers reclassified 95 patients (31.7% of the total cohort) with iron loading. Plotting this relationship continues to demonstrate a strong association between the 2 parameters. Similar findings were seen in the Italian study by Torlasco et al, with 138 patients with transfusion dependent thalassaemia where a cut-off T2* value of 28.7ms was described.(134)

Of the 4 patients with high T1 values, 3 had sickle cell disease - a disease linked with myocardial fibrosis.(135) T1 values are raised in the presence of fibrosis or oedema.(136)

Heart failure is the leading cause of significant morbidity and mortality in patients with iron overload.(2) In a prospective study of patients with thalassaemia major the occurrence of heart failure in patients with severe iron within one year was 47% in patients with T2* less than 6ms, 21% when T2* was between 6 and 10ms, and 0.2% when T2* was greater than 10ms.(57) We did not replicate this finding. In this cohort of patients, 3 patients with severe iron loading had mild heart failure at most with calculated systolic function on the lower limit of normal (LVEF 59.6 \pm 6.7%). The lowest measured EF in the severe iron group was 50% in a patient with a T2* value

of 8ms and a corresponding T1 of 575ms. The lowest T2* and T1 value were measured in the same patient who had mildly impaired LV function (T2* 2.1ms, T1 349ms, LVEF 52%). Overall, the lowest measured LVEF in the entire cohort was 42% (normal >55%) in a patient with hereditary haemochromatosis (HH) and normal myocardial iron by both T2* and T1. In the absence of iron the aetiology of heart failure in HH is likely to be multifactorial. Possible explanations for this finding include previous myocardial iron loading, gene polymorphisms associated with ischaemic heart disease by increasing lipoprotein oxygenation, and an increased incidence of cardiac arrhythmias. (137, 138)

On assessment of longitudinal RV function, TAPSE was significantly lower in patients with normal T2* and low T1 compared with patients with normal T2*/T1, although all values were within the normal range. Although uncommon in the absence of LV dysfunction, RV impairment is a recognised finding in iron overload patients and may reflect a restrictive phenotype.(23, 139) The functional vulnerability of the RV is likely secondary to iron deposition within the thin walled ventricle, and RV impairment has been linked to higher iron burden and an increased frequency of red cell transfusions.(2, 139, 140, 141) Additionally this group of patients had smaller LV cavity volumes when compared to patients with normal T2*/T1 (p< 0.05). LV remodelling leading to dilatation is a recognised consequence of iron deposition. The observed preservation of LV size and reduced TAPSE suggests an early restrictive phenotype pattern in this subset of patients highlighting the potential role of T1 mapping in the identification of patients

with preclinical disease. No differences were found in the assessment of left ventricular ejection fraction, mass, and left atrial area between the two groups.

This study was performed using the conventional BB T2* sequence used in our clinical practice. The recent technical improvement using a double inversion preparation pulse, dark blood T2* (DBT2*), suppresses the blood signal and provides an improved myocardial/blood interface thus avoids contamination of the myocardium. Fifty patients had the DBT2* sequence in addition to BBT2* and T1 mapping to assess the relationship between the 3 parameters. As expected, there was a good relationship between DBT2* and BBT2* ($R^2 = 0.78$, p< 0.001), and DB T2* and T1 mapping ($R^2 = 0.88$, p< 0.001).

Twenty-one paediatric patients were recruited in this study. Reference ranges were inferred from the adult healthy volunteer population, as a control group was not scanned. Using the adult range, 2 patients had low T2* values (severe and moderate) with corresponding low T1 values and overall, 4 patients had low T1 values. The youngest patient with a low T1 value was 11 years old (T1 874ms; T2* 24ms) suggesting an early onset of myocardial iron deposition in transfusion dependent young children despite early chelation therapy not identified by T2*. Unlike the adult population, T1 values did not reach exceed the upper limit of normal suggesting that fibrosis occurs later in the disease process.

This study has shown that T1 mapping for iron has potential advantages:

- There is increased sensitivity for subtle iron deposition "not seen" by the gold-standard T2* method and therefore may have an important role as a complementary diagnostic tool in patients with equivocal disease particularly patients with T2* values less than 29ms.
- The colour maps allow a rapid visual assessment of myocardial iron without the need for complex off-line analysis.
- Requires a shorter breath hold (9 heart beats (T1) versus 21 heart beats (T2*)). This is reflected in the number of repeated scans for optimal images. In this study 27% required repeated T2* scans for diagnostic images versus 12% for T1 mapping.

There are limitations to this study:

- It is likely that the varied underlying primary and secondary aetiologies
 of iron loading are linked to confounders that may affect the disease
 process or patterns of deposition (T1 is affected by scar and fibrosis).
 Further studies recruiting patients according to underlying disease may
 provide more understanding of the pathophysiology of iron loading.
- The lack of longitudinal and interval scans in this study limits the understanding of subtle iron deposition.
- Patient recruitment, imaging acquisition, and image analysis were all performed by the author of this thesis. To minimise bias in future studies, the imaging datasets can be stored anonymously under a serial number unique to each patient and analysed by an independent assessor blinded to patient background.

4.6 Conclusion

Native myocardial T1 mapping has the potential to have a significant impact in the management of cardiac iron overload. In this large cohort of patients T1 mapping correlated well with T2* and all patients with low T2* values had corresponding short T1. The advantages of T1 mapping are also related to the shorter breath-hold required over 9 heart beats, which is easier for patients to complete the acquisition in one attempt. T1 mapping can also be used at 3T(88), and appears to have specific advantages in mild iron overload. The immediacy of iron quantification through the colour map is of significant workflow utility, and T1 can be used to provide confirmation data for the T2* analysis results. The utility of a simple test, which is easy to interpret, may be key in countries with patients who would benefit the most.

CHAPTER 5 RESULTS: Ultrafast CMR for iron in the

developing world

The work described in this chapter was shortlisted for the SCMR Early Career Award category and is based on the publications listed below. This study was conducted to address an important heath concern in a country with a large population at risk of iron overload. My contribution was study design, obtaining ethical approval, teaching scanning methods to the local Thai team with supervision throughout, and reporting the scans. I also performed the analysis and wrote the manuscript. This study led to the RapidCMR project taking ultrafast CMR to over 10 low-income countries.

- <u>Abdel-Gadir A</u>, Vorasettakarnkij Y, Ngamkasem H, Nordin S, Ako EA, Tumkosit M, Sucharitchan P, Uprasert N, Kellman P, Piechnik SK, Fontana M, Fernandes JL, Manisty C, Westwood M, Porter JB, Walker JM, Moon JC. Ultrafast magnetic resonance imaging for iron quantification in thalassemia participants in the developing world: The TIC-TOC Study (Thailand and UK International Collaboration in Thalassemia optimising ultrafast CMR). Circulation. 2016 Aug 2;134(5):432-4.
- <u>Amna Abdel-Gadir</u>, Yongkasem Vorasettakarnkij, Hataichanok Ngamkasem, Sabrina Nordin, Emmanuel O Ako, Monravee Tumkosit, Pranee Sucharitchan, Peter Kellman, Stefan K Piechnik, Juliano L Fernandes, Mark Westwood, John Porter, John Malcolm Walker, James Moon. Ultrafast CMR to deliver high volume screening of an at risk thalassaemia population in the developing world: Preliminary results from the TIC-TOC study (Thailand and UK international collaboration in thalassaemia using an optimised ultrafast CMR protocol). J Cardiovasc Magn Reson. 2016;18:39.
- <u>Amna Abdel-Gadir</u>, Yongkasem Vorasettakarnkij, Hataichanok Ngamkasem, Sabrina Nordin, Katia Menacho, Heerajnarain Bulluck, Emmanuel Ako, Peter Kellman, Stefan K Piechnik, Juliano L Fernandes, Charlotte Manisty, Mark Westwood, Pranee Sucharitchan, Noppacharn Uprasert, Marianna Fontana, J Malcolm Walker, James Moon, Monravee Tumkosit. Extra-cardiac findings detected by CMR in a Thai population with Thalassaemia major - findings from the TIC- TOC study. Presented at SCMR 2018, Barcelona, Spain.

5.1 Introduction

It is estimated that 1.5% of the world's population are heterozygous carriers of thalassemia mutations, and approximately 60,000 homozygous infants are born every year with TM, making it the most common monogenetic disorder worldwide. (142, 143) Morbidity and mortality of patients is variable worldwide, and a lack of reliable registries raises the suspicion of an underestimation of global prevalence. Survival depends on the availability of regular blood transfusions to correct anaemia and reduce ineffective erythropoiesis, but this can result in organ failure. (11) As described in chapter 1, CMR assessment is the gold standard tool for iron quantification and to help guide chelation therapy, however this method is often perceived as expensive and complex. (127) Serum ferritin levels are used as an alternative surrogate measure, which as previously described can be unreliable.

The idea for this study was conceived when conducting the study described in chapter 4. A cardiologist visiting our institution from Thailand described the need for CMR for iron quantification. Despite the recognised benefits of CMR, MRI scanners in low-socioeconomic countries are often prioritised for other indications including neurology and musculoskeletal pathology. Dedicated magnet time for more rare indications is deemed expensive and there is often a lack of necessary expertise to perform and report dedicated scans. Abbreviated MRI protocols focusing on sequences that provide instantly diagnostic images without the need for complex analysis may provide the solution. The reduction in costs may allow implementation of a CMR for iron service into healthcare particularly when resources are limited.

The aim of this chapter was to demonstrate that abbreviated (ultrafast) CMR protocols using distinctive colour maps, as used in the previous study, can be diagnostic and cost-effective in the management of iron overload. The author wanted to trial this concept in Thailand, which has a high prevalence of thalassaemia, at a government hospital with access to MRI scanners, and with patients likely to benefit from intervention. Additionally, the concept of ultrafast scanning, reducing costs and improving workflow is not limited to countries with low socioeconomic status. In the UK utilisation of ultrafast scanning into the national healthcare system can potentially reduce waiting times, improve productivity and efficiency.

5.2 Hypotheses

We hypothesised that performing CMR scans with abbreviated protocols utilising mapping sequences would provide immediate diagnoses of iron loading and eliminate the need for complex analysis. Additionally, the shorter scanning time would translate into reduced scanning costs allowing implementation into local clinical services. We also hypothesised that T1 mapping would identify iron overload in patients with low T2* values.

5.3 Materials and Methods

A single centre feasibility study performed over a two-day period at the Chulalongkorn Memorial Hospital, Bangkok, Thailand. This is a large public general and tertiary referral centre operated by the Thai Red Cross Society. Thalassaemia patients are referred from local district hospitals and centres close to Bangkok to the dedicated thalassaemia service. The author of this

thesis initiated a collaboration with a Thai cardiologist, and the hospital's haematologists and radiologists. The research proposal and ethics applications were written by the author and principal supervisor (Professor James Moon), and translated to Thai. The author arranged a team consisting of UK and Thai healthcare professionals to execute the study. The UK team included 3 cardiologists, the principal supervisor, and a cardiac physiologist. The Thai team consisted of 2 cardiologists, 1 radiologist, 1 haematologist, and 2 radiographers. Technical support during the study period was provided by a Siemens representative for Southeast Asia, and remotely from a physicist at the National Institute of Health. The research received approval by the Institutional Review Board, Faculty of Medicine, at Chulalongkorn University (IRB No 060/58). All participants provided written informed consent.

5.3.1 Patient cohort

A total of 100 patients with thalassemia major were identified and recruited, by the Chulalongkorn Thalassemia Support Group for CMR assessment at the King Chulalongkorn Memorial Hospital in Bangkok, Thailand. The support group invited all members who were undergoing long-term regular red cell transfusions and taking chelation therapy. Patients were under the care of a regular haematologist at rural satellite units outside of Bangkok linked to Chulalongkorn Memorial Hospital. An up to date medical and drug history was obtained from each patient on the day of scanning. None of the patients had undergone previous cardiac imaging (CMR or echocardiography) as part of their ongoing management.

5.3.2 Normal volunteers

Healthy volunteers were recruited by the Chulalongkorn Memorial Hospital

collaborators through advertising at the Chulalongkorn Memorial Hospital and the affiliated University. All volunteers had no previous history of cardiovascular disease, hypertension, diabetes mellitus, and were not on regular cardioactive medications. Normal ranges for native T1 values were established as recommended.(86)

5.3.3 CMR scanning

All patients underwent a CMR scan using a 1.5T scanner (Aera, Siemens). Each scan comprised of ten breath-holds including a localiser and pilot images, T2*, and T1 mapping of the myocardium (with the liver included), an anatomical HASTE stack, and long axis left ventricular SSFP cine images (figure 21). An optional short axis cine stack was acquired to assess LV function, consisting of an additional two breath-holds, if the long axis cine images were visually abnormal. The protocol was adaptable to clinical findings with options for further more detailed imaging if indicated. T1 and T2* sequences were performed on the same mid-left ventricular short axis slice.

As T1 mapping was not fully standardised at the time of this study, two separate implementations (MOLLI and ShMOLLI sequences from Siemens MyoMaps) were acquired. Quality control of T1 maps, by accredited CMR reporters, was performed by review of the error maps generated with the sequence, and review of the raw images, looking for any artefacts.

The T2* sequence was acquired using an ECG gated single breath hold multiecho sequence to generate eight images with a range of echo times (TE: 2.68-20.11ms at 2.49ms increments) for the heart. Shorter echo times are required for the liver and therefore a standard transverse T2* was acquired with twelve predefined echo times, with a shorter minimum TE (0.99ms) to generate 12 images.

Test: re-test repeatability assessment was performed in sixteen subjects (n=10 patients, n=6 healthy volunteers).

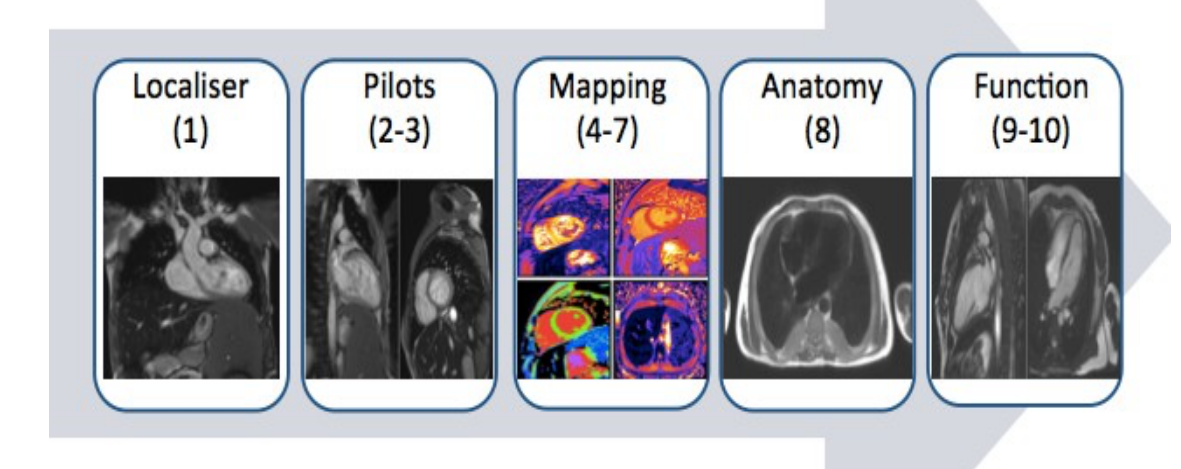


Figure 21. Ultrafast scanning protocol. In 10 breath-holds, iron quantification of liver and heart, cardiac function and extra-cardiac anatomy is acquired. This could be shortened (by omitting one of the T1 mapping sequences) or lengthened (by doing a whole short-axis cine stack in 2 breath- holds).

5.3.4 Image analysis

CMR images were analysed as they were acquired in real-time to ensure excellent quality and no, or minimum, artefacts. Scans were fully reported by the author, with supervision from the primary supervisor, within one minute of scan completion providing diagnostic assessments of myocardial and liver

iron loading status, ventricular function, and extra-cardiac anatomy. These analyses were later repeated using conventional off-line analysis methods. The author and primary supervisor were not blinded to the patients' medical diagnoses, medications, or previous blood biomarkers.

Myocardium: A single region of interest was manually traced in the midventricular short axis septum in all maps (figure 22a, b, c). Care was taken to avoid the endo- and epicardial contours to minimize partial voluming effect.

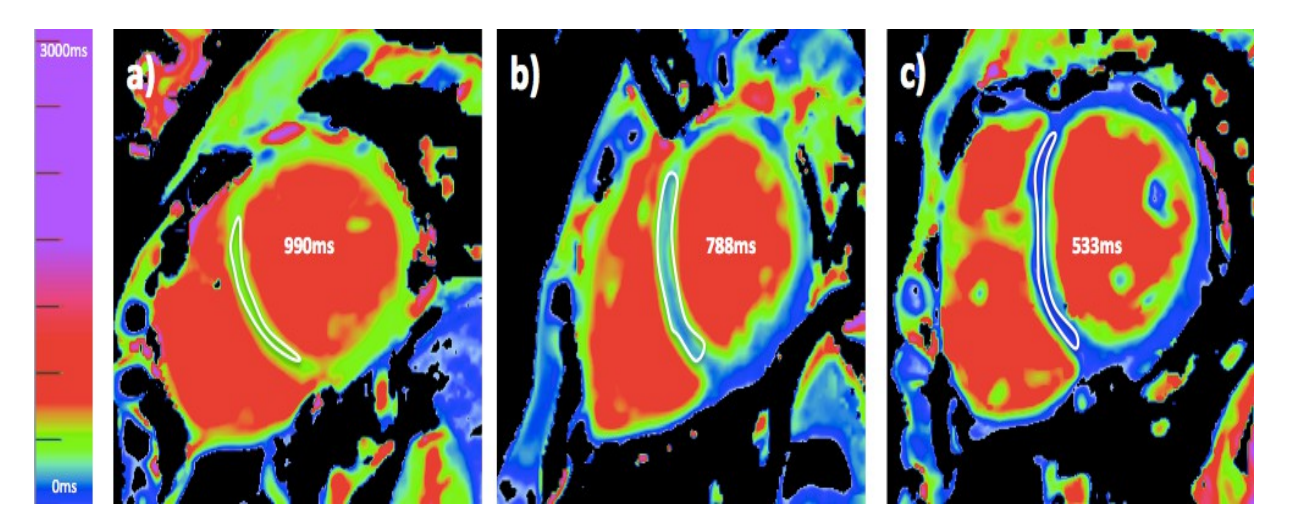


Figure 22. Native T1 myocardial short axis map using the ShMOLLI technique with a) no iron "green"; b) moderate and c) severe iron "blue". The difference is instantly visually recognisable.

Liver: A single axial slice was acquired separately for T2* measurement as lower TE values are required (minimum TE: 0.99ms). A large ROI was traced carefully avoiding the hepatic vasculature (figure 23a, b, c). T1 values were obtained by tracing a ROI in the liver in the myocardial short axis images.

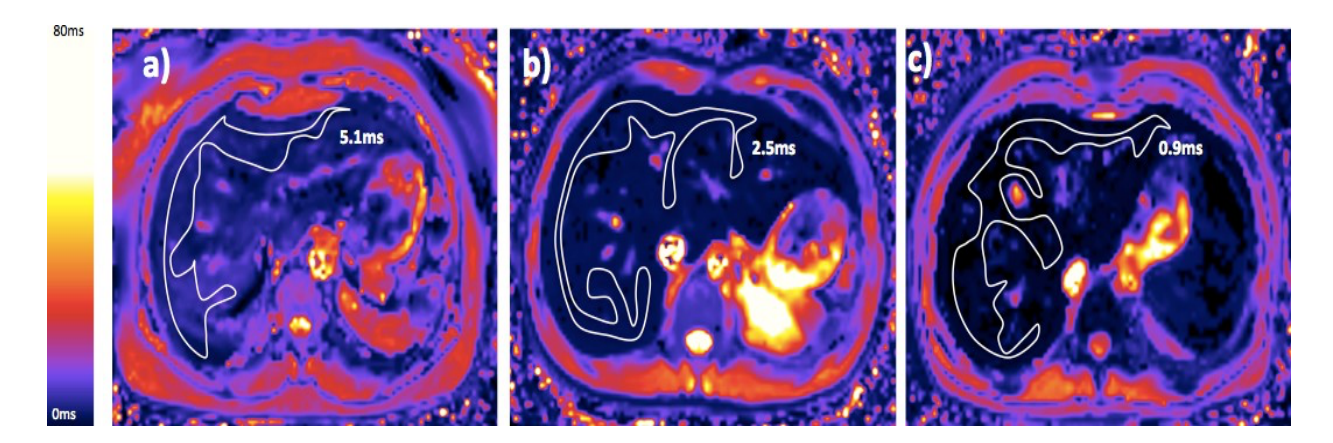


Figure 23. T2* of the liver with region of interest shown. a) mild iron appears purple; b) moderate iron; c) severe liver iron appears dark and almost black.

5.3.5 Blood sampling

Blood samples were taken from each patient prior to the CMR scan for assessment of ferritin and analysed by the hospital laboratory using an electrochemiluminescence immunoassay (Roche Diagnostics International Ltd, Rotkreuz, Switzerland). Average ferritin values were also collated for each patient over the preceding 12months from the hospital electronic database. A minimum of three ferritin measurements was available for each patient.

5.3.6 Statistical analysis

Statistical analysis was performed using IBM SPSS Statistics (version 22).

Normality was assessed using Shapiro-Wilk test. Correlation was assessed using either Pearson's correlation coefficient for normally distributed data or

Spearman's rho for non-normally distributed data. Correlation was used to assess the association between T2* and T1 values with ferritin. For inter- study repeatability the intraclass correlation coefficient (ICC) was calculated. Statistical significance was defined as p<0.05.

5.4 Results

Patients

One hundred patients were invited to participate in the study. 97 patients were scanned (age 34.1 ± 12.1 years; 68% female). Two patients had attended the hospital but felt too unwell to continue with the study. One patient consented to the study but was claustrophobic during the CMR scan and therefore scanning was stopped early. The baseline patient characteristics are shown in table 9.

Normal volunteers

Eleven healthy volunteers were scanned (age 46 ± 12 years; 73% female). Their CMR scans did not reveal any cardiac or extracardiac abnormalities. The healthy range for T2* (heart 33ms ± 4ms; liver 26ms ± 5ms) and T1 (MOLLI 1042ms ± 30ms and ShMOLLI 985ms ± 40ms) were as expected when compared to the UK cohort. Normal liver T1 values for MOLLI were 645ms ± 50ms, and 533ms ± 41ms for ShMOLLI. The lower limit of normal was taken as two standard deviations below the mean healthy volunteer T1.(66) The normal ranges for myocardial and liver T2* were predefined by international consensus.(2)

5.4.1 CMR scan duration

In total, including re-testing for repeatability, 123 scans were performed over the course of 2 days consisting of 12-hour working days. Mean scan duration was 8.3 ± 2.4 minutes with complete analysis within one minute of last image acquisition.

	Patients
N	97
Age (years)	34.1 ± 12.1
Gender (male/female)	31/66
Height (m)	1.57 ± 0.08
Weight (kg)	50.7 ± 9.2
BSA (m ²)	1.48 ± 0.16
Chelation (number of patients)	
DFO	13
DPO	63
Deferasirox	6
DFO + DPO	5
DPO + Deferasirox	2
None	8
Average ferritin (ug/L)	3533 ± 2897
Hb (g/dL)	8.03 ± 1.24

Table 9. Thailand patient baseline characteristics. DFO desferrioxamine; DPO Deferiprone. Average ferritin over one year.

5.4.2 Assessment of cardiac iron in patients

Median myocardial T2* values were 30.9ms (range 1.2ms to 53.7ms). Sixteen patients (16.4%) had myocardial iron loading as defined by T2*: 10 severe, 3 moderate, and 3 mild. Both MOLLI and ShMOLLI had excellent agreement with T2* identifying patients with myocardial iron loading. There was good correlation between myocardial T2* and T1 maps (T2* versus MOLLI r^2 =0.81 (figure 24), and T2* versus ShMOLLI r^2 =0.83; both p<0.0001). This correlation was stronger in the patient population with iron overload as defined by T2* less than 20ms (T2* versus MOLLI r^2 =0.86 and T2* versus ShMOLLI r^2 =0.87).

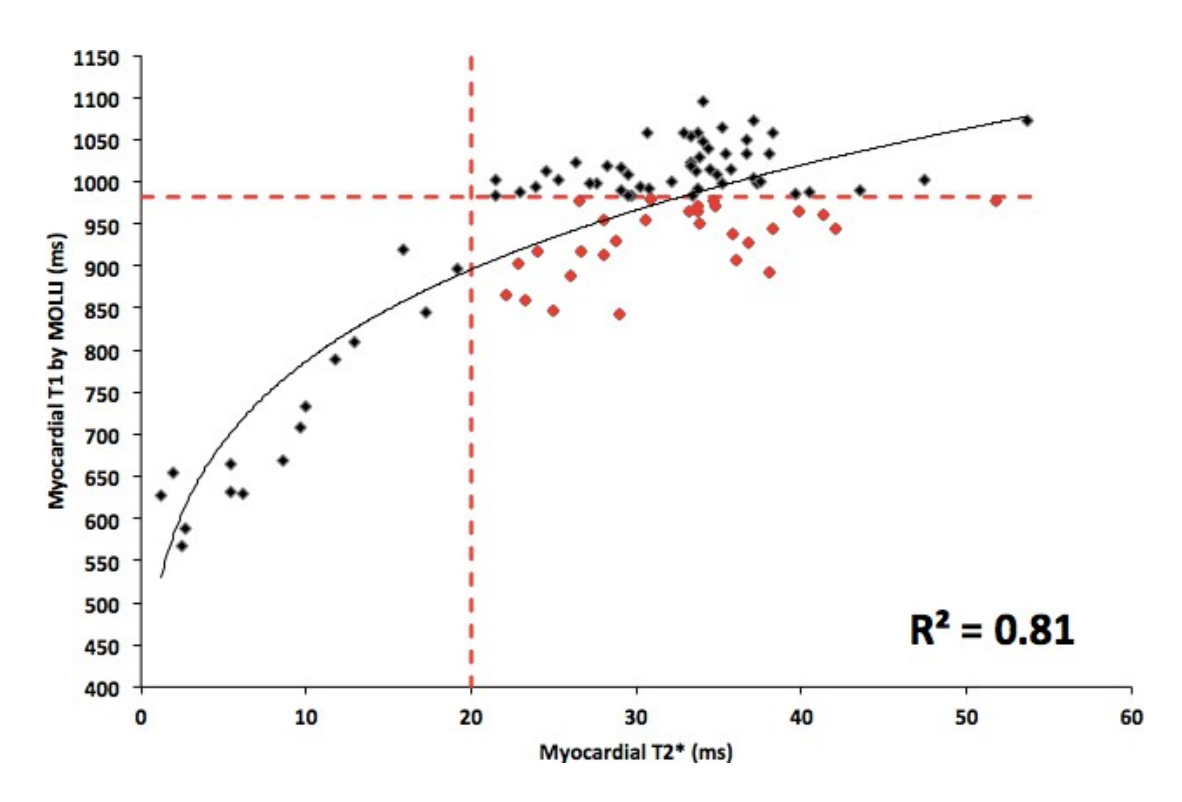


Figure 24. Correlation between T2* and T1 mapping in patients. Red dotted lines equal lower limits of normal. 30 patients with normal T2* values (>20ms) had low T1 MOLLI values (red dots).

All patients with myocardial iron by T2* had low T1 values using both ShMOLLI and MOLLI sequences. However, 30 patients with normal myocardial T2* values (>20ms) had low T1 MOLLI values (less than 982ms); ShMOLLI analysis was similar as 27 patients with normal T2* values had low T1 values (less than 905ms).

5.4.3 Left ventricular systolic function

Visual assessment of LV systolic function on long-axis cine imaging was normal in all patients, including those with cardiac iron. LVEF in all patients was visually greater than 55%. A short axis stack was not required or acquired for any of the patients in this study.

5.4.4 Assessment of liver iron in patients

Median liver T2* values in patients were 1.4ms (0.1ms to 8.8ms). Ninety-six patients had liver iron by the gold standard T2* measurement: 46 (47.9%) with severe loading, 33 with moderate (34.4%), and 17 were mild (17.7%). One patient had a normal liver T2* value. Liver T2* mapping correlated with T1 mapping (T2* versus MOLLI r²=0.33, T2* versus ShMOLLI r²=0.36, both p<0.0001). Using the reference ranges derived from the healthy volunteers MOLLI was normal in 3 patients and ShMOLLI was normal in 2 patients. Of those with liver iron as measured by T2*, MOLLI was normal in 2 patients and normal in 1 via the ShMOLLI method.

5.4.5 Serum ferritin and myocardial iron

Mean ferritin values (at least 3 measurements over 12 months) were 2785ug/L (113 to 15483ug/L) and mean contemporaneous ferritin values were 1995ug/L (147.7 to 13389ug/L). Overall, there was a weak correlation between myocardial T2* and mean ferritin and contemporaneous ferritin ($r^2 = 0.17$, p <0.0001 and $r^2 = 0.16$, p<0.0001, respectively). In severe myocardial iron overload (T2* <10ms) there was no correlation with serum ferritin (p=0.2). Myocardial T1 mapping with both MOLLI and ShMOLLI also correlated weakly with serum ferritin ($r^2 = 0.17$, p<0.005).

The highest measured and mean serum ferritin values in the patient population were 13389.0ug/L and 15483ug/L, respectively, in the same patient who had normal myocardial iron by T2* (30.6ms) but low using T1 mapping (ShMOLLI 856ms). The patient with the lowest cardiac T2* value (T2* 1.2ms, ShMOLLI 570ms, MOLLI 628ms) had an average serum ferritin of 7706ug/L. Eleven patients had serum ferritin levels less than 1000ug/L all of whom had normal T2* values. However, three patients with ferritin levels between 500 -1000ug/L had low T1 values.

Serum ferritin and liver iron

Correlation between liver T2* map and mean ferritin values was also weak ($r^2 = 0.15$, p<0·0001). There was no correlation between severe liver iron (n = 46) and ferritin (p = 0.1). Liver T1 also correlated weakly with ferritin (ShMOLLI $r^2 = 0.21$; MOLLI $r^2 = 0.13$; p<0·005).

5.4.6 CMR analysis quality

Sixteen subjects (10 patients and 6 healthy volunteers) were scanned twice, with a delay of one patient between scans (approximately 6-10minutes), to assess interstudy repeatability. This was high for both T2* and T1 imaging (average ICC 0.97; table 10).

Automated maps with instant analysis were compared with traditional off-line manual analysis. There was excellent agreement between the two methods (T2* ICC 0.91 95% CI 0.86 - 0.94; T1 using both sequences ICC 0.99 95% CI 0.98 - 0.99).

	Mean difference (SD)	ICC (95%CI)
T2* map	2·2ms (1·64)	0.94 (0.84- 0.98)
T1 MOLLI	8·8ms (0·79)	0.99 (0.97-0.99)
T1 ShMOLLI	4·7ms (3·9)	0.99 (0.995- 0.999)

Table 10. Interstudy repeatability in 10 patients and 6 healthy volunteers.

5.4.7 Incidental findings

Sixty patients had incidental findings identified on CMR (table 11). Fifty-eight patients had recognised changes related to thalassemia (figures 25a and 25b). One patient had a newly diagnosed secundum atrial septal defect with a significant shunt (figure 25c) and one patient had changes suggestive of

hepatocellular carcinoma and was referred for urgent assessment. One patient requested plastic surgery following his scan due to longstanding changes in his appearance and difficulties breathing. His CMR showed severe iron loading and extensive extramedullary haematopoiesis. He was referred to the local Ear, Nose, and Throat team for further assessment (figure 26).

Incidental Findings	n
Extramedullary haematopoiesis	
 Paravertebral 	45
Rib expansion	2
Enlarged Thymus	3
MPA dilatation	11
Pericardial effusion	2
Aortic dilatation	1
Pleural effusions	1
Cysts	
• Liver	2
• Thyroid	1
ASD	1
Liver mass	1
Breast prosthesis	1

Table 11. Incidental anatomical findings in the Thailand group using CMR.

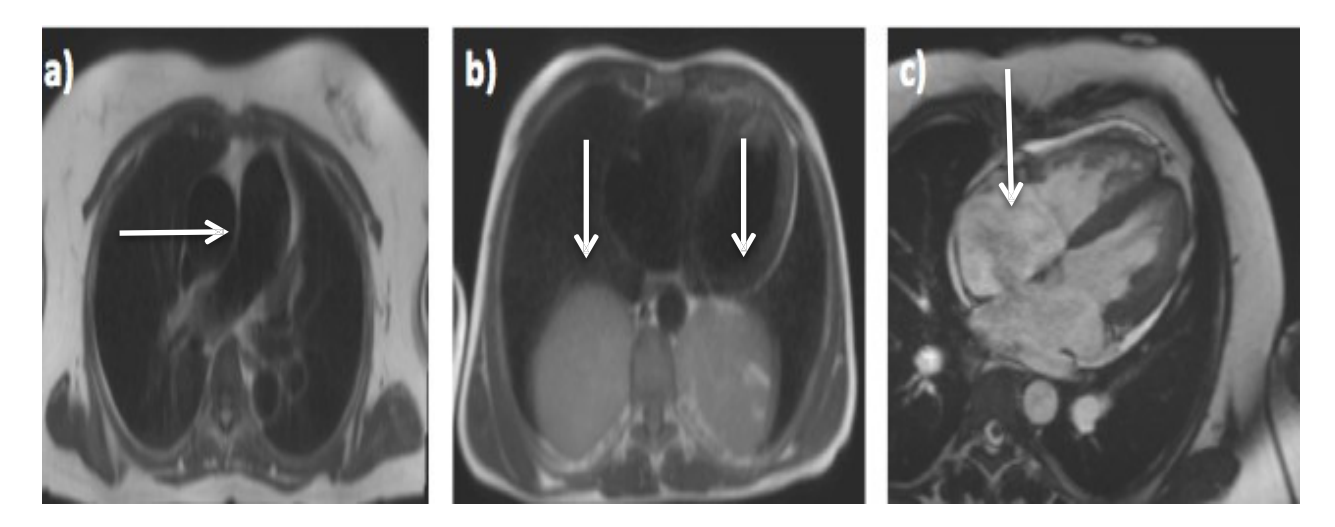


Figure 25. Significant extra-cardiac findings a) dilated main pulmonary artery; b) massive paravertebral extramedullary haematopoiesis; and c) unrelated to thalassaemia a secundum atrial septal defect with significant shunt.

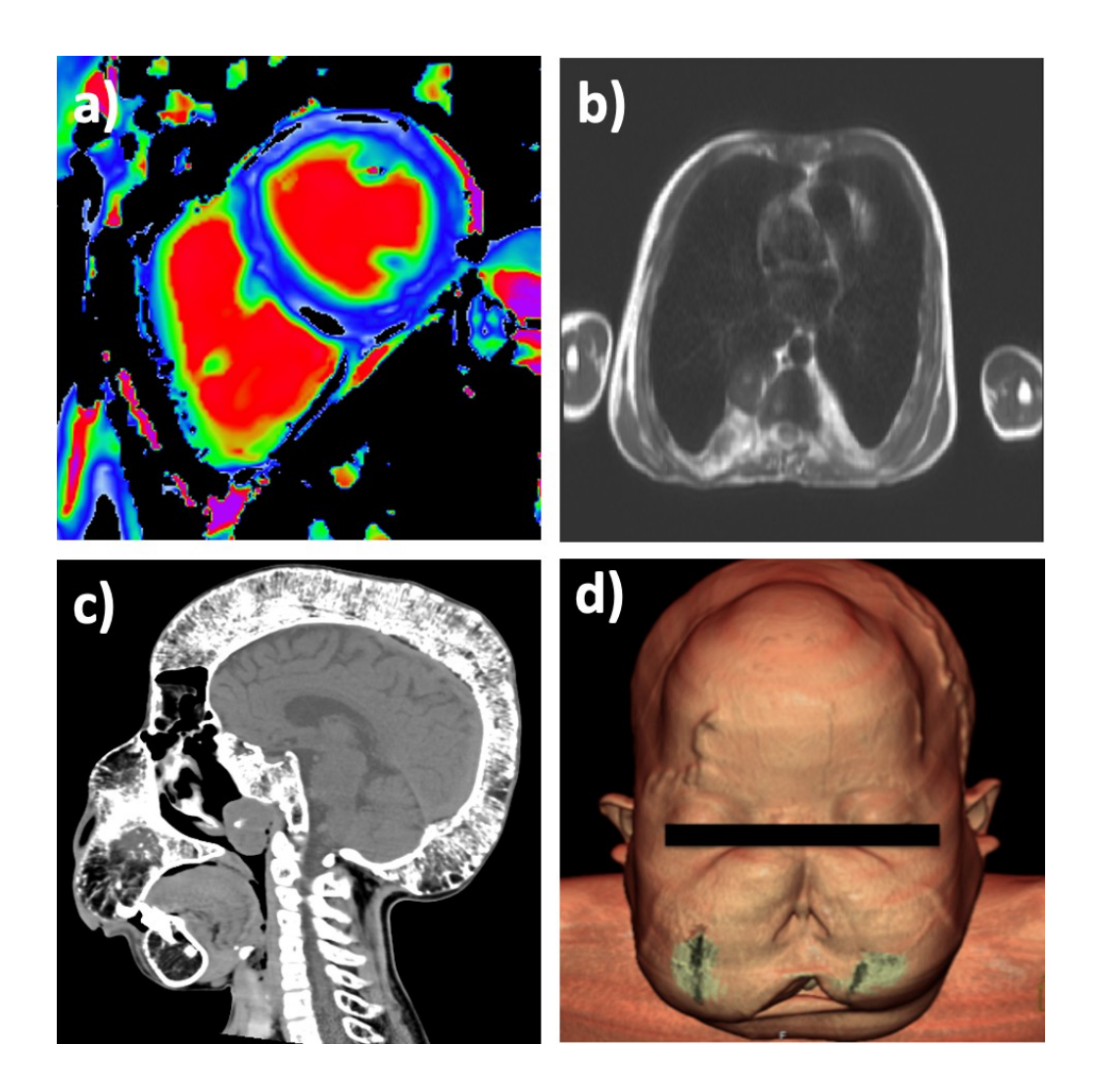


Figure 26. Patient with severe cardiac iron loading and evidence of extensive extramedullary haematopoiesis: a) ShMOLLI T1 indicating severe myocardial iron overload; b) paravertebral extramedullary haematopoiesis on CMR; c) widened diploic space and vertical striations giving rise to the characteristic hair-on-end appearance; d) CT facial reconstruction. Images used with patient's permission.

5.5 Discussion

In the developed world, the MRI T2* method when linked to therapy has changed the prognosis of patients dependent on multiple blood transfusions. However, patients most likely to benefit from this technique live in low and middle-income countries where MRI is seldom used for iron, and serum ferritin is the primary method used for the clinical management of iron loading.

This is the first large-scale ultrafast CMR study for the diagnosis of iron and the aim was 2-fold. Firstly, to demonstrate the cost-effective and diagnostic advantages of abbreviated CMR protocols for iron loading using mapping sequences, and secondly to demonstrate that T1 mapping for iron can be diagnostic in an at-risk population.

In total, including patients, volunteers, and scanning for repeatability, 123 scans were performed over a period of 2 days. Local Thai MRI radiographers were trained by the author and the principal supervisor (Professor James Moon) to perform the predefined protocol for iron to ensure continued scanning of patients after the study. Scan duration was 8.3 ± 2.4 minutes including analysis time, which is approximately 4 times faster than a standard non-contrast CMR. The shortest recorded scanning time was 4 minutes and 13 seconds.

This study diagnosed new myocardial iron in 16% of patients using the gold standard T2* method of whom 62.5% had severe iron loading, a finding lower than expected based on previous studies in South East Asia.(144) None of

the patients involved had previous CMR scans to compare. As expected T1 mapping, using both preparations, showed good agreement with T2* as demonstrated in the UK T2*/T1 work in this thesis (chapter 4). Thirty patients with normal T2* values had low T1 values suggesting increased sensitivity of T1 in the recognition of mild iron deposition undetected by T2*. As the incidence of heart failure increases by up to 50% in iron overload the clinical implications of this finding may benefit patients with borderline T2* values who may require more intense monitoring or changes in chelation therapy to prevent further iron loading.(57) Contrary to previous findings left ventricular function was visually normal in all patients including those with the highest iron content.(140) As formal volume assessments for function were not conducted in this study subtle changes in ventricular function may have been missed.

Almost all patients were diagnosed with previously unknown liver iron loading. T2* correlated with T1 mapping, however 2 patients with low T2* had normal T1. This may be explained by the confounding effect of co-existing liver pathology. In Thailand there is an increased prevalence of hepatitis B and C, which may lead to fibrosis.(145, 146)

Serum ferritin is a reflection of body iron stores, but measured values are affected by a number of confounding factors including inflammation, liver disease, and excess alcohol consumption.(17, 147) Although a poor indicator of myocardial iron loading long term control of ferritin can provide valuable diagnostic information.(148) Ferritin levels less than 1000ug/L have been

linked to a lower probability of heart failure and prolonged survival.(61) In this cohort, ferritin values correlated poorly with cardiac iron ($r^2 = 0.17$) but also unexpectedly poorly with liver iron ($r^2 = 0.15$). Three patients with ferritin levels between 500 -1000ug/L had low T1 values.

For liver, the reduced correlation may be explained by the increased prevalence of hepatitis in Thailand(145, 146) or the narrow range of liver iron found as most patients were found to have severe iron loading. Categorising the ferritin levels further into mild, moderate, and severe (>3000ug/L) did not show or strengthen the relationship.

This study has demonstrated that by scaling down the protocols and using mapping with instantaneous analysis, MRI can be high volume, reliable and low cost with important clinical yield. MRI scans at the study centre typically cost \$300 USD per scan (allocated time 1 hour). By reducing scanning times and completing a minimum of 6 scans per hour, the suggested reduction cost to \$50 USD makes CMR a highly feasible option. This study also demonstrates that not all patients require regular CMR scans. Although recognised as a poor quality test for iron loading, ferritin is a potential gatekeeper to the MRI department as all patients in this study with cardiac iron had ferritin levels greater than 1000ug/L. Algorithms to triage could be developed where MRI could be targeted for optimal yield.

There were limitations in this study. This study was conducted in a city hospital where disease prevalence may be underestimated and not reflective

of Thailand's urban areas where patients may be on the extreme end of the disease spectrum. Additionally, the increasing use of 3T scanners in Thailand, and Southeast Asia, limits our data to 1.5T as we did not determine the feasibility of ultrafast scanning on a 3T scanner.

5.6 Conclusion

Ultrafast scanning for iron can be diagnostic with the advantage of cost reduction and an improvement in workflow. The international consensus limiting T2* to 1.5T makes T1 mapping a more attractive option in countries where access to 3T scanners is available. The concept of ultrafast scanning is not limited to countries with low socioeconomic status. In the UK utilisation of ultrafast scanning into the national healthcare system has the potential to reduce waiting times, improve productivity and efficiency. Based on this project further work is currently in motion focusing on delivery, cost- effectiveness, and outcomes with the aim to distribute this technology globally.

CHAPTER 6 RESULTS: CMR FOR COBALT

This chapter is based on the publications and abstract presentations listed below. My contribution was study design, obtaining ethical approval, patient consent, performing and reporting the CMR scans. I analysed the data and wrote the manuscripts.

- Abdel-Gadir A, Berber R, Rosmini S, Captur G, Nordin S, Culotta V, Palla L, Kellman P, Lloyd GW, Skinner JA, Noon JC, Manisty C, Hart AJ. Assessing for cardiotoxicity from metal-on-metal hip implants with advanced multimodality imaging techniques. J Bone Joint Surg Am. 2017 Nov 1:00(21):1827-1835
- Abdel-Gadir A, Berber R, Porter JB, Quinn PD, Suri D, Kellman P, Hart AJ, Moon JC, Manisty C, Skinner JA. Detection of metallic cobalt and chromium liver deposition following failed hip replacement using T2* and R2 magnetic resonance. J Cardiovasc Magn Reson. 2016 May 6:18(1):29

6.1 **Introduction**

There has been great concern regarding the over one million implanted metal-on-metal (MoM) hip prostheses.(7) Release of non-particulate debris and cobalt and chromium ions, from repeated wear and corrosion, have been reported to cause significant harm.(149) The resulting local and systemic toxicity led to highly prolific safety alerts by the regulatory agencies, device recall, and a subsequent increase in the number of surgical revisions performed.(7, 150, 151) Elevated circulating levels of cobalt have also been linked to thyroid, neuro-ocular, fatal cardiac events, and a reported 3-fold increased risk of heart failure in male patients with MoM hips.(9, 10, 152, 153) Cobalt is considered predominantly responsible for the local and systemic reactions seen. As described in chapter 1, the systemic effects of cobalt are well described with both beneficial and deleterious actions recognised. Reported cases of cardiomyopathy where biopsies or autopsies have been performed confirmed presence of cobalt in the heart.(113, 122, 123)

Chromium, an essential nutrient for humans required for sugar and fat metabolism, exists in a number of valence states (II, III, and VI) and toxicity depends on the oxidation state in which it circulates.(154, 155) Trivalent (Cr³⁺) appears to be the most stable form, and forms stable organic complexes with proteins, amino acids, and other organic salts.(155) Hexavalent chromium (Cr⁶⁺) is the most toxic form and has mutagenic characteristics.(156) Analytical studies of tissues surrounding MoM prostheses have only identified the trivalent form, typically as chromium phosphate.(157)

Serial measurements of blood metal levels are recommended by the medical device regulatory bodies, including the US Food and Drug Administration (FDA) and the Medicines and Healthcare products Regulatory Agency (MHRA) to help guide management. In patients with MoM implants a threshold of 7 parts per billion (ppb) (119 nmol/L cobalt or 134.5nmol/L chromium) is used to track the risk of local soft tissue reactions and the potential for further surgery.(116) Presently non-invasive methods for the detection of systemic toxicity or organ deposition do not exist. Non-invasive iron quantification of the myocardium and liver using the T2* MRI sequence is a well-recognised method for the assessment of iron overload.(55, 64) As cobalt exhibits similar magnetic properties to iron, CMR has the potential to non-invasively detect tissue deposition of metal ions and act as a screening tool for patients at risk of systemic toxicity.(117)

The aim of this chapter was 2-fold. Firstly, to seek evidence of metal deposition using CMR in patients with high circulating blood metal levels. Secondly, to use advanced multi-imaging modalities to assess for early cardiotoxicity.

6.2 Hypotheses

We hypothesised that native T1 mapping and T2* values would be shortened in patients with metal-on-metal hips with high blood metal-ion levels, and that changes may be an early marker of organ dysfunction.

6.3 Materials and Methods

The research received approval by the University College London/ University College London Hospitals Joint Committees on the Ethics of Human Research Committee (reference 14/LO/1722). The study was also registered on Clinicaltrials.gov (NCT02331264).

6.3.1 Patient cohort

Patients over the age of 18 with MoM hips or ceramic-on-ceramic (CoC, control) hip implants were recruited from the UK's national centre for hip revision surgery. All had hip implants for at least 12 months at the point of recruitment. The groups were divided into 3 age and sex-matched groups (Group A, B and C) based on the type of hip prosthesis and the measured blood metal ion levels at point of recruitment:

- Group A comprised of patients with CoC-bearing implant and normal whole-blood metal ion levels
- Group B patients with a MoM implant and low whole-blood metal ion levels (<7 ppb)
- Group C patients with a MoM implant and raised whole-blood metal ion levels (<7ppb).

CoC was chosen over the other prosthetic hip implant metal-on-polyethylene as there was concern regarding metal debris arising through trunnionosis. Trunnionosis, a process defined as wear of the femoral head and neck interface, is increasingly acknowledged as a growing cause of arthroplasty failure and accounts for approximately 2% of all revisions.(158) Seven ppb

was used as a normal cut-off as this represents the UK Medicines and Healthcare products Regulatory Agency (MHRA) recommended threshold.(115)

Exclusion criteria included prior hip revision surgery, atrial fibrillation, and impaired renal function in addition to standard contraindications for MRI including claustrophobia and pacemakers.

All tests were completed in a single visit (figure 27). The investigators were blinded to the study groups during data acquisition and analysis until the study was completed.

6.3.2 Normal volunteers

Healthy subjects were recruited through advertising in our local hospital and University sites. All subjects had no history of cardiovascular disease, hypertension, diabetes mellitus, and were not on regular cardioactive medications. Normal ranges for myocardial T2* and native T1 values, for the scanner used in this study, were established (as previously described).

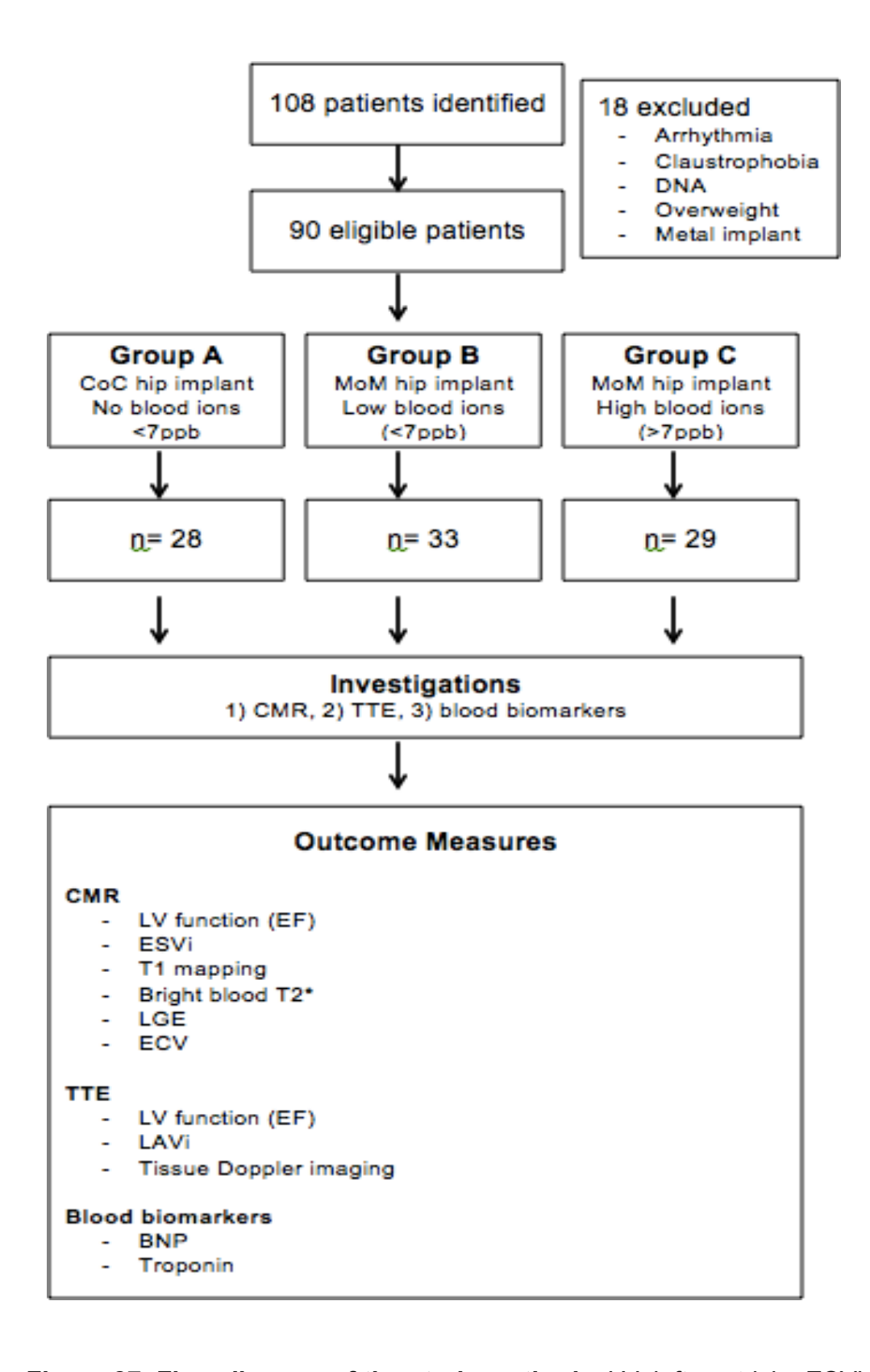


Figure 27. Flow diagram of the study methods. LV: left ventricle. ESVi: end systolic volume indexed. LGE: late gadolinium enhancement. ECV: extracellular volume. TTE: transthoracic echocardiogram. LAVi: left atrial volume indexed. BNP: B-type natriuretic peptide

6.3.3 CMR scanning

All patients underwent a single CMR scan with a Siemens 1.5T clinical scanner (Avanto, Siemens Healthcare, Germany). Each scan included acquisition of long and short axis left ventricular SSFP cine images, and assessment of left ventricular volumes, mass, BBT2*, and T1 mapping sequences (MOLLI and ShMOLLI), using previously published techniques.(65, 83) Additional T2* liver sequences were acquired with a shorter first TE than for the myocardium (0.99 – 16.5ms).

Late gadolinium-enhancement images were acquired using a motion corrected phase sensitive inversion recovery sequence to identify scaring and fibrosis of the myocardium. Patients were administered 0.1mmol/kg of gadolinium-based contrast medium (gadoterate meglumine – Dotarem, Guerbet SA, Paris, France). Fifteen minutes post-contrast injection, T1 sequences were repeated for automated ECV quantification displayed as parametric maps.

6.3.4 Image analysis

Image acquisition, analyses, and clinical reporting were performed by the author and verified by a Level 3 certified CMR reporter. The author was blinded to the study groups. An independent statistician performed unblinding once all the data had been acquired and analysed.

Left ventricular volumes, ejection fraction, and mass were calculated offline from the acquired CMR data using standard techniques and the dedicated software CMR tools (Cardiovascular Imaging Solutions, London, UK). Thresholding methods were used, and papillary muscles were

considered part of the left ventricular myocardium. Volumes were indexed to body surface area. For T2* and T1 mapping measurements, a single region of interest (ROI) was manually traced in the mid-ventricular short axis septum carefully avoiding the endo- and epicardial contours to minimize partial-voluming effect. BBT2* decay was calculated using the FDA approved Thalassaemia-Tools plugin for CMR tools (Cardiovascular Imaging Solutions, London, UK). The signal intensity was plotted against each echo time and the T2* value was calculated from the resulting exponential decay curve. The presence of LGE was determined by visual assessment by two independent reporters. ECV was calculated via a fully automated method that calculates ECV parametric maps(126), based on the standard formula:

$$ECV = (1 - haematocrit)*[\Delta R1_{myocardium}] / [\Delta R1_{blood}]$$

6.3.5 Blood and cardiac biomarkers

Blood sampling was performed prior to undergoing CMR scanning. Whole-blood cobalt and chromium levels were measured using inductively coupled mass plasma mass spectrometry in the same UK reference laboratory to eliminate interlaboratory variation. The MHRA advises that cobalt and chromium ion measurements are carried out by laboratories participating in the Trace Elements External Quality Assessment Scheme (TEQAS). The accuracy and reliability of these measurements are regularly audited and have excellent agreement (96.4%; SD 2.33%, coefficient of variation 2.3%) across the laboratories. Brain natriuretic peptide

(BNP) and troponin levels were also measured as markers of myocardial involvement.

6.3.6 Transthoracic echocardiography

Transthoracic echocardiograms (TTE) were performed using a Vivid E9 ultrasound machine (GE Healthcare) to assess early changes suggestive of systolic dysfunction. Measurements were in keeping with The British Society of Echocardiography standard minimum dataset protocol.(159) These included acquisition of standard 2-dimensional views, M-mode, and longitudinal Tissue Doppler Imaging (LV lateral S' and septal S').

6.3.7 Statistical analysis

Statistical analysis was performed by an independent statistician as the author was blinded to the groups. The 3 groups were assessed for matching using chi-square tests for binary variables and analysis of variance (ANOVA) for continuous variables. The metal ions were not normal distributed and therefore non-parametric tests on medians were used to compare ion levels between groups. Correlations between ion levels and T1 mapping, T2* and left ventricular function were calculated using Pearson correlation coefficient.

6.4 Results

One hundred and eight patients were identified and recruited. Eighteen patients were excluded from the study: six patients were found to have a cardiac arrhythmia with rapid ventricular rates and therefore difficult to obtain images for diagnostic interpretation, 5 did not attend their allocated scan

appointments, 4 patients were claustrophobic, 2 were overweight and could not fit in the MRI scanner, and 1 patient was found to have a pacemaker on the day of the study and therefore excluded. In total ninety patients enrolled and completed the study These groups comprised of 28 patients with CoC implants (Group A), 33 patients with MoM implants with a low metal-ion levels (Group B), and 29 patients with MoM implants and high metal-ion levels (Group C). Patients were matched for age and sex, and their baseline characteristics are summarised in table 12. There were no significant differences between the groups with regards to cardiovascular risk factors or cardioprotective medications.

	All patients	Group A	Group B	Group C	P value
N	90	28	33	29	
Age (yr)	64.9± 10.5	65.3±8.80	61.9±11.9	67.6±10.8	0.115
Male/female	30/60	7/21	12/21	11/18	0.525
Time since implantation (yr)	8.76±2.34	7.86±2.62	9.03±1.87	9.39±2.52	0.041
BMI (kg/m2)	28	28	28	27	0.929
Comorbidities					
Diabetes (no.;%)	3; 3	1; 4	1; 3	1; 3	0.982
Hypertension	32; 36	11; 39	12: 36	9; 31	0.715
Hypercholesterolaemia	20; 22	9; 32	4; 12	7; 24	0.105
Medications (no.; %)					
Beta-blocker	5; 6	2; 7	0	3; 10	0.181
ACE inhibitor*	10; 11	5; 18	3; 9	2; 7	0.326
Thiazide diuretic	8; 9	2; 7	4; 12	2; 7	0.741
Calcium channel blocker	15; 17	7; 25	4; 12	4; 14	0.289
Aspirin	3; 3	1; 4	0	2; 7	0.317
Statin	20; 22	9; 32	4; 12	7; 24	0.121
Proton pump inhibitor	18; 20	8; 29	3; 9	7; 24	0.101
Thyroxine	8; 9	4; 14	4; 12	0	0.108
Whole blood levels					
Cobalt level (ppb)	10.9	0.17 (0.10-0.47)	2.47 (0.73-6.97)	30.0(7.54-118)	<0.0001
Chromium level (ppb)	7.7	0.74 (0.53-1.42)	2.84(0.94-10.5)	19.6(1.71-69)	<0.0001

Table 12. Patient demographics by study group. Age is displayed as mean and SD. Cobalt and chromium levels are displayed as mean with range in ppb. *ACE= angiotensin-converting enzyme.

The mean cobalt levels in groups A, B, and C were 0.17 ± 0.08 , 2.47 ± 1.81 , and 30.0 ± 29.1 ppb, p<0.0001, respectively. The mean chromium levels (ppb) were 0.7 ± 0.18 , 2.84 ± 2.34 , and 19.6 ± 20.33 ppb, p<0.0001, for groups A, B, and C respectively. The overall mean time from implantation of the hip prosthesis to the date of recruitment was marginally shorter in group A than in group B or C (7.9 ± 2.6 versus 9.0 ± 1.9 and 9.4 ± 2.5 years, p<0.05).

6.4.1 CMR T1 mapping

Using the ShMOLLI and MOLLI techniques myocardial T1 values were within the normal range in all 3 groups. MOLLI values were 1030 ± 42ms in Group A, 1014 ± 33ms in Group B, and 1022 ± 37ms in Group C, p=0.64. Myocardial ShMOLLI values were 961± 31ms, 957± 30ms, and 956 ± 44ms in groups A, B, and C respectively, p=0.82. All patients with high metal-ion levels (Group C) had T1 values within the normal range, with no outliers. Combining the MoM groups together (groups B and C) and comparing the T1 values with group A (CoC) did not reveal significant difference in T1 results using MOLLI or ShMOLLI, p=0.15 and p=0.54 respectively.

Liver T1 values did not differ between or among the 3 groups using MOLLI and ShMOLLI. Liver MOLLI values were 615.6 ± 71.7 ms in Group A, 596.0 ± 77.7 ms in Group B, and 583.7 ± 49.5 ms in Group C. ShMOLLI values were 558.3 ± 45.9 ms in Group A, 538.9 ± 50 ms in Group B, and 543 ± 45.8 ms in Group C. All patients in Group C had normal liver T1 values (table 13).

6.4.2 CMR T2*

Myocardial T2* values were normal in the 3 groups with no significant difference among them (p = 0.69). Combining the MoM groups (Group B and C) and comparing T2* values with Group A did not reveal any differences in T2* values. All patients with high blood metal-ion levels had T2* values above 20ms. Liver T2* values were normal in all groups with no difference detected within the groups or when the MoM groups were combined and compared with group A.

6.4.3 Left ventricular size and function

By CMR assessment all patients had normal left ventricular function as defined by an ejection fraction greater than 55%. There was no significant difference among the groups (group A 70.1% \pm 6% versus group B 69.5 \pm 7% versus group C 70.6% \pm 5%, p=0.75). Additionally left ventricular end systolic volumes indexed (LVESVi) to body surface area did not differ when comparing the patient groups (p=0.86). Combining the MoM groups (B and C) and comparing to the CoC group (A) did not reveal any significant differences in LVEF or LVESVi.

Like the CMR assessment echocardiography did not show significant differences between the groups with regards to LV function (group A $65\% \pm 6\%$ versus group B $62\% \pm 7\%$, versus group C $63\% \pm 6\%$, p=0.28). There were also no significant differences in lateral and septal S' velocities between the groups (p=0.24 and 0.16,respectively). Left atrial volume was similar among the 3 groups (p=0.19).

		А	В	С	A vs. B vs. C	A vs. B and C
N		28	33	29		
CMR						
Olviix	LVEF (%)	70 ± 5	69 ± 7	71 ± 5	p= 0·75	p= 0·96
	ESVi (ml/m²)	21 ± 6	21 ± 8	20 ± 5	p= 0·86	p=0·99
	T1 MOLLI heart	1030 ± 42	1014 ± 33	1022 ± 37	p=0·64	p=0·15
	(NR 949- 1101ms)					
	T1 ShMOLLI heart	961 ± 31	957 ± 30	956 ± 44	p= 0.82	p=0.54
	(NR 900- 1020ms)					
	T2* heart	31 ± 5	31 ± 6	32 ± 6	p=0·69	p=0.85
	(Normal >20ms)					
	ECV heart	0.28 ± 0.03	0.27 ± 0.03	0.29 ± 0.04	p=0·28	p=0·62
	T1 mapping liver	616 ± 72	596 ± 78	584 ± 49	p=0·21	p=0·11
	(ms)					
	T2* liver	25 ± 4	26 ± 7	25 ± 5	p= 0.67	p=0.92
	(Normal >6.3ms)					
	ECV liver	0.29 ± 0.04	0.30 ± 0.03	0.30 ± 0.04	p=0·62	p=0·36
	(Normal <0.31)					
Blood						
	BNP (pmol/L)	11 ± 10	10 ± 8	25 ± 61	p=0·32	p=0·52
	Troponin (ng/L)	7.38 ± 6.9	7.16 ± 5.0	8.62 ± 10.2	p=0.77	p=0.78

Table 13. Summary of CMR and biomarker results. Comparison of CMR findings between the 3 groups. Group A: CoC; Group B: MoM with low blood levels; Group C: MoM with high blood levels.

6.4.4 Assessment of fibrosis and scar

Late gadolinium enhancement (LGE) was detected in 5 patients: 3 patients in Group B, 1 in group C, and 1 patient in group A. In group B, 2 patients had a small amount of mid-wall fibrosis, and one had a small area of subendocardial scar in the mid anterolateral wall. In group C, one patient had basal inferolateral LGE in a non-ischaemic distribution (figure 28). The patient in group A had a small area of midwall LGE (figure 29).

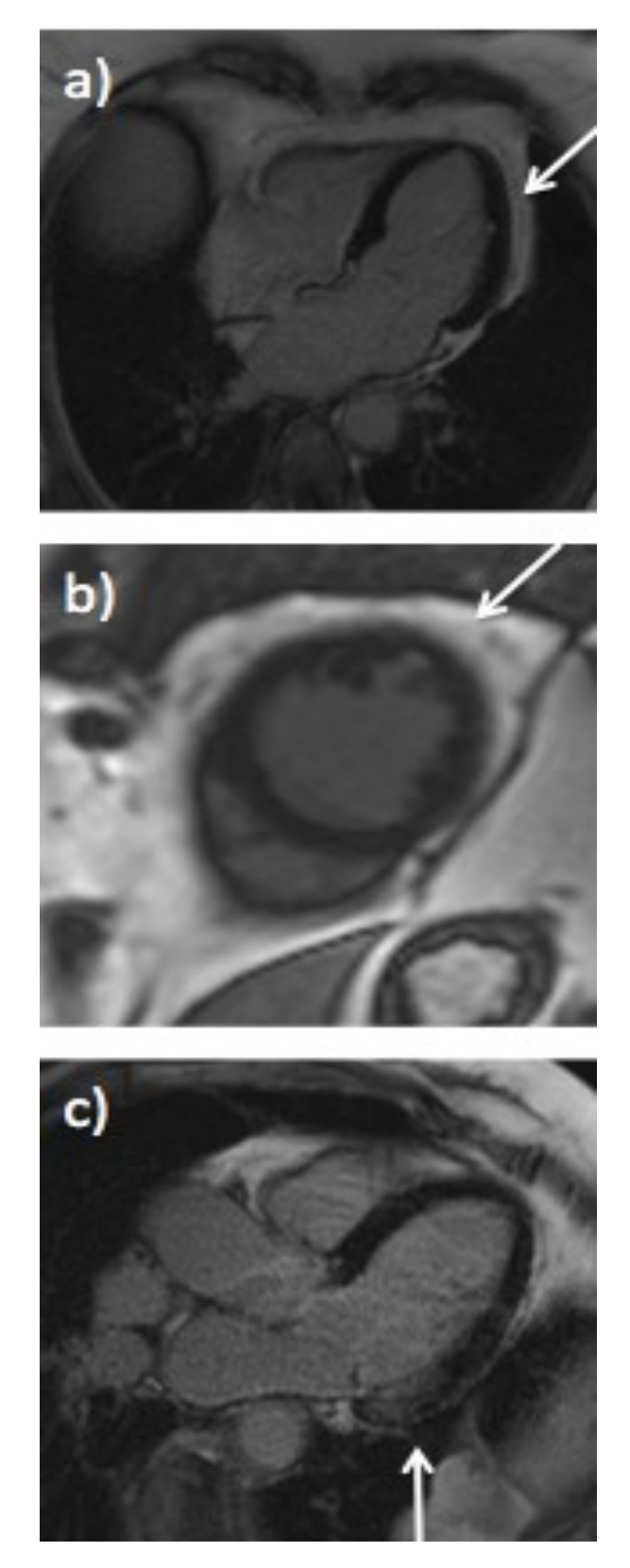


Figure 28. CMR images of late gadolinium enhancement. Examples of (a) 4-chamber view and b) SAX view demonstrating subendocardial LGE in the same patient; and (c) basal inferolateral LGE

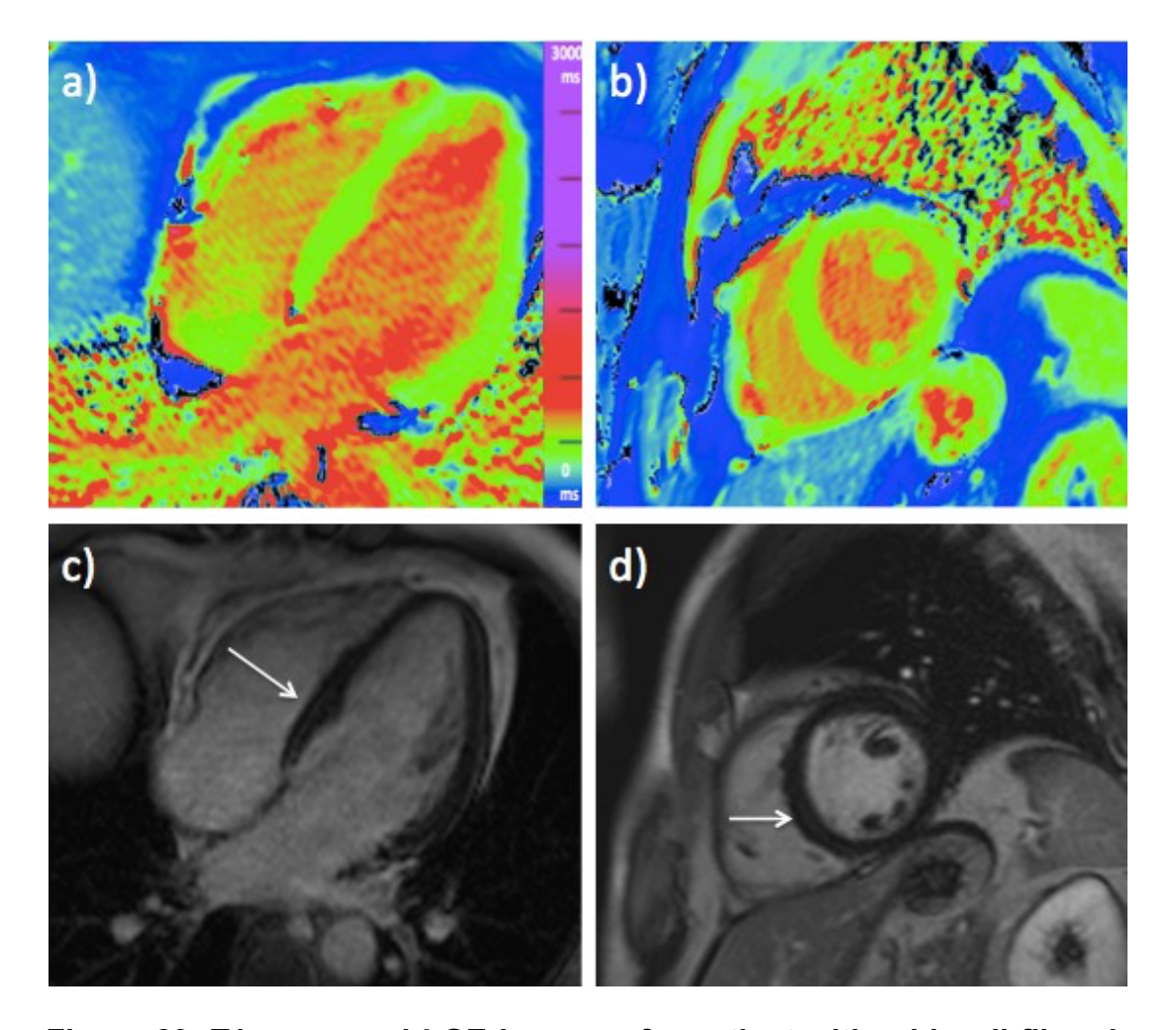


Figure 29. T1 maps and LGE images of a patient with mid-wall fibrosis. ShMOLLI images of a) 4-chamber and b) 2-chamber view and the corresponding LGE images (c and d) on the same patient. The patient had normal T1 values.

Assessment of diffuse fibrosis using post-contrast T1 mapping did not reveal any differences between the groups (p = 0.28). ECV was normal in all patients with no outliers (figure 30).

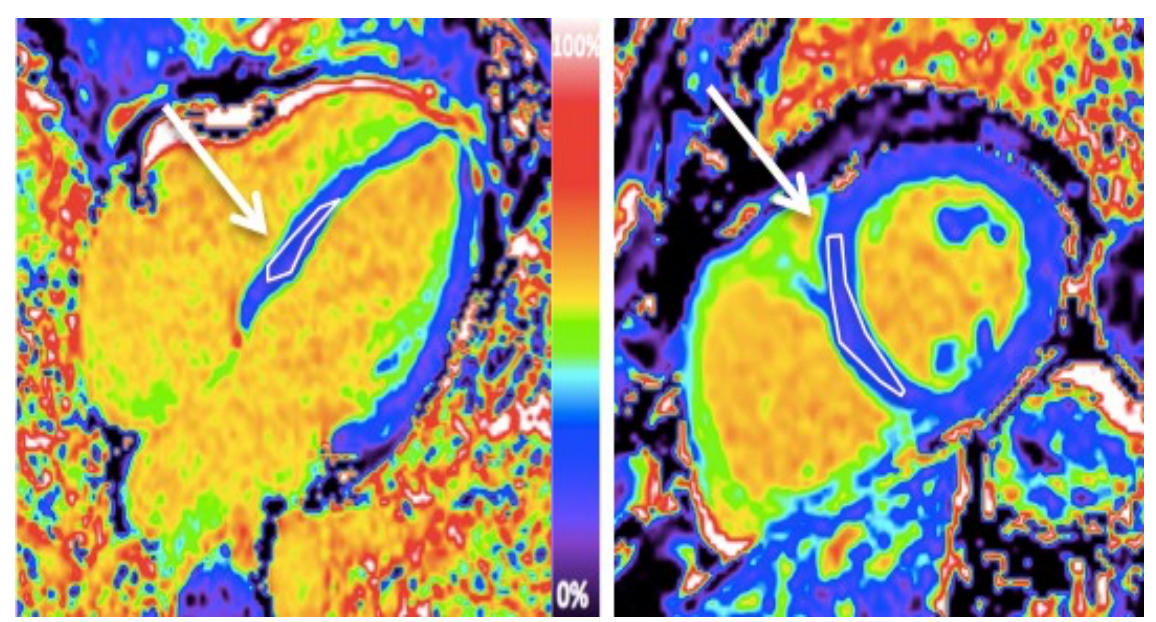


Figure 30. Examples of ECV maps of a 4Ch view and a SAX slice. A map is generated after acquisition of a post-contrast T1 map 15 minutes after an intravenous bolus of contrast is administered. A ROI of interest is drawn to provide an ECV value. All patients had normal ECV values.

6.5 Discussion

Cardiotoxicity from cobalt/chromium has caused much anxiety from healthcare professionals and patients alike, fueled by the increasing number of isolated cases reported in the literature. A non-invasive method for organ assessment of metal deposition from implanted prostheses does not exist.

In this study we investigated the use of CMR for the assessment of myocardial and liver involvement in 3 distinct groups defined by their hip prosthesis and levels of circulating blood cobalt and chromium. Gold standard methods were used to quantify metal deposition, and assess cardiac function and fibrosis. The author was blinded to details regarding group allocations, type of prosthesis, and circulating blood metal ion levels.

Previous work by the author demonstrated the potential use of CMR for the detection of cobalt and chromium deposition in the liver in a patient with high blood levels in which T2* had detected biopsy proven cobalt/chromium.(117) We therefore hypothesised that states of metal deposition would mirror the effect of iron, shortening the T1 and T2* values in patients with high circulating levels. However, in this study both T1 mapping and T2* techniques failed to identify any changes suggestive of metal deposition in the myocardium and liver. Patients with the highest amount of circulating blood metal ions had normal T1 and T2* values. Additionally using post-contrast T1 mapping for the assessment of diffuse fibrosis failed to demonstrate abnormal values. These methods may have been unsuccessful in identifying metal deposition due to:

- 1. T1 mapping, T2* and fibrosis imaging may lack sensitivity for detecting early or mild disease in the myocardium and liver.
- There was no metal deposition in the myocardium or liver occurring in this patient population despite recruiting patients with circulating levels defined as "high" by MHRA standards.

Scar imaging using LGE sequences identified 5 patients with abnormal fin–ings - none in keeping with previous case reports.(152, 160) One patient with high circulating blood metal ion levels (cobalt 13ppb and chromium 11ppb) had basal inferolateral LGE in a non-ischaemic distribution with no other abnormalities found on analysis of T1, T2*, ECV, and ventricular size and function. Basal inferolateral scar can be a non-specific finding, but has also

been implicated in Anderson-Fabry disease (AFD), myocarditis, desminrelated hypertrophic cardiomyopathy, and cardiomyopathies related to
muscular dystrophy.(161, 162, 163, 164) The patient did not have other MRI
features consistent with cardiomyopathy. Although the ion levels were on the
lower end of the high spectrum within this group, this finding may reflect preclinical disease. Mid-wall fibrosis was seen in 2 patients with low circulating
blood metal ions and 1 patient with CoC hip implant. A small area of
subendocardial scar in the mid-anterolateral wall was seen in a patient in the
low blood metal ions group. The significance of this finding is unclear as
ventricular function, T1, T2*, and ECV were normal, and may be secondary to
a previous coronary embolic event. The finding of non-ischaemic scar in this
group of patients may provide prognostic information based on the ICELANDMI study (n= 936) study had shown that non-ischaemic patterns signified a
worse prognosis than those without.(165)

This is the largest blinded-study conducted thus far in the assessment of cardiotoxicity from MoM prostheses, using gold-standard imaging modalities for volume assessment and tissue characterisation. Both CMR and echocardiography were not able to demonstrate LV systolic dysfunction or cavity dilatation in patients with the highest levels of circulating blood metal ions. Our findings were not consistent with Gillam et al who reported an association between a specific subtype of MoM implant and hospitalisation for heart failure in men.(10)

Cobalt induced cardiomyopathy is well recognised in the literature but the pathophysiology behind the link between raised cobalt levels and cardiac toxicity remains unclear.(4, 166, 167, 168) Suggested theories include the interference of cobalt with cardiac myocyte oxygen uptake, disruption of transmembrane transport systems, and generation of reactive oxygen species.(4, 169) Histological findings in cobalt-related cardiac toxicity include myofibrillar hypertrophy. interstitial fibrosis, and muscle fibre degeneration. (104) The development of cardiac toxicity is likely to be multifactorial and partly due to additional predisposing factors including poor nutritional status and excess alcohol intake as seen in the Quebec beer drinkers cobalt cardiomyopathy epidemic where foam stabiliser containing large quantities of cobalt were used. The case reports detailing cobalt induced cardiomyopathy in association with MoM prostheses involved patients with circulating levels greater than our patient population (>100ppb). The highest level measured in this study was 82ppb recruited by one the UK's leading retrieval centres. The current national surveillance programme with regular blood sampling means patients with extremely high levels are likely to have undergone revision surgery with a presumed resultant reduction in systemic toxicity.

Limitations of this study include the lack of histological validation of T1 mapping. Liver and myocardial tissue biopsies are highly invasive, challenging procedures, and prone to sampling error. Longitudinal data is required to monitor changes. Additionally, the echocardiogram study protocol did not include all measurements of diastolic dysfunction including mitral valve early filling (E Vmax), E/A ratio, deceleration time, and pulmonary vein flow.

Therefore, conclusions regarding diastolic dysfunction cannot be made based on the limited measurements in this study

6.6 Conclusion

This is the first imaging study to assess the effects of cobalt and chromium on cardiac function. Although the results were negative this unique study may provide reassurance to patients and surgeons, and a platform for further work.

CHAPTER 7: DISCUSSION AND CONCLUSION

Heart failure remains the leading cause of significant morbidity and mortality in patients with iron overload and results from the accumulation of cardiac iron. (1, 2) CMR for the detection and quantification of iron loading in the heart and liver has changed the prognosis of those at risk, but only for those with access to the necessary resources.(3) T1 mapping has shown promise as a complimentary tool for the diagnosis of early iron deposition and reduce morbidity.

Like iron, cobalt has ferromagnetic properties and heart failure secondary to toxicity is reversible.(4) Serum metal levels do not predict end organ damage, and there is no reliable measure of metal deposition. Cardiotoxicity relies on symptoms and established impairment. CMR may provide the answer.

As a result of the work outlined in this thesis:

- I have scanned the largest cohorts of patients for the CMR assessment of iron and Cobalt/chromium loading (combined numbers 520 patients in total).
- 2. In chapter 4, I explored the relationship between the gold-standard measurement T2* and the experimental method T1 in both adult and paediatric populations at risk of iron loading. I have shown the agreement between both measurements and that T1 may diagnose mild iron not detected by T2*. Additionally, that there may be a

subgroup of patients with pre-clinical iron loading (as evidenced by a low T1/normal T2*) where early RV dysfunction was seen.

- 3. In chapter 5, I have shown that refining CMR scanning for iron in resource limited countries can be a diagnostic and cost-effective method to improve diagnosis and management of iron loading leading to reduced morbidity and mortality. This method has now been adopted in over 10 countries worldwide in the Rapid CMR project.
- 4. By using CMR for tissue characterisation and metal quantification, and echocardiography for function, and Tissue Doppler Imaging in chapter 6, I have shown that patients referred from the UK's national hip prosthesis retrieval service with the highest levels of circulating cobalt/chromium did not develop heart failure or features suggestive of cardiomyopathy.

Clinical insights and potential

Myocardial iron quantification by T1 mapping

Prior to my work, low native T1 had been observed in the presence of iron in a small pilot study led by the primary supervisor of this thesis.(85) Myocardial T1 was lower in patients than healthy volunteers (p<0.001), and correlated well with T2* (p<0.0001).(85)

In this thesis, I demonstrated that native T1 has the potential to play a complimentary role to T2* in the management of iron loading. T1 correlated with the gold standard measurement in both adults and children at risk, and identified patients with potential subclinical disease in nearly 50% of patients with normal T2* values. Contrary to findings in the literature demonstrating the

association of low T2* values with heart failure we did not replicate this finding (57). In a multi-centre study with 652 thalassaemia major patients heart failure occurred in 47% of patients (mean EF 43.1 ± 7.2%) within 1 year in patients with cardiac T2* values less than 6ms.(57) In our cohort, 7 patients had T2* values less than 6ms with a mean ejection fraction of 61.7 ± 8.9%. We did however show a significant difference in longitudinal RV function and LV dimensions in patients with normal T2*/low T1 when compared with patients with normal T2*/T1, suggesting a subgroup of patients with a restrictive phenotype. Further studies including longitudinal data and multi-imaging modalities using echocardiographic methods including global longitudinal strain, may provide further insight. This thesis also investigated the role of T1 mapping in a paediatric population. A similar association was seen between T2* and T1 mapping. The youngest patient with evidence of iron loading by T1 mapping was 11 years old, despite regular chelation. This is in keeping with the literature that iron loading can occur as early as 6 years of age and may reflect transfusion requirements increased due to severe thalassaemia, hypersplenism, infection, or inadequate chelation.(170, 171) Identification of patients with evidence of early cardiac involvement allows a more intensive chelation regime to reduce the risk of heart failure.

Ultrafast CMR in the developing world

Patients with iron loading conditions most likely to benefit from CMR iron quantification live in countries where MRI scanners are available but used for other indications. Instead, blood markers are used as surrogate measures of organ involvement.

In this thesis, I demonstrated the feasibility of a large-scale ultrafast CMR study for the diagnosis of iron. Over a period of 2 days, 123 scans were performed using a 10-minute protocol aimed at removing complex scanning and analysis, by using T1 mapping with instant colour maps for diagnosis. Local teams were trained to perform and analyse the scans for future clinical use. Scan duration, including analysis time, was 8.3 ± 2.4 minutes, which is approximately 4 times quicker than a standard scan for iron. New myocardial iron was diagnosed in 16% of patients and almost all patients had liver iron. As with the UK data, T1 maps were diagnostic and in agreement with T2* in all patients with myocardial iron. An additional 30 patients were identified to have low myocardial T1 in the presence of a normal T2* highlighting a group of patients with possible imminent cardiac loading.

This study has shown that dedicated protocols with easy to analyse sequences can diagnose iron accurately and are cost-effective. The suggested cost reduction from \$300 to \$50USD, by King Chulalongkorn Hospital, makes CMR a more feasible option. This study has also crucially demonstrated that not all patients require regular CMR scans. Serum ferritin levels can be used to assess whether cardiac monitoring is required, as all patients in this study with cardiac iron had ferritin levels greater than 1000ug/L. Since publication of this work, the ultrafast CMR protocol for iron has been recommended in an algorithm for healthcare services with limited MRI availability.(172) Furthermore, the RapidCMR project, which stems from this work, has now taken ultrafast CMR to over 10 countries. This health

initiative aims to provide educational and pastoral support to hospitals to continue providing a fully functioning CMR service.

CMR for cobalt and chromium

Prior to my work, concerns regarding iatrogenic cobalt cardiomyopathy were triggered by an increasing number of isolated case reports describing heart failure in patients with metal-on-metal (MoM) hip prostheses.(4, 152) A recent retrospective cohort study including 4019 patients demonstrated increased hospitalisation rates for heart failure in men with MoM hips.(10) These findings have been inconsistent.(173, 174) This is the largest blinded-study conducted thus far in the assessment of cardiotoxicity from MoM prostheses, using gold-standard imaging modalities for volume assessment, tissue characterisation, and Tissue Doppler Imaging.

Three distinct groups of patients were recruited from the UK's largest hip retrieval service defined by the type of prosthetic hip and circulating blood metal ion levels. Patients with the highest levels of circulating cobalt/chromium had normal biventricular function by both CMR, and normal Tissue Doppler Imaging on echocardiography. Patients with the highest levels of circulating cobalt/chromium had normal biventricular function by both CMR and echocardiography.

There were no significant differences between the groups when assessing focal and diffuse fibrosis by LGE and ECV assessment. However, 5 patients had LGE (4 in the MoM group and 1 control). Although the scar patterns were

considered non-specific (n=2 midwall, n=1 inferolateral, n=1 subendocardial) these may reflect early disease. LGE patterns have not been reported in previous publications.(152, 160)

Although a negative study, the findings are important and may provide reassurance to both patients and surgeons. Longitudinal data is required to monitor changes.

On-going and Future work

This thesis has pioneered work in the field of ultrafast CMR. Further projects have since stemmed with many international units using the abbreviated protocol to diagnose iron including India and Peru. Furthermore, the concept of ultrafast scanning has been adapted with the use of contrast in other cardiac conditions.(175) A multicentre study is currently in progress to continue to explore the long-term health and cost benefit of CMR for iron cardiomyopathy (the Rapid CMR project).

Conclusion

This thesis evaluated the use of CMR in the assessment of myocardial and liver iron, and myocardial cobalt deposition. I have demonstrated the potential impact of native T1 mapping in the diagnosis and management of cardiac iron overload in a large at risk adult and paediatric population. The additional advantage of shorter time acquisitions and immediate results through a colour map has shown significant workflow utility, as was demonstrated in the Thailand study. In the UK, utilisation of ultrafast scanning into the national healthcare system can reduce waiting times, improve productivity and efficiency. Finally,

this thesis explored the effects of cobalt and chromium on cardiac function using advanced imaging techniques in the largest blinded-study conducted thus far. The negative findings may provide reassurance to patients and healthcare practitioners.

.

CHAPTER 8: PUBLICATIONS

PRIZES

- Finalist: Early Career Award (clinical) SCMR 2016
 Ultrafast CMR to Deliver High Volume Screening of an at Risk Thalassemia Population in the Developing World: Preliminary Results from the TIC-TOC Study (Thailand and UK International Collaboration in Thalassaemia Using an Optimised Ultrafast CMR Protocol).
- Winner of SCMR Regional Travel Award, SCMR, USA 2016
- Finalist: Seed Grant Award SCMR 2017
 Ultrafast CMR scanning for Iron

PUBLICATIONS

- Abdel-Gadir A, Berber R, Rosmini S, Captur G, Nordin S, Culotta V, Palla L, Kellman P, Lloyd GW, Skinner JA, Moon JC, Manisty C, Hart AJ. Assessing cardiotoxicity from metal-on-metal hip implants with multi-modality imaging. J Bone Joint Surg Am. 2017 Nov 1:00(21):1827-1835
- Abdel-Gadir A, Vorasettakarnkij Y, Ngamkasem H, Nordin S, Ako EA, Tumkosit M, Sucharitchan P, Uprasert N, Kellman P, Piechnik SK, Fontana M, Fernandes JL, Manisty C, Westwood M, Porter JB, Walker JM, Moon JC. Ultrafast magnetic resonance imaging for iron quantification in Thalassemia patients in the developing world: The TICTOC Study. Circulation. 2016 Aug 2;134(5):432-4.
- Abdel-Gadir A, Berber R, Porter JB, Quinn PD, Suri D, Kellman P, Hart AJ, Moon JC, Manisty C, Skinner JA. Detection of metallic cobalt and chromium liver deposition following failed hip replacement using

T2* and R2 magnetic resonance. Journal of Cardiovascular Magnetic Resonance. 2016 May 6; 18(1):29

Amna Abdel-Gadir, Thomas Treibel, James Moon. Myocardial T1
 Mapping: Where are we now and where are we going? Research
 Reports in Clinical Cardiology 2014, 5:339-34

CO AUTHOR PULICATIONS DURING THIS THESIS

- Menacho K, Ramirez S, Segura P, Nordin S, <u>Abdel-Gadir A</u>, Illatopa V, Bhuva A, Benedetti G, Boubertakh R, Abad P, Rodriguez B, Medina F, Treibel TA, Westwood M, Fernandes J, Walker M, Litt,H, Moon JC. The INCA (Peru) study: Impact of Non-invasive CMR Assessment in the Developing World. Journal of the American Heart Association. 2018.
- Rosmini S, Bulluck H, Captur G, Treibel TA, <u>Abdel-Gadir A</u>, Bhuva AN, Culotta V, Merghani A, Fontana M, Maestrini V, Herrey AS, Chow K, Thompson RB, Piechnik SK, Kellman P, Manisty C, Moon JC. Myocardial native T1 and extracellular volume with healthy ageing and gender. *Eur Heart J Cardiovasc Imaging*. 2018 Jun;19(6):615-621.
- Torlasco C, Cassinerio E, Roghi A, Faini A, Capecchi M, <u>Abdel-Gadir A</u>, Giannattasio C, Parati G, Moon JC, Cappellini MD, Pedrotti P. Role of T1 mapping as a complementary tool to T2* for non-invasive cardiac iron overload assessment. *PLoS One*. 2018 Feb 21;13(2):e0192890. doi: 10.1371/journal.pone.0192890. PubMed PMID: 29466447; PubMed Central PMCID: PMC5821344.
- CMR verified regression of cardiac AL amyloid after chemotherapy.
 Martinez-Naharro A, <u>Abdel-Gadir A</u> et al. JACC Cardiovascular Imaging. 2017 Apr 7.

- Defining left ventricular remodelling following acute ST-segment elevation myocardial infarction using cardiovascular magnetic resonance. Bulluck H, Go YY, Crimi G, Ludman AJ, Rosmini S, <u>Abdel-Gadir A</u> et al. Journal of Cardiovascular Magnetic Resonance. 2017 Mar 13;19(1):26.
- Diagnostic performance of T1 and T2 mapping to detect intramyocardial hemorrhage in reperfused ST-segment elevation myocardial infarction (STEMI) patients: T1 and T2 mapping and IMH. Bulluck H, Rosmini S,
 Abdel-Gadir A et al. Journal of Magnetic Resonance Imaging. 2017 Feb 15.
- Impact of microvascular obstruction on semiautomated techniques for quantifying acute and chronic myocardial infarction by cardiovascular magnetic resonance. Bulluck H, Rosmini S, <u>Abdel-Gadir A</u> et al. Open Heart. 2016 Dec 12;3(2).
- Residual myocardial iron following intramyocardial hemorrhage during the convalescent phase of reperfused ST-segment-elevation myocardial infarction and adverse left ventricular remodelling. Bulluck H, Rosmini S,
 Abdel-Gadir A et al. Circ Cardiovasc Imaging. 2016 Oct;9(10).
- Cardiac Fabry disease with late gadolinium enhancement is a chronic inflammatory cardiomyopathy evidence from multi parametric mapping by cardiovascular magnetic resonance. Nordin S, Kozor R, Bulluck H, Rosmini S, <u>Abdel-Gadir A</u> et al. J Am Coll Cardiol. 2016 Oct 11;68(15):1707-1708.
- Automated extracellular volume fraction mapping provides insights into the pathophysiology of left ventricular remodelling post-reperfused STelevation myocardial infarction. Bulluck H, Rosmini S, <u>Abdel-Gadir A</u>, et al. J Am Heart Assoc. 2016 Jul 11;5(7).

- Response to Letters Regarding Article, "Prognostic Value of Late Gadolinium Enhancement Cardiovascular Magnetic Resonance in Cardiac Amyloidosis. Fontana M, Pica S, Reant P, <u>Abdel-Gadir A</u> et al. Circulation 2016 Mar 22;133(12).
- Automatic Measurement of the Myocardial Interstitium: Synthetic Extracellular Volume Quantification without Hematocrit Sampling. Treibel TA, Fontana M, Maestrini V, Castelletti S, Rosmini S, Simpson J, Nasis A, Bhuva AN, Bulluck H, <u>Abdel-Gadir A</u> et al. JACC Cardiovasc Imaging 2016 Jan;9(1):54-63.
- Prognostic Value of Late Gadolinium Enhancement Cardiovascular Magnetic Resonance in Cardiac Amyloidosis. Fontana M, Pica S, Reant P, <u>Abdel-Gadir A</u> et al. Circulation 2015 Oct 20;132(16).
- T1 mapping and T2 mapping at 3T for quantifying the area-at-risk in reperfused STEMI patients. Bulluck H, White SK, Rosmini S, Bhuva A, Treibel TA, Fontana M, <u>Abdel-Gadir A</u> et al. J Cardiovasc Magn Reson 2015 Aug 12;17(1):73
- Differential myocyte responses in patients with cardiac transthyretin amyloidosis and light-chain amyloidosis: A cardiac MR imaging study.
 Fontana M, Banypersad SM, Treibel TA, <u>Abdel-Gadir A</u> et al. Radiology. 2015 May 21:141744
- Free-breathing T2* mapping using respiratory motion corrected averaging. Kellman P, Xue H, Spottiswoode BS, Sandino CM, Hansen MS, <u>Abdel-Gadir A</u> et al. J Cardiovasc Magn Reson 2015 Jan 24;17(1):3

- Myocardial T1 mapping, Bulluck H, Maestrini V, Rosmini S, <u>Abdel-Gadir A.</u> Treibel TA, Castelletti S, Bucciarelli-Ducci C, Manisty C, Moon JC. Circ J 2015;79(3)487-94
- New Generation Cardiac Parametric Mapping: the Clinical Role of T1 and T2 Mapping. Viviana Maestrini; <u>Amna Abdel-Gadir</u>; Anna S. Herrey; James C. Moon. Magnetom Flash 2013.

BOOK CHAPTER

 Standards for the Clinical Care of Children and Adults with Thalassaemia in the UK, 3rd Edition (2016). Chapter: Management of the cardiovascular system in the thalassaemia population. ISBN: 978- 1-900254-20-5.

PRESENTATIONS and INVITED LECTURES RELATED TO THIS THESIS

- 2018 Extra-cardiac findings detected by CMR in a Thai population with Thalassaemia major - findings from the TIC-TOC study. Poster presentation, SCMR, Barcelona, Spain
- 2018 T1 Mapping for Cardiac Iron in Children. Poster presentation, SCMR, Barcelona, Spain
- 2017 Non-ischemic Primary and Secondary CMP: Non-invasive assessment for cardiotoxicity from metal-on-metal hip implants using CMR. Abstract, SCMR 2017
- 2017 Cardiac Complications in Thalassaemia, Manchester
- 2016 Ultrafast CMR scanning in the Developing World, First International Congress in CMR, Peru. Invited Speaker.
- 2016 A New MRI Sequence to Assess Iron Overload in Thalassaemia.
 Sixth International Thalassaemia Conference, <u>India</u>. Invited Speaker.

- 2016 Cardiac MRI and Iron Overload Workshop, King Chulalongkorn Hospital, Bangkok, <u>Thailand</u>. Presenter and course organiser.
- 2016 Detection of metallic cobalt and chromium liver deposition following failed hip replacement using MRI T2* and R2 sequences. EuroCMR, Florence, <u>Italy</u>.
- 2016 Ultrafast CMR to deliver high volume screening of an at risk thalassemia population in the developing world: Results from the TIC-TOC Study. Early Career Award category, SCMR, LA, <u>USA</u>.
- 2016 Out of the frying pan, into the fire: From untreated thalassemia to severe iron overload. A reflection on modern healthcare. SCMR, LA, USA.
- 2015 Myocardial iron quantification using T2* and native T1 mapping a 250 patient study. SCMR/EuroCMR Joint Scientific Sessions, Nice, France.

CHAPTER 9: REFERENCES

- 1. Gujja P, Rosing DR, Tripodi DJ, Shizukuda Y. Iron overload cardiomyopathy: better understanding of an increasing disorder. J Am Coll Cardiol. 2010;56(13):1001-12.
- 2. Pennell DJ, Udelson JE, Arai AE, Bozkurt B, Cohen AR, Galanello R, et al. Cardiovascular function and treatment in beta-thalassemia major: a consensus statement from the American Heart Association. Circulation. 2013;128(3):281-308.
- 3. Modell B, Khan M, Darlison M, Westwood MA, Ingram D, Pennell DJ. Improved survival of thalassaemia major in the UK and relation to T2* cardiovascular magnetic resonance. J Cardiovasc Magn Reson. 2008;10:42.
- 4. Packer M. Cobalt Cardiomyopathy: A Critical Reappraisal in Light of a Recent Resurgence. Circ Heart Fail. 2016;9(12).
- 5. Devlin JJ, Pomerleau AC, Brent J, Morgan BW, Deitchman S, Schwartz M. Clinical features, testing, and management of patients with suspected prosthetic hip-associated cobalt toxicity: a systematic review of cases. J Med Toxicol. 2013;9(4):405-15.
- 6. Allen LA, Ambardekar AV, Devaraj KM, Maleszewski JJ, Wolfel EE. Clinical problem-solving. Missing elements of the history. N Engl J Med. 2014;370(6):559-66.
- 7. Matharu GS, Judge A, Pandit HG, Murray DW. Follow-up for patients with metal-on-metal hip replacements: are the new MHRA recommendations justified? BMJ. 2018;360:k566.
- 8. Pandit H, Glyn-Jones S, McLardy-Smith P, Gundle R, Whitwell D, Gibbons CL, et al. Pseudotumours associated with metal-on-metal hip resurfacings. J Bone Joint Surg Br. 2008;90(7):847-51.
- 9. Bradberry SM, Wilkinson JM, Ferner RE. Systemic toxicity related to metal hip prostheses. Clin Toxicol (Phila). 2014;52(8):837-47.
- 10. Gillam MH, Pratt NL, Inacio MC, Roughead EE, Shakib S, Nicholls SJ, et al. Heart failure after conventional metal-on-metal hip replacements. Acta Orthop. 2017;88(1):2-9.
- 11. Andrews NC. Disorders of iron metabolism. N Engl J Med. 1999;341(26):1986-95.
- 12. Wang CY, Babitt JL. Liver iron sensing and body iron homeostasis. Blood. 2019;133(1):18-29.
- 13. Porter JB, Garbowski M. The pathophysiology of transfusional iron overload. Hematol Oncol Clin North Am. 2014;28(4):683-701, vi.
- 14. Chifman J, Laubenbacher R, Torti SV. A systems biology approach to iron metabolism. Adv Exp Med Biol. 2014;844:201-25.
- 15. Gulec S, Anderson GJ, Collins JF. Mechanistic and regulatory aspects of intestinal iron absorption. American journal of physiology Gastrointestinal and liver physiology. 2014;307(4):G397-409.
- 16. McKie AT, Barrow D, Latunde-Dada GO, Rolfs A, Sager G, Mudaly E, et al. An iron-regulated ferric reductase associated with the absorption of dietary iron. Science. 2001;291(5509):1755-9.
- 17. Cullis JO, Fitzsimons EJ, Griffiths WJ, Tsochatzis E, Thomas DW, British Society for H. Investigation and management of a raised serum ferritin. Br J Haematol. 2018;181(3):331-40.

- 18. Anderson GJ, Frazer DM. Current understanding of iron homeostasis. Am J Clin Nutr. 2017;106(Suppl 6):1559S-66S.
- 19. Nemeth E. Hepcidin in beta-thalassemia. Annals of the New York Academy of Sciences. 2010;1202:31-5.
- 20. Origa R, Galanello R, Ganz T, Giagu N, Maccioni L, Faa G, et al. Liver iron concentrations and urinary hepcidin in beta-thalassemia. Haematologica. 2007;92(5):583-8.
- 21. Walker JM. Thalassaemia major and the heart: a toxic cardiomyopathy tamed? Heart. 2013;99(12):827-34.
- 22. Siddique A, Kowdley KV. Review article: the iron overload syndromes. Aliment Pharmacol Ther. 2012;35(8):876-93.
- 23. Kremastinos DT, Farmakis D. Iron overload cardiomyopathy in clinical practice. Circulation. 2011;124(20):2253-63.
- 24. Pietrangelo A. Ferroportin disease: pathogenesis, diagnosis and treatment. Haematologica. 2017;102(12):1972-84.
- 25. Shander A, Cappellini MD, Goodnough LT. Iron overload and toxicity: the hidden risk of multiple blood transfusions. Vox Sang. 2009;97(3):185-97.
- 26. Harmatz P, Butensky E, Quirolo K, Williams R, Ferrell L, Moyer T, et al. Severity of iron overload in patients with sickle cell disease receiving chronic red blood cell transfusion therapy. Blood. 2000;96(1):76-9.
- 27. Hoffbrand AV, Taher A, Cappellini MD. How I treat transfusional iron overload. Blood. 2012;120(18):3657-69.
- 28. Porter JB. Practical management of iron overload. Br J Haematol. 2001;115(2):239-52.
- 29. Porter J. Assessing iron overload and toxicity. Hematology Education: the education program for the annual congress of the European Hematology Association. 2012(6):45-352.
- 30. Limdi JK, Crampton JR. Hereditary haemochromatosis. Qjm. 2004;97(6):315-24.
- 31. Pietrangelo A. Hereditary hemochromatosis--a new look at an old disease. N Engl J Med. 2004;350(23):2383-97.
- 32. Carpenter JP, Grasso AE, Porter JB, Shah F, Dooley J, Pennell DJ. On myocardial siderosis and left ventricular dysfunction in hemochromatosis. J Cardiovasc Magn Reson. 2013;15:24.
- 33. Aydinok Y. Thalassemia. Hematology. 2012;17 Suppl 1:S28-31.
- 34. Dev S, Babitt JL. Overview of iron metabolism in health and disease. Hemodial Int. 2017;21 Suppl 1:S6-S20.
- 35. Weatherall DJ. Thalassaemia: the long road from bedside to genome. Nature reviews Genetics. 2004;5(8):625-31.
- 36. Rees DC, Williams TN, Gladwin MT. Sickle-cell disease. Lancet. 2010;376(9757):2018-31.
- 37. Adams RJ, McKie VC, Hsu L, Files B, Vichinsky E, Pegelow C, et al. Prevention of a first stroke by transfusions in children with sickle cell anemia and abnormal results on transcranial Doppler ultrasonography. N Engl J Med. 1998;339(1):5-11.
- 38. Scott BL, Deeg HJ. Myelodysplastic syndromes. Annual review of medicine. 2010;61:345-58.
- 39. Mahesh S, Ginzburg Y, Verma A. Iron overload in myelodysplastic syndromes. Leukemia & lymphoma. 2008;49(3):427-38.

- 40. Boddaert N, Le Quan Sang KH, Rotig A, Leroy-Willig A, Gallet S, Brunelle F, et al. Selective iron chelation in Friedreich ataxia: biologic and clinical implications. Blood. 2007;110(1):401-8.
- 41. Batts KP. Iron overload syndromes and the liver. Mod Pathol. 2007;20 Suppl 1:S31-9.
- 42. Li CK, Chik KW, Lam CW, To KF, Yu SC, Lee V, et al. Liver disease in transfusion dependent thalassaemia major. Arch Dis Child. 2002;86(5):344-7.
- 43. Chapoutot C, Esslimani M, Joomaye Z, Ramos J, Perney P, Laurent C, et al. Liver iron excess in patients with hepatocellular carcinoma developed on viral C cirrhosis. Gut. 2000;46(5):711-4.
- 44. Srisukh S, Ongphiphadhanakul B, Bunnag P. Hypogonadism in thalassemia major patients. J Clin Transl Endocrinol. 2016;5:42-5.
- 45. Simcox JA, McClain DA. Iron and diabetes risk. Cell Metab. 2013;17(3):329-41.
- 46. Murphy CJ, Oudit GY. Iron-overload cardiomyopathy: pathophysiology, diagnosis, and treatment. J Card Fail. 2010;16(11):888-900.
- 47. Lekawanvijit S, Chattipakorn N. Iron overload thalassemic cardiomyopathy: iron status assessment and mechanisms of mechanical and electrical disturbance due to iron toxicity. Can J Cardiol. 2009;25(4):213-8.
- 48. Ludwiczek S, Theurl I, Muckenthaler MU, Jakab M, Mair SM, Theurl M, et al. Ca2+ channel blockers reverse iron overload by a new mechanism via divalent metal transporter-1. Nat Med. 2007;13(4):448-54.
- 49. Oudit GY, Trivieri MG, Khaper N, Liu PP, Backx PH. Role of L-type Ca2+ channels in iron transport and iron-overload cardiomyopathy. J Mol Med (Berl). 2006;84(5):349-64.
- 50. Kumfu S, Chattipakorn S, Srichairatanakool S, Settakorn J, Fucharoen S, Chattipakorn N. T-type calcium channel as a portal of iron uptake into cardiomyocytes of beta-thalassemic mice. Eur J Haematol. 2011;86(2):156-66.
- 51. Link G, Pinson A, Hershko C. Heart cells in culture: a model of myocardial iron overload and chelation. J Lab Clin Med. 1985;106(2):147-53.
- 52. Wood JC, Enriquez C, Ghugre N, Otto-Duessel M, Aguilar M, Nelson MD, et al. Physiology and pathophysiology of iron cardiomyopathy in thalassemia. Annals of the New York Academy of Sciences. 2005;1054:386-95.
- 53. Buja LM, Roberts WC. Iron in the heart. Etiology and clinical significance. Am J Med. 1971;51(2):209-21.
- 54. Schellhammer PF, Engle MA, Hagstrom JW. Histochemical studies of the myocardium and conduction system in acquired iron-storage disease. Circulation. 1967;35(4):631-7.
- 55. Carpenter JP, He T, Kirk P, Roughton M, Anderson LJ, de Noronha SV, et al. On T2* magnetic resonance and cardiac iron. Circulation. 2011;123(14):1519-28.
- 56. Carpenter JP, Alpendurada F, Deac M, Maceira A, Garbowski M, Kirk P, et al. Right ventricular volumes and function in thalassemia major patients in the absence of myocardial iron overload. J Cardiovasc Magn Reson. 2010;12:24.
- 57. Kirk P, Roughton M, Porter JB, Walker JM, Tanner MA, Patel J, et al. Cardiac T2* magnetic resonance for prediction of cardiac complications in thalassemia major. Circulation. 2009;120(20):1961-8.

- 58. Olson LJ, Edwards WD, McCall JT, Ilstrup DM, Gersh BJ. Cardiac iron deposition in idiopathic hemochromatosis: histologic and analytic assessment of 14 hearts from autopsy. J Am Coll Cardiol. 1987;10(6):1239-43.
- 59. Fitchett DH, Coltart DJ, Littler WA, Leyland MJ, Trueman T, Gozzard DI, et al. Cardiac involvement in secondary haemochromatosis: a catheter biopsy study and analysis of myocardium. Cardiovasc Res. 1980;14(12):719-24.
- 60. Porter JV, V. Iron Overload and Chelation. Guidelines for the Management of Tranfusion Dependent Thalasaemia (TDT) [Internet]. 3rd ed. Nicosia (CY)2014.
- 61. Borgna-Pignatti C, Rugolotto S, De Stefano P, Zhao H, Cappellini MD, Del Vecchio GC, et al. Survival and complications in patients with thalassemia major treated with transfusion and deferoxamine. Haematologica. 2004;89(10):1187-93.
- 62. Olivieri NF, Nathan DG, MacMillan JH, Wayne AS, Liu PP, McGee A, et al. Survival in medically treated patients with homozygous betathalassemia. N Engl J Med. 1994;331(9):574-8.
- 63. Bellenger NG, Davies LC, Francis JM, Coats AJ, Pennell DJ. Reduction in sample size for studies of remodeling in heart failure by the use of cardiovascular magnetic resonance. J Cardiovasc Magn Reson. 2000;2(4):271-8.
- 64. Anderson LJ, Holden S, Davis B, Prescott E, Charrier CC, Bunce NH, et al. Cardiovascular T2-star (T2*) magnetic resonance for the early diagnosis of myocardial iron overload. Eur Heart J. 2001;22(23):2171-9.
- 65. Westwood M, Anderson LJ, Firmin DN, Gatehouse PD, Charrier CC, Wonke B, et al. A single breath-hold multiecho T2* cardiovascular magnetic resonance technique for diagnosis of myocardial iron overload. J Magn Reson Imaging. 2003;18(1):33-9.
- 66. Moon JC, Messroghli DR, Kellman P, Piechnik SK, Robson MD, Ugander M, et al. Myocardial T1 mapping and extracellular volume quantification: a Society for Cardiovascular Magnetic Resonance (SCMR) and CMR Working Group of the European Society of Cardiology consensus statement. J Cardiovasc Magn Reson. 2013;15:92.
- 67. Wood JC, Ghugre N. Magnetic resonance imaging assessment of excess iron in thalassemia, sickle cell disease and other iron overload diseases. Hemoglobin. 2008;32(1-2):85-96.
- 68. Pepe A, Positano V, Santarelli MF, Sorrentino F, Cracolici E, De Marchi D, et al. Multislice multiecho T2* cardiovascular magnetic resonance for detection of the heterogeneous distribution of myocardial iron overload. J Magn Reson Imaging. 2006;23(5):662-8.
- 69. He T. Cardiovascular magnetic resonance T2* for tissue iron assessment in the heart. Quant Imaging Med Surg. 2014;4(5):407-12.
- 70. Collins W, Taylor WH. Determination of iron in cardiac and liver tissues by plasma emission spectroscopy. Ann Clin Biochem. 1987;24 (Pt 5):483-7.
- 71. Alam MH, He T, Auger D, Smith GC, Drivas P, Wage R, et al. Validation of T2* in-line analysis for tissue iron quantification at 1.5 T. J Cardiovasc Magn Reson. 2016;18(1):23.
- 72. Wood JC, Otto-Duessel M, Aguilar M, Nick H, Nelson MD, Coates TD, et al. Cardiac iron determines cardiac T2*, T2, and T1 in the gerbil model of iron cardiomyopathy. Circulation. 2005;112(4):535-43.

- 73. Bull S, White SK, Piechnik SK, Flett AS, Ferreira VM, Loudon M, et al. Human non-contrast T1 values and correlation with histology in diffuse fibrosis. Heart. 2013;99(13):932-7.
- 74. Ferreira VM, Piechnik SK, Dall'Armellina E, Karamitsos TD, Francis JM, Choudhury RP, et al. Non-contrast T1-mapping detects acute myocardial edema with high diagnostic accuracy: a comparison to T2-weighted cardiovascular magnetic resonance. J Cardiovasc Magn Reson. 2012;14:42.
- 75. Karamitsos TD, Piechnik SK, Banypersad SM, Fontana M, Ntusi NB, Ferreira VM, et al. Noncontrast T1 mapping for the diagnosis of cardiac amyloidosis. JACC Cardiovasc Imaging. 2013;6(4):488-97.
- 76. Sado DM, White SK, Piechnik SK, Banypersad SM, Treibel T, Captur G, et al. Identification and assessment of Anderson-Fabry disease by cardiovascular magnetic resonance noncontrast myocardial T1 mapping. Circ Cardiovasc Imaging, 2013;6(3):392-8.
- 77. Banypersad SM, Fontana M, Maestrini V, Sado DM, Captur G, Petrie A, et al. T1 mapping and survival in systemic light-chain amyloidosis. Eur Heart J. 2015;36(4):244-51.
- 78. Messroghli DR, Radjenovic A, Kozerke S, Higgins DM, Sivananthan MU, Ridgway JP. Modified Look-Locker inversion recovery (MOLLI) for high-resolution T1 mapping of the heart. Magn Reson Med. 2004;52(1):141-6.
- 79. Messroghli DR, Greiser A, Frohlich M, Dietz R, Schulz-Menger J. Optimization and validation of a fully-integrated pulse sequence for modified look-locker inversion-recovery (MOLLI) T1 mapping of the heart. J Magn Reson Imaging. 2007;26(4):1081-6.
- 80. Kellman P, Hansen MS. T1-mapping in the heart: accuracy and precision. J Cardiovasc Magn Reson. 2014;16:2.
- 81. Chow K, Flewitt JA, Green JD, Pagano JJ, Friedrich MG, Thompson RB. Saturation recovery single-shot acquisition (SASHA) for myocardial T(1) mapping. Magn Reson Med. 2014;71(6):2082-95.
- 82. Roujol S, Weingartner S, Foppa M, Chow K, Kawaji K, Ngo LH, et al. Accuracy, precision, and reproducibility of four T1 mapping sequences: a head-to-head comparison of MOLLI, ShMOLLI, SASHA, and SAPPHIRE. Radiology. 2014;272(3):683-9.
- 83. Piechnik SK, Ferreira VM, Dall'Armellina E, Cochlin LE, Greiser A, Neubauer S, et al. Shortened Modified Look-Locker Inversion recovery (ShMOLLI) for clinical myocardial T1-mapping at 1.5 and 3 T within a 9 heartbeat breathhold. J Cardiovasc Magn Reson. 2010;12:69.
- 84. Moon J, Abdel-Gadir A, Treibel T. Myocardial T1 mapping: where are we now and where are we going? Research Reports in Clinical Cardiology. 2014:339.
- 85. Sado DM, Maestrini V, Piechnik SK, Banypersad SM, White SK, Flett AS, et al. Noncontrast myocardial T1 mapping using cardiovascular magnetic resonance for iron overload. J Magn Reson Imaging. 2015;41(6):1505-11.
- 86. Messroghli DR, Moon JC, Ferreira VM, Grosse-Wortmann L, He T, Kellman P, et al. Clinical recommendations for cardiovascular magnetic resonance mapping of T1, T2, T2* and extracellular volume: A consensus statement by the Society for Cardiovascular Magnetic Resonance (SCMR) endorsed by the European Association for Cardiovascular Imaging (EACVI). J Cardiovasc Magn Reson. 2017;19(1):75.

- 87. Alam MH, Auger D, Smith GC, He T, Vassiliou V, Baksi AJ, et al. T1 at 1.5T and 3T compared with conventional T2* at 1.5T for cardiac siderosis. J Cardiovasc Magn Reson. 2015;17:102.
- 88. Camargo GC, Rothstein T, Junqueira FP, Fernandes E, Lima RL, Greiser A, et al. Myocardial iron quantification using modified Look-Locker inversion recovery (MOLLI) T1 mapping at 3 Tesla. Journal of Cardiovascular Magnetic Resonance. 2013;15(Suppl 1):W8.
- 89. Brown L. Cardiac extracellular matrix: a dynamic entity. Am J Physiol Heart Circ Physiol. 2005;289(3):H973-4.
- 90. Kellman P, Wilson JR, Xue H, Bandettini WP, Shanbhag SM, Druey KM, et al. Extracellular volume fraction mapping in the myocardium, part 2: initial clinical experience. J Cardiovasc Magn Reson. 2012;14:64.
- 91. Wong TC, Piehler K, Meier CG, Testa SM, Klock AM, Aneizi AA, et al. Association between extracellular matrix expansion quantified by cardiovascular magnetic resonance and short-term mortality. Circulation. 2012;126(10):1206-16.
- 92. Weatherall DJ, Pippard MJ, Callender ST. Editorial retrospective. Iron loading in thalassemia--five years with the pump. N Engl J Med. 1983;308(8):456-8.
- 93. Wolfe L, Olivieri N, Sallan D, Colan S, Rose V, Propper R, et al. Prevention of cardiac disease by subcutaneous deferoxamine in patients with thalassemia major. N Engl J Med. 1985;312(25):1600-3.
- 94. Easley RM, Jr., Schreiner BF, Jr., Yu PN. Reversible cardiomyopathy associated with hemochromatosis. N Engl J Med. 1972;287(17):866-7.
- 95. Rivers J, Garrahy P, Robinson W, Murphy A. Reversible cardiac dysfunction in hemochromatosis. Am Heart J. 1987;113(1):216-7.
- 96. Short EM, Winkle RA, Billingham ME. Myocardial involvement in idiopathic hemochromatosis. Morphologic and clinical improvement following venesection. Am J Med. 1981;70(6):1275-9.
- 97. Freeman AP, Giles RW, Berdoukas VA, Walsh WF, Choy D, Murray PC. Early left ventricular dysfunction and chelation therapy in thalassemia major. Ann Intern Med. 1983;99(4):450-4.
- 98. Farmaki K, Tzoumari I, Pappa C, Chouliaras G, Berdoukas V. Normalisation of total body iron load with very intensive combined chelation reverses cardiac and endocrine complications of thalassaemia major. Br J Haematol. 2010;148(3):466-75.
- 99. Leyssens L, Vinck B, Van Der Straeten C, Wuyts F, Maes L. Cobalt toxicity in humans-A review of the potential sources and systemic health effects. Toxicology. 2017;387:43-56.
- 100. Simonsen LO, Harbak H, Bennekou P. Cobalt metabolism and toxicology--a brief update. Sci Total Environ. 2012;432:210-5.
- 101. Czarnek K, Terpilowska S, Siwicki AK. Selected aspects of the action of cobalt ions in the human body. Cent Eur J Immunol. 2015;40(2):236-42.
- 102. Schade SG, Felsher BF, Bernier GM, Conrad ME. Interrelationship of cobalt and iron absorption. J Lab Clin Med. 1970;75(3):435-41.
- 103. Catalani S, Rizzetti MC, Padovani A, Apostoli P. Neurotoxicity of cobalt. Hum Exp Toxicol. 2012;31(5):421-37.
- 104. Alexander CS. Cobalt-beer cardiomyopathy. A clinical and pathologic study of twenty-eight cases. Am J Med. 1972;53(4):395-417.

- 105. Morin YL, Foley AR, Martineau G, Roussel J. Quebec beer-drinkers' cardiomyopathy: forty-eight cases. Can Med Assoc J. 1967;97(15):881-3.
- 106. Lauwerys R, Lison D. Health risks associated with cobalt exposure--an overview. Sci Total Environ. 1994;150(1-3):1-6.
- 107. Lippi G, Franchini M, Guidi GC. Cobalt chloride administration in athletes: a new perspective in blood doping? Br J Sports Med. 2005;39(11):872-3.
- 108. Cheung AC, Banerjee S, Cherian JJ, Wong F, Butany J, Gilbert C, et al. Systemic cobalt toxicity from total hip arthroplasties: review of a rare condition Part 1 history, mechanism, measurements, and pathophysiology. Bone Joint J. 2016;98-B(1):6-13.
- 109. Keegan GM, Learmonth ID, Case CP. A systematic comparison of the actual, potential, and theoretical health effects of cobalt and chromium exposures from industry and surgical implants. Crit Rev Toxicol. 2008;38(8):645-74.
- 110. Beyersmann D, Hartwig A. Carcinogenic metal compounds: recent insight into molecular and cellular mechanisms. Arch Toxicol. 2008;82(8):493-512.
- 111. Harrow JA, Das PK, Dhalla NS. Influence of some divalent cations on heart sarcolemmal bound enzymes and calcium binding. Biochem Pharmacol. 1978;27(22):2605-9.
- 112. Kleinfeld M, Stein E. Action of divalent cations on membrane potentials and contractility in rat atrium. Am J Physiol. 1968;215(3):593-9.
- 113. Zywiel MG, Brandt JM, Overgaard CB, Cheung AC, Turgeon TR, Syed KA. Fatal cardiomyopathy after revision total hip replacement for fracture of a ceramic liner. Bone Joint J. 2013;95-B(1):31-7.
- 114. Choi HI, Hong JA, Kim MS, Lee SE, Jung SH, Yoon PW, et al. Severe Cardiomyopathy Due to Arthroprosthetic Cobaltism: Report of Two Cases with Different Outcomes. Cardiovasc Toxicol. 2019;19(1):82-9.
- 115. Agency MHpR. Medicines & Healthcare products Regulatory Agency. All metal-on-metal (MoM)
- hip replacements. 2017 [Available from: https://www.gov.uk/drug-device-alerts/all-metal-on-metal-mom-hip-replacements-updated-advice-for-follow-up-of-patients.
- 116. Agency MHpR. All metal-on-metal (MoM) hip replacements: updated advice for follow-up of patients
- https://assets.publishing.service.gov.uk/media/5954ca1ded915d0baa00009b/MDA-2017-018 Final.pdf [20th May 2019].
- 117. Abdel-Gadir A, Berber R, Porter JB, Quinn PD, Suri D, Kellman P, et al. Detection of metallic cobalt and chromium liver deposition following failed hip replacement using T2* and R2 magnetic resonance. J Cardiovasc Magn Reson. 2016;18(1):29.
- 118. D'Ambrosi R, Ursino N. N-Acetyl-Cysteine Reduces Blood Chromium and Cobalt Levels in Metal-on-Metal Hip Arthroplasty. Arthroplast Today. 2020;6(2):149-52.
- 119. Giampreti A, Lonati D, Ragghianti B, Ronchi A, Petrolini VM, Vecchio S, et al. N-Acetyl-Cysteine as Effective and Safe Chelating Agent in Metal-on-Metal Hip-Implanted Patients: Two Cases. Case Rep Orthop. 2016;2016:8682737.

- 120. Pelclova D, Sklensky M, Janicek P, Lach K. Severe cobalt intoxication following hip replacement revision: clinical features and outcome. Clin Toxicol (Phila). 2012;50(4):262-5.
- 121. Dahms K, Sharkova Y, Heitland P, Pankuweit S, Schaefer JR. Cobalt intoxication diagnosed with the help of Dr House. Lancet. 2014;383(9916):574.
- 122. Goel SH, Sumedh. 1625: Cobalt-induced cardiomyopathy requiring Venoarterial ECMO. Critical care medicine. 2016;44(12).
- 123. Fox KA, Phillips TM, Yanta JH, Abesamis MG. Fatal cobalt toxicity after total hip arthroplasty revision for fractured ceramic components. Clin Toxicol (Phila). 2016;54(9):874-7.
- 124. American College of Cardiology Foundation Task Force on Expert Consensus D, Hundley WG, Bluemke DA, Finn JP, Flamm SD, Fogel MA, et al. ACCF/ACR/AHA/NASCI/SCMR 2010 expert consensus document on cardiovascular magnetic resonance: a report of the American College of Cardiology Foundation Task Force on Expert Consensus Documents. J Am Coll Cardiol. 2010;55(23):2614-62.
- 125. Kellman P, Arai AE, McVeigh ER, Aletras AH. Phase-sensitive inversion recovery for detecting myocardial infarction using gadolinium-delayed hyperenhancement. Magn Reson Med. 2002;47(2):372-83.
- 126. Kellman P, Wilson JR, Xue H, Ugander M, Arai AE. Extracellular volume fraction mapping in the myocardium, part 1: evaluation of an automated method. J Cardiovasc Magn Reson. 2012;14:63.
- 127. Kramer CM, Barkhausen J, Flamm SD, Kim RJ, Nagel E, Society for Cardiovascular Magnetic Resonance Board of Trustees Task Force on Standardized P. Standardized cardiovascular magnetic resonance (CMR) protocols 2013 update. J Cardiovasc Magn Reson. 2013;15:91.
- 128. Townsend A, Drakesmith H. Role of HFE in iron metabolism, hereditary haemochromatosis, anaemia of chronic disease, and secondary iron overload. Lancet. 2002;359(9308):786-90.
- 129. Sado DM, Maestrini V, Piechnik SK, Banypersad SM, White SK, Flett AS, et al. Noncontrast myocardial T mapping using cardiovascular magnetic resonance for iron overload. J Magn Reson Imaging. 2014.
- 130. Westwood MA, Anderson LJ, Firmin DN, Gatehouse PD, Lorenz CH, Wonke B, et al. Interscanner reproducibility of cardiovascular magnetic resonance T2* measurements of tissue iron in thalassemia. J Magn Reson Imaging. 2003;18(5):616-20.
- 131. Westwood MA, Firmin DN, Gildo M, Renzo G, Stathis G, Markissia K, et al. Intercentre reproducibility of magnetic resonance T2* measurements of myocardial iron in thalassaemia. The international journal of cardiovascular imaging. 2005;21(5):531-8.
- 132. Kirk P, He T, Anderson LJ, Roughton M, Tanner MA, Lam WW, et al. International reproducibility of single breathhold T2* MR for cardiac and liver iron assessment among five thalassemia centers. J Magn Reson Imaging. 2010;32(2):315-9.
- 133. Wood JC. History and current impact of cardiac magnetic resonance imaging on the management of iron overload. Circulation. 2009;120(20):1937-9.

- 134. Torlasco C, Cassinerio E, Roghi A, Faini A, Capecchi M, Abdel-Gadir A, et al. Role of T1 mapping as a complementary tool to T2* for non-invasive cardiac iron overload assessment. PLoS One. 2018;13(2):e0192890.
- 135. Niss O, Fleck R, Makue F, Alsaied T, Desai P, Towbin JA, et al. Association between diffuse myocardial fibrosis and diastolic dysfunction in sickle cell anemia. Blood. 2017;130(2):205-13.
- 136. Haaf P, Garg P, Messroghli DR, Broadbent DA, Greenwood JP, Plein S. Cardiac T1 Mapping and Extracellular Volume (ECV) in clinical practice: a comprehensive review. J Cardiovasc Magn Reson. 2016;18(1):89.
- 137. Shizukuda Y, Tripodi DJ, Zalos G, Bolan CD, Yau YY, Leitman SF, et al. Incidence of cardiac arrhythmias in asymptomatic hereditary hemochromatosis subjects with C282Y homozygosity. Am J Cardiol. 2012;109(6):856-60.
- 138. Rasmussen ML, Folsom AR, Catellier DJ, Tsai MY, Garg U, Eckfeldt JH. A prospective study of coronary heart disease and the hemochromatosis gene (HFE) C282Y mutation: the Atherosclerosis Risk in Communities (ARIC) study. Atherosclerosis. 2001;154(3):739-46.
- 139. Alpendurada F, Carpenter JP, Deac M, Kirk P, Walker JM, Porter JB, et al. Relation of myocardial T2* to right ventricular function in thalassaemia major. Eur Heart J. 2010;31(13):1648-54.
- 140. Kremastinos DT, Farmakis D, Aessopos A, Hahalis G, Hamodraka E, Tsiapras D, et al. Beta-thalassemia cardiomyopathy: history, present considerations, and future perspectives. Circ Heart Fail. 2010;3(3):451-8.
- 141. Bornaun H, Dedeoglu R, Oztarhan K, Dedeoglu S, Erfidan E, Gundogdu M, et al. Detection of Early Right Ventricular Dysfunction in Young Patients With Thalassemia Major Using Tissue Doppler Imaging. Iran J Pediatr. 2016;26(3):e5808.
- 142. Higgs DR, Engel JD, Stamatoyannopoulos G. Thalassaemia. Lancet. 2012;379(9813):373-83.
- 143. Modell B, Khan M, Darlison M, King A, Layton M, Old J, et al. A national register for surveillance of inherited disorders: beta thalassaemia in the United Kingdom. Bull World Health Organ. 2001;79(11):1006-13.
- 144. Carpenter JP, Roughton M, Pennell DJ, Myocardial Iron in Thalassemia I. International survey of T2* cardiovascular magnetic resonance in beta-thalassemia major. Haematologica. 2013;98(9):1368-74.
- 145. Leroi C, Adam P, Khamduang W, Kawilapat S, Ngo-Giang-Huong N, Ongwandee S, et al. Prevalence of chronic hepatitis B virus infection in Thailand: a systematic review and meta-analysis. Int J Infect Dis. 2016;51:36-43.
- 146. Wanachiwanawin W, Luengrojanakul P, Sirangkapracha P, Leowattana W, Fucharoen S. Prevalence and clinical significance of hepatitis C virus infection in Thai patients with thalassemia. Int J Hematol. 2003;78(4):374-8.
- 147. Kell DB, Pretorius E. Serum ferritin is an important inflammatory disease marker, as it is mainly a leakage product from damaged cells. Metallomics. 2014;6(4):748-73.
- 148. Kondur AK, Li T, Vaitkevicius P, Afonso L. Quantification of myocardial iron overload by cardiovascular magnetic resonance imaging T2* and review of the literature. Clin Cardiol. 2009;32(6):E55-9.

- 149. Hart AJ, Sabah S, Henckel J, Lewis A, Cobb J, Sampson B, et al. The painful metal-on-metal hip resurfacing. J Bone Joint Surg Br. 2009;91(6):738-44.
- 150. Smith AJ, Dieppe P, Howard PW, Blom AW, National Joint Registry for E, Wales. Failure rates of metal-on-metal hip resurfacings: analysis of data from the National Joint Registry for England and Wales. Lancet. 2012;380(9855):1759-66.
- 151. Smith AJ, Dieppe P, Vernon K, Porter M, Blom AW, National Joint Registry of E, et al. Failure rates of stemmed metal-on-metal hip replacements: analysis of data from the National Joint Registry of England and Wales. Lancet. 2012;379(9822):1199-204.
- 152. Khan AH, Verma R, Bajpai A, Mackey-Bojack S. Unusual case of congestive heart failure: cardiac magnetic resonance imaging and histopathologic findings in cobalt cardiomyopathy. Circ Cardiovasc Imaging. 2015;8(6).
- 153. Prentice JR, Clark MJ, Hoggard N, Morton AC, Tooth C, Paley MN, et al. Metal-on-metal hip prostheses and systemic health: a cross-sectional association study 8 years after implantation. PLoS One. 2013;8(6):e66186.
- 154. Anderson RA. Chromium as an essential nutrient for humans. Regul Toxicol Pharmacol. 1997;26(1 Pt 2):S35-41.
- 155. Gad SC. Acute and chronic systemic chromium toxicity. Sci Total Environ. 1989;86(1-2):149-57.
- 156. Junaid M, Hashmi MZ, Malik RN, Pei DS. Toxicity and oxidative stress induced by chromium in workers exposed from different occupational settings around the globe: A review. Environ Sci Pollut Res Int. 2016;23(20):20151-67.
- 157. Hart AJ, Quinn PD, Sampson B, Sandison A, Atkinson KD, Skinner JA, et al. The chemical form of metallic debris in tissues surrounding metal-on-metal hips with unexplained failure. Acta Biomater. 2010;6(11):4439-46.
- 158. Berstock JR, Whitehouse MR, Duncan CP. Trunnion corrosion: what surgeons need to know in 2018. Bone Joint J. 2018;100-B(1 Supple A):44-9.
- 159. Wharton G, Steeds R, Allen J, Phillips H, Jones R, Kanagala P, et al. A minimum dataset for a standard adult transthoracic echocardiogram: a guideline protocol from the British Society of Echocardiography. Echo Res Pract. 2015;2(1):G9-G24.
- 160. Samar HY, Doyle M, Williams RB, Yamrozik JA, Bunker M, Biederman RW, et al. Novel Use of Cardiac Magnetic Resonance Imaging for the Diagnosis of Cobalt Cardiomyopathy. JACC Cardiovasc Imaging. 2015;8(10):1231-2.
- 161. Deva DP, Hanneman K, Li Q, Ng MY, Wasim S, Morel C, et al. Cardiovascular magnetic resonance demonstration of the spectrum of morphological phenotypes and patterns of myocardial scarring in Anderson-Fabry disease. J Cardiovasc Magn Reson. 2016;18:14.
- 162. Friedrich MG, Sechtem U, Schulz-Menger J, Holmvang G, Alakija P, Cooper LT, et al. Cardiovascular magnetic resonance in myocarditis: A JACC White Paper. J Am Coll Cardiol. 2009;53(17):1475-87.
- 163. Mavrogeni S, Markousis-Mavrogenis G, Papavasiliou A, Kolovou G. Cardiac involvement in Duchenne and Becker muscular dystrophy. World J Cardiol. 2015;7(7):410-4.
- 164. He Y, Zhang Z, Hong D, Dai Q, Jiang T. Myocardial fibrosis in desmin-related hypertrophic cardiomyopathy. J Cardiovasc Magn Reson. 2010;12:68.

- 165. Shanbhag SM, Greve AM, Aspelund T, Schelbert EB, Cao JJ, Danielsen R, et al. Prevalence and prognosis of ischaemic and non-ischaemic myocardial fibrosis in older adults. Eur Heart J. 2019;40(6):529-38.
- 166. Bonilla HMG, Bhimaraj A. A CASE OF COBALT CARDIOMYOPATHY. Journal of the American College of Cardiology. 2018;71(11 Supplement):A2386.
- 167. Tilney R, Burg MR, Sammut MA. Cobalt Cardiomyopathy Secondary to Hip Arthroplasty: An Increasingly Prevalent Problem. Case Rep Cardiol. 2017;2017:5434571.
- 168. Morin Y, Tetu A, Mercier G. Cobalt cardiomyopathy: clinical aspects. Br Heart J. 1971;33:Suppl:175-8.
- 169. Barceloux DG. Cobalt. J Toxicol Clin Toxicol. 1999;37(2):201-6.
- 170. Fernandes JL, Fabron A, Jr., Verissimo M. Early cardiac iron overload in children with transfusion-dependent anemias. Haematologica. 2009;94(12):1776-7.
- 171. Borgna-Pignatti C, Meloni A, Guerrini G, Gulino L, Filosa A, Ruffo GB, et al. Myocardial iron overload in thalassaemia major. How early to check? Br J Haematol. 2014;164(4):579-85.
- 172. Viprakasit V, Ajlan A, Aydinok Y, Al Ebadi BAA, Dewedar H, Ibrahim AS, et al. MRI for the diagnosis of cardiac and liver iron overload in patients with transfusion-dependent thalassemia: An algorithm to guide clinical use when availability is limited. Am J Hematol. 2018;93(6):E135-E7.
- 173. van Lingen CP, Ettema HB, Timmer JR, de Jong G, Verheyen CC. Clinical manifestations in ten patients with asymptomatic metal-on-metal hip arthroplasty with very high cobalt levels. Hip Int. 2013;23(5):441-4.
- 174. Sabah SA, Moon JC, Jenkins-Jones S, Morgan CL, Currie CJ, Wilkinson JM, et al. The risk of cardiac failure following metal-on-metal hip arthroplasty. Bone Joint J. 2018;100-B(1):20-7.
- 175. Menacho K, Ramirez S, Segura P, Nordin S, Abdel-Gadir A, Illatopa V, et al. INCA (Peru) Study: Impact of Non-Invasive Cardiac Magnetic Resonance Assessment in the Developing World. J Am Heart Assoc. 2018;7(17):e008981.